An Analysis of the Multi-scale Structure of Rough Surfaces

by

Xiaohan Zhang

A thesis submitted to the Graduate Faculty of
Auburn University
in partial fulfillment of the
requirements for the Degree of
Master of Science

Auburn, Alabama
December 13, 2014

Keywords: surface finishing techniques; surface roughness; models; topography

Approved by

Robert L. Jackson, Chair, Associate Professor of Mechanical Engineering
Dan B. Marghitu, Professor of Mechanical Engineering
Andres L. Carrano, Associate Professor of Industrial and Systems Engineering

Abstract

Even with the various surface finishing techniques, all surfaces are rough with different structures and geometric characteristics over multiple scales. The roughness impacts significantly the friction, wear, and surface fatigue of applications, and also affects the electrical and thermal resistance. In this work, a profilometer was utilized to measure the profiles of different rough surfaces, and the profiles were characterized using a variety of statistical, multi-scale spectrum, and fractal methodologies. Since the fractal dimension, *D*, is a very popular and arguably important parameter in describing the fractal rough surfaces, four different methods are implemented in calculating the value and these four methods are then compared. The relationship between the fractal dimension, *D*, and the fractal scaling constant, *G*, is investigated as well. The measured rough surfaces are also compared with W-M function generated rough surfaces. After comparing a series of statistical and fractal parameters which are calculated based on the surface profile data, it can be found that the Weierstrass-Mandelbrot (W-M) function does not appear to be very suitable for characterizing real rough surfaces. Another important conclusion is that many surfaces are not consistent with the quality of self-affinity that many of the popular fractal models assume. Therefore, a discrepancy exists between idealized fractal equations and real surfaces.

Table of Contents

Abstract ii

List of Figures vi

List of Tables viii

List of Abbreviations ix

1 Introduction 1

1.1 Surface height distributions 1

1.2 Statistical parameters in describing rough surfaces 2

1.3 Rough surfaces geometrical characterizations 6

1.4 Fractal parameters for fractal geometry 9

1.5 Method of generating rough surfaces 12

a) Random midpoint displacement 12

b) Weierstrass-Mandelbrot (W-M) fractal function 13

1.6 Relationship between statistical parameters and fractal parameters 15

1.7 Goal of the work 16

2 Experiment and methodology 17

2.1 Experiment 17

2.1.1 Preprocessing of surface data 17

2.1.2 Different methods in calculating the fractal dimension, *D* 25

(1) Methods description 25

a) Fourier analysis 26

b) Roughness-length method 26

c) Box-counting method 28

d) Power spectrum method 30

(2) Results and discussion 32

2.1.3 Discussion of *G* value 34

2.1.4 Parameters calculated in the experiment 36

2.2 Bearing area curve 37

3 Generated W-M fractal rough surfaces 40

3.1 Surfaces generation based on the W-M function 40

3.2 Discussion of parameters in generated rough surfaces 41

3.3 Parameters comparison between measured rough surfaces and generated rough surfaces 47

4 Analysis 52

4.1 The analysis of the W-M function 52

4.2 The analysis of different methods in calculating the fractal dimension, *D* 53

4.3 The analysis of autocorrelation function (ACF) in power spectrum method 57

5 Conclusions and future work 58

References 61

Appendices 68

A: The other five measured rough surface profiles after leveling 68

B: Plots of relationship between amplitude (Δ) versus wavelength (λ) for the other four measured rough surfaces 69

C: Plots of relationship between B and λ for the other four measured rough surfaces 70

D: Schematical illustration of fractal dimension of the other five measured rough surfaces calculated by using different four methods 71

E: The other five generated rough surface profiles after leveling 76

F: Plots of relationship between amplitude (Δ) versus wavelength (λ) for the other four generated rough surfaces 78

G: Plots of relationship between B and λ for the other four measured rough surfaces 79

H: Schematical illustration of fractal dimension of generated rough surfaces calculated by using different four methods 80

List of Figures

Figure 1: Schematic illustration of the rough surface 3

Figure 2: Details of an asperity profile in rough surface profile 5

Figure 3: Fractal self-similarity 8

Figure 4: Fractal self-affinity 8

Figure 5: The influence of *D* on rough surfaces 10

Figure 6: The influence of *G* on rough surfaces 11

Figure 7: Profilometer used in the experiment 18

Figure 8: Standard reference surface 18

Figure 9: 8L Rough surface profile after leveling 19

Figure 10: Multi-scale nature of rough surfaces 20

Figure 11: Multi-scale surface profile 20

Figure 12: Δ vs. λ for measured rough surfaces 23

Figure 13: *B* vs. λ for measured rough surfaces 24

Figure 14: Computational process of roughness-length method 27

Figure 15: Process of box-counting method 30

Figure 16: Autocorrelation function for 8L rough surface 31

Figure 17: The results of four different ways in calculating D 33

Figure 18: Relationship between D and G 35

Figure 19: Bearing area curve for 8L surface 38

Figure 20: Generated 8L surface by using the W-M function 40

Figure 21: Δ vs. λ for the generated rough surfaces 44

Figure 22: B vs. λ for the generated rough surfaces 45

Figure 23: $dB/d\lambda$ vs. λ 46

Figure 24: Comparison of statistical parameters between original rough surfaces and generated rough surfaces 48

Figure 25: Comparison of multi-scale parameters between original rough surfaces and generated rough surfaces 49

Figure 26: Comparison of $db/d\lambda$ calculated with varying l values and FFT method for measured rough surfaces and generated rough surfaces 51

Figure 27: Random fractal outlines generated with varying fractal dimensions 56

Figure 28: The other five rough surface profiles after leveling 69

Figure 29: Δ vs. λ for the other measured rough surfaces 70

Figure 30: B vs. λ for the other four measured rough surfaces 71

Figure 31: D values calculated by four different methods for the other five measured rough surfaces 76

Figure 32: Surface profiles after leveling for the other five generated rough surfaces 77

Figure 33: Δ vs. λ for the other four generated rough surfaces 78

Figure 34: B vs. λ for the other four generated rough surfaces 79

Figure 35: D values calculated by four different methods for the other five measured rough surfaces 85

List of Tables

Table 1: *D* and *G* values for measured rough surfaces 35

Table 2: Parameters needed in the experiment 37

Table 3: Values of $db/d\lambda$ for varying *l* and FFT method 37

Table 4: Fractal dimension values for generated rough surfaces 42

Table 5: Parameters calculated based on W-M function 42

Table 6: Values of $db/d\lambda$ for different *l* and FFT method of generated surfaces 46

Table 7: Comparison between different methods in evaluating *D* 53

List of Abbreviations

$(\frac{dy}{dx})_i$ Mean square slope

$(\frac{d^2y}{dx^2})_i$ Mean square curvature

A Amplitude of each scaled sinusoidal wave

B Asperity aspect ratio or Fourier series slope

c Scaling parameter

D Fractal dimension

f Spatial frequency

G Scaling constant

H Hurst exponent

K Kurtosis

L Sampling length

l Self-similar fractal scaling parameter

M Number of superposed ridges used to construct the surface

m_0, m_2, m_4 Spectral moments

N Number of sampling points

N_r Number of boxes in the box-counting method

n Fractal scale index

n_1 Lowest cutoff frequency index

n_2 Highest cutoff frequency index

n_w Total number of window in roughness-length method

R_a Average roughness

R_q Root mean square roughness or standard deviation of the distribution

r Box side length in the box-counting method

SK Skewness

s Sampling interval

y_i Height of rough surface profile

$\bar{y}$ Surface average height

z Surface height

μ Mean of the distribution

φ Random phase

γ Fractal scaling parameter

Δ Amplitude

λ Wavelength

β Slope of fitted line

w Window length in the roughness-length method

ω_h Higher wave number limit

ω_l Lower wave number limit

τ Changing distance in the power spectrum method

Subscript

i Surface roughness scale or frequency level

Chapter 1

1 Introduction

1.1 Surface height distributions

The surfaces of objects play important roles in natural phenomena. The geometric structure of rough surfaces has a great impact on some physical phenomena which are related to many engineering areas, such as electrical contact, microelectronics, bearings and seals. Additionally, it can be applied to geology and the navigation of autonomous vehicles.

Regarding the height distribution of engineering surfaces as Gaussian distribution has already become the mainstay of surface characterization. Therefore, most of the studies of surface roughness effects on the engineering phenomena as lubricant, contact mechanics, and thermal contact are obtained by using Gaussian surfaces [1].

The Gaussian distribution, also called the normal distribution, is a famous probability distribution that is wildly used in the field of mathematics, physics and engineering. Its probability density function is:

$$f(x) = \frac{1}{\sqrt{2\pi}R_q} \exp\left(-\frac{(y-\mu)^2}{2R_q^{\,2}}\right) \tag{1}$$

where μ is the mean of the distribution, it determines the central position of the distribution; R_q is the standard deviation that describes the dispersion degree, the larger it is , the more

dispersive the distribution will be.

In particularly, the skewness (*SK*) and kurtosis (*K*) are two important parameters in describing the shape of a distribution. Skewness represents the measure of the degree of asymmetry for a distribution. For a Gaussian distribution, the value of skewness is zero. Kurtosis determines the degree of peakedness for the height distribution of a surface. It equals 3 if the height distribution is a Gaussian distribution. The expression of these two parameters will be shown in section 1.2.

However, except for the Gaussian height distribution, many engineering surfaces can also be recognized as processing non-Gaussian height distributions, which sometimes is difficult to formalize using an equation. Whether the surface height distribution follows the Gaussian distribution or non-Gaussian distribution depends on the nature of the processing method [2]. Cumulative processes, such as peening and lapping, can make the surface height distribution act as the Gaussian distribution because of the final shape of each region is the cumulative result of a large number of random discrete local events and irrespective of the distribution governing each individual event. Generally, non-Gaussian surfaces can be caused by the single-point processes (such as turning and shaping) and extreme-value processes (such as grinding and milling) [2].

1.2 Statistical parameters in describing rough surfaces

Surfaces are not as smooth as what we observe, there are many asperities on surfaces (see Figure 1). The deviation of the surface from its smooth contour is the roughness. The

characterization of roughness is very significant in a multitude of engineering problems, such as wear, friction and wave scattering.

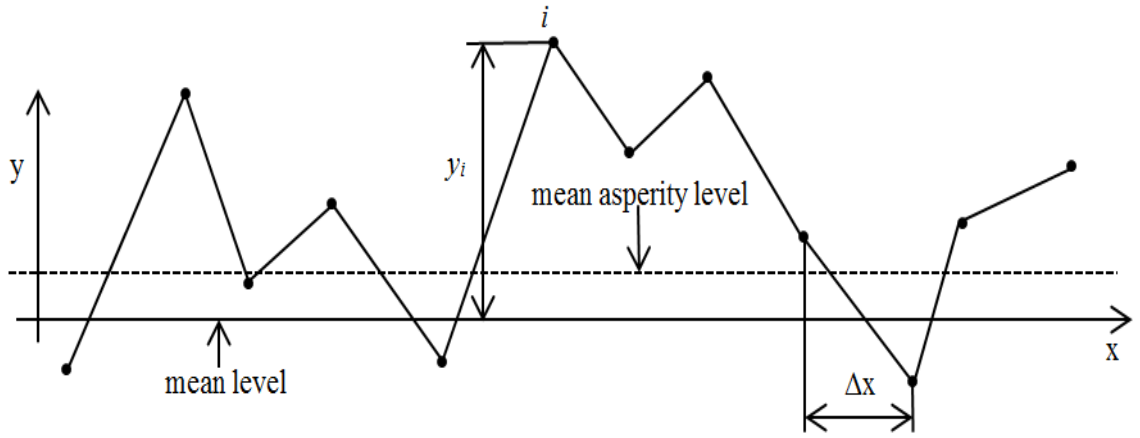

Figure 1: Schematic illustration of the rough surface

Note: mean level – the average height of the asperities and the valleys
mean asperity level - the average height of all the asperities

There are many different statistical parameters in use to characterize the surface roughness. Among which R_a (arithmetic average) is the most common one because of its easy measurement and explanation:

$$R_a = \frac{1}{N}\sum_{i=1}^{N}\left|y_i\right| \tag{2}$$

where N is number of sampling points, y_i is the height of rough surface profile.

For process engineers, the specification of R_a can be used to finish a surface [3]. However, the shortcoming of R_a is that it makes no distinction between peaks and valleys, and it cannot provide the insight into the spatial structure [3]. Therefore, engineers formulated several other statistical parameters, such as R_q (root mean squared roughness or standard deviation), SK (Skewness) and K (kurtosis), to make up for the deficiencies of R_a. R_q is another widely used

parameter which is similar to R_a and for large deviations from the mean line, R_q is more sensitive than R_a [4] and for a surface having a Gaussian statistical height distribution, R_q=1.25R_a:

$$R_q = \sqrt{\frac{1}{N}\sum_{i=1}^{N} y_i^2} \tag{3}$$

The expressions for SK and K are shown below:

$$SK = \frac{1}{R_q^{\,3}(N+1)}\sum_{i=1}^{N}(y_i - \bar{y})^3 \tag{4}$$

$$K = \frac{1}{R_q^{\,4}N}\sum_{i=1}^{N}(y_i - \bar{y})^4 \tag{5}$$

where $\bar{y}$ is the average height, and the equation of $\bar{y}$ is:

$$\bar{y} = \frac{1}{N}\sum_{i=1}^{N} y_i \tag{6}$$

In 1987, McCool [5] described how to use spectral moments, m_0, m_2 and m_4, to obtain the statistical parameters:

$$m_0 = \frac{1}{N}\sum_{i=1}^{N} y_i^2 \tag{7}$$

$$m_2 = \frac{1}{N-2}\sum_{i=2}^{N-1}\left(\frac{dy}{dx}\right)_i^{\,2} \tag{8}$$

$$m_4 = \frac{1}{N-2}\sum_{i=2}^{N-1}\left(\frac{d^2y}{dx^2}\right)_i^2 \tag{9}$$

where $\left(\frac{dy}{dx}\right)_i$ and $\left(\frac{d^2y}{dx^2}\right)_i$ can be calculated by using the central finite difference scheme (see Figure 2):

$$\left(\frac{dy}{dx}\right)_i = \frac{y_{i+1} - y_{i-1}}{2\Delta_x} \tag{10}$$

$$\left(\frac{d^2y}{dx^2}\right)_i = \frac{y_{i+1} - 2y_i + y_{i-1}}{\Delta_x^2} \tag{11}$$

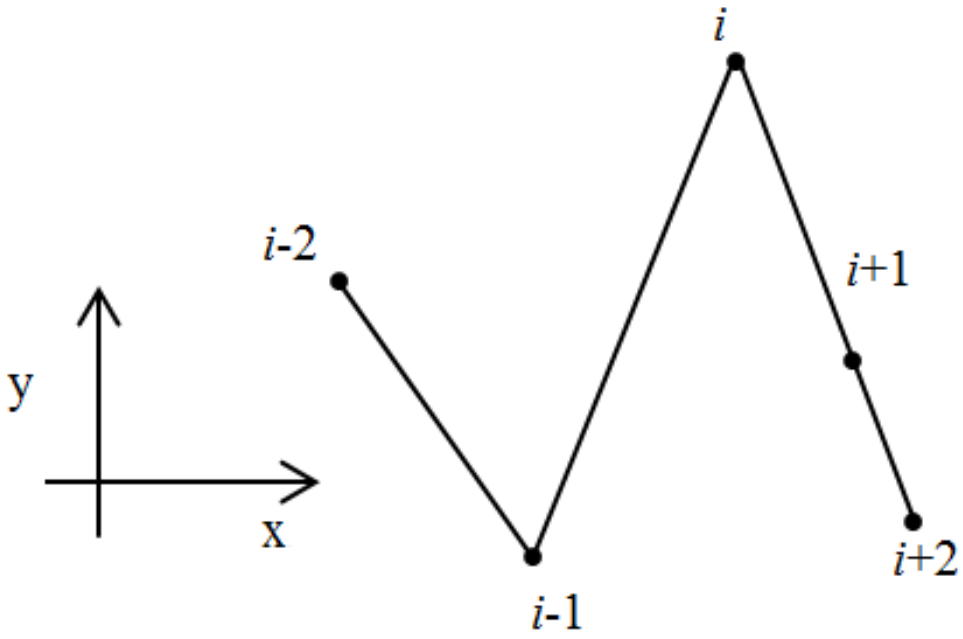

Figure 2: Details of an asperity profile in rough surface profile

From the equations above, it may be found that the expression of m_0 is the same as the square of R_q, i.e., $m_0=R_q^2$. m_2 and m_4 can also be called the mean square slope and curvature respectively [6].

However, experimental results [4, 7, 8] show that these statistical parameters are instrument-dependent, and that they can change with the scan length and the resolution of the measuring instrument. They are therefore not intrinsic properties of the surface. Despite this defect, these parameters are still very useful. They can be regarded as the numerical characteristics of a surface height distribution.

1.3 Rough surfaces geometrical characterizations

According to previous studies [9-12], essentially two different types of geometries were utilized in the study of surfaces in nature: Euclidean and Fractal geometry. Euclidean geometry is a mathematical system which is a branch of geometry. Normally, Euclidean shapes have some characteristic sizes or length scales (e.g. the radius of a circle or the length of the side of a cube) [9]. For ages, Euclidean geometry has dominantly been used to describe numerous natural phenomena. However, the classical Euclidean geometry merely describes artificial objects and it can only work with objects that have integer fractal dimensions (i.e.1-D, 2-D or 3-D).

With the discovery of "non-Euclidean" geometries, such as the Koch curve shown in [13], the Sierpinski fractal shown in [14] and the Menger sponge in [15], the previous concepts of mathematics were violated. The dimensions of these geometries are non-integer, so the Euclidean geometrical descriptions cannot be used anymore. To better characterize "rough" phenomena in the natural and artificial world, new approaches needed to be introduced in addition to the Euclidean geometry.

Mandelbrot first proposed that the fractal geometry seems to fit much of the natural world [16] and it can be regarded as a workable geometric middle ground which is between the excessive geometric order of Euclid [11] and the geometric chaos of general mathematics [10]. Mandelbrot declared a more general definition of a fractal, as "a shape made of parts similar to the whole in some way" [17]. Burrough [18] also emphasized that the strictly defined fractal refers to a series in which the Hausdorf-Besicovith dimension exceeds the topological dimension.

This kind of geometry can be used to describe the profile of objects with non-integer dimensions.

Fractal geometry is often used to simplify rough surfaces as following a specific mathematical definition over many scales. Majumdar [19] emphasized that the essence of the fractal definition Mandelbrot [17] has proposed lied in the concepts of self-similarity and self-affinity.

The work by Majumdar provides a description of these two phenomena of self-similarity and self-affinity as well. For example, Figure 3 [20] is a typical self-similar shape for which the scaling ratio is the same as in all directions. When a local region is enlarged, it appears to be exactly the same to the larger regions. In other words, self-similar means the appearance of an object is much the same at any the magnification or scale. While Figure 4 [21] shows an example of self-affinity, where the scaling ratio is unequal in different directions. Therefore, self-affinity is a generalization of self-similar fractals. Russ suggested that many natural surfaces as produced by deposition, erosion, wear, fracture, etc., seem to be self-affine rather than self-similar [22]. Fractal surfaces are then always classified as by either self-similarity or self-affinity.

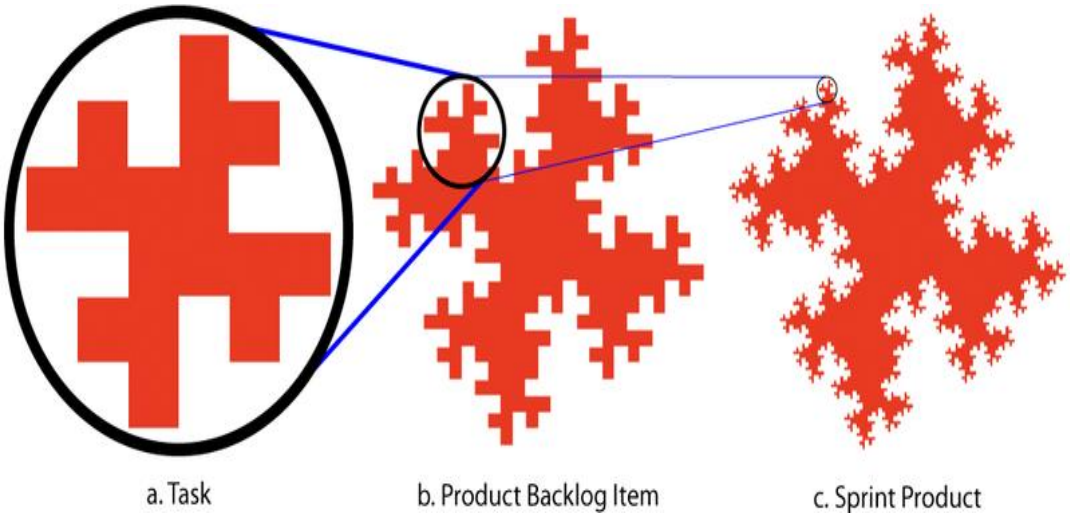

Scrum Self-Similarity: Creating Organizational Fractals

Figure 3: Fractal self-similarity [20]

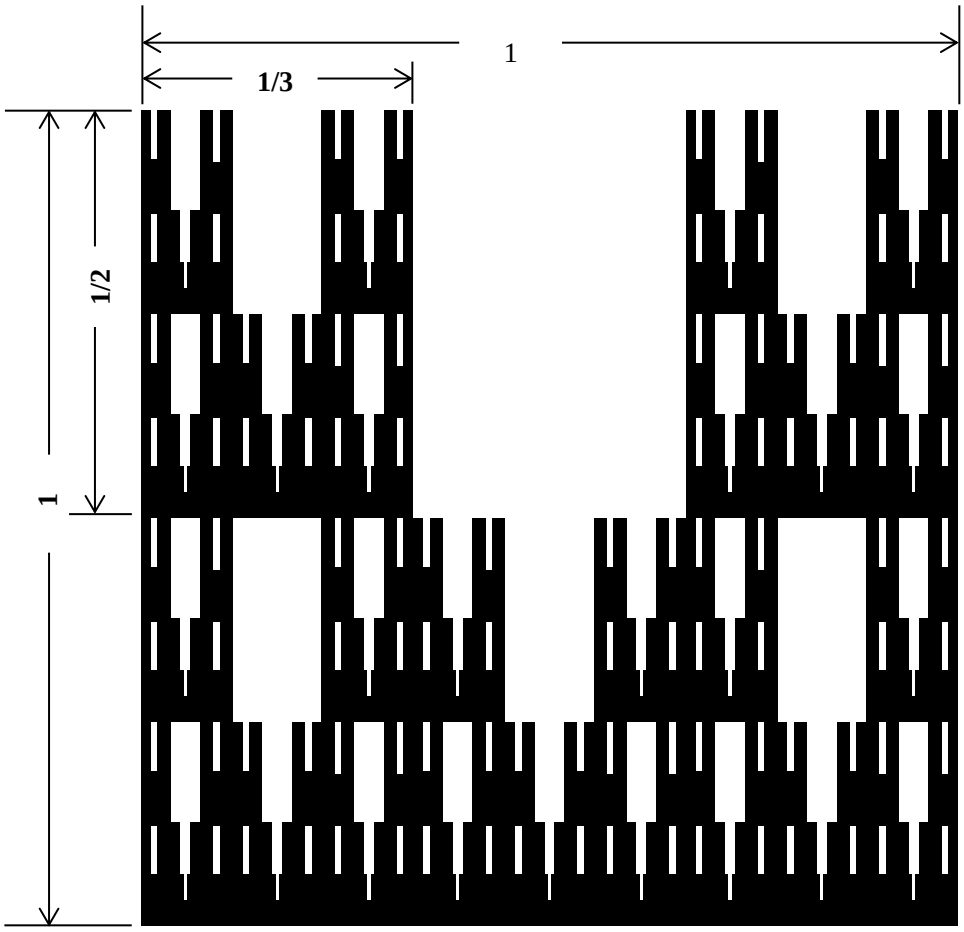

Fractal Geometry

Figure 4: Fractal self-affinity [21]

1.4 Fractal parameters for fractal geometry

Majumdar and Bhushan [8] characterized fractal surfaces with two parameters: a non-integer Hausdorff-Besicovitch dimension (fractal dimension) D and a scaling constant G (often referred to as fractal roughness). The fractal dimension, D, provides a description of how close a geometry is to being a point (D=0), a perfect line (D=1), a plane (D=2) or a volume (D=3). Only the dimensions of surface profiles are considered in the current work, and therefore 1<D<2. The surface dimension (D_s) can be combined with the profile dimension (D) using $D_s=D+1$. This equation is based on the statement [22] that adding two fractal data sets with dimensions D_a and D_b together can produce a dimension of D_a+D_b.

The impact of D when generating surface profiles is shown in Figure 5 (G is kept constant). Sometimes G is also called the fractal roughness parameter [23], as it may have influence on the height of a fractal rough surface, as shown in Figure 6 (D is a constant).

Fractal parameters can all be extracted from rough surface data. Compared to the scale-dependent parameters discussed in section 1.2, D and G are scale-independent according to [7, 24]. These two fractal parameters helped much in studying the surface phenomenon by providing the information about the roughness structure over multiple scales.

Klinkenberg [25] discussed that determining the fractal dimension of a self-similar objective is much easier than determining the fractal dimension of a self-affine objective. In the current work, four different methods are used in determining the fractal dimension and will be discussed in chapter 2.

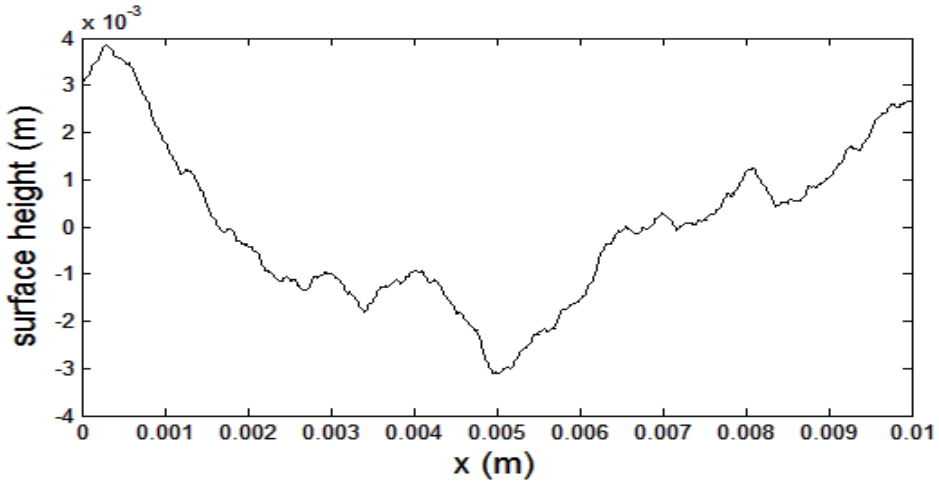

G=1
D=1

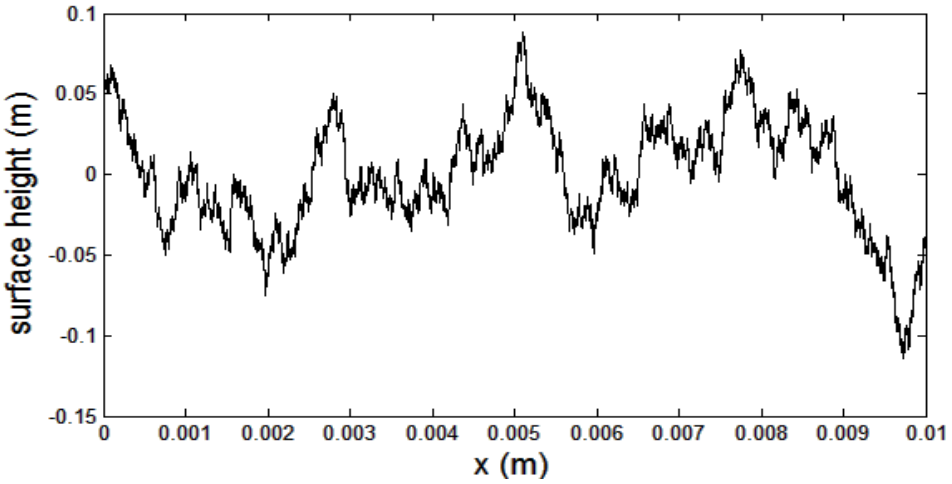

G=1
D=1.5

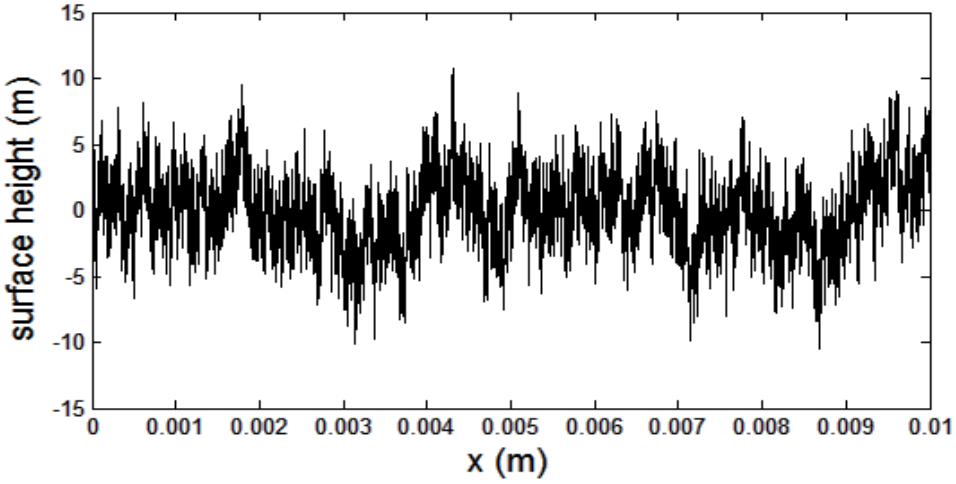

G=1
D=2

Figure 5: The influence of *D* on rough surfaces

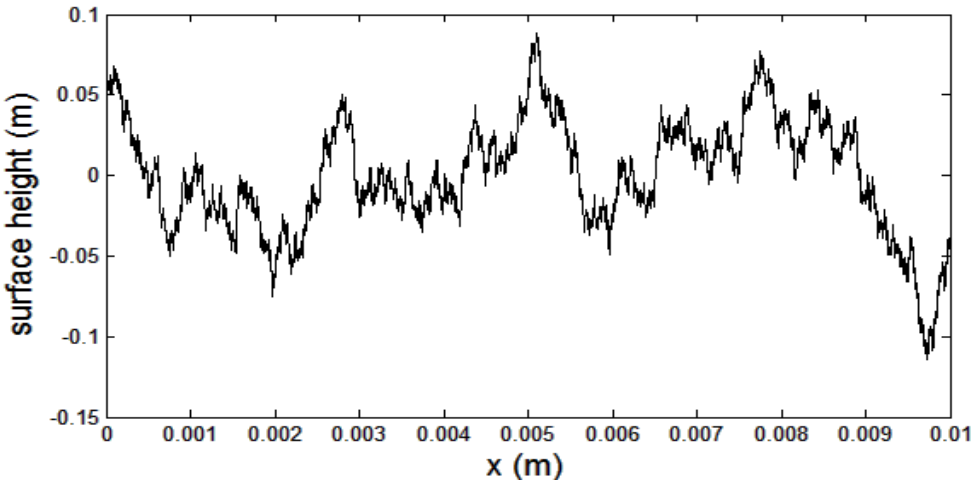

D=1.5
G=1

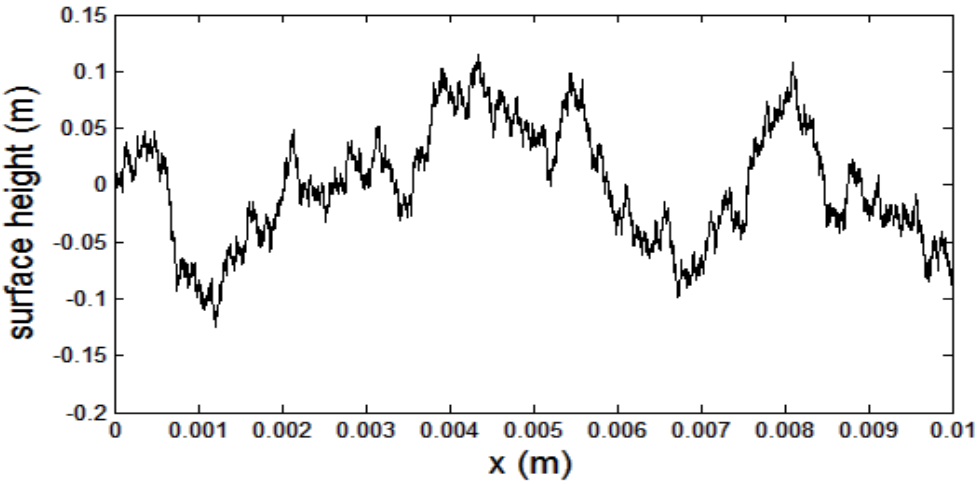

D=1.5
G=1.5

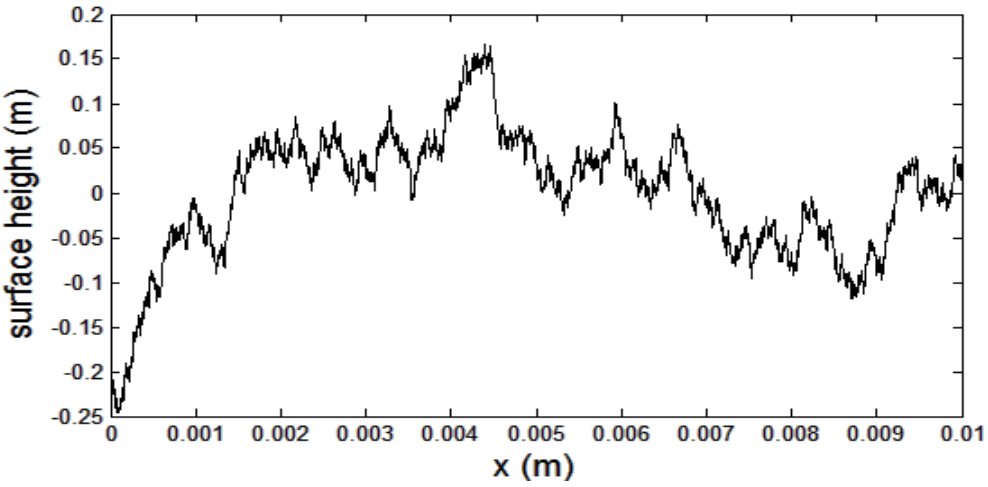

D=1.5
G=2

Figure 6: The influence of *G* on rough surfaces

1.5 Method of generating rough surfaces

Commonly, rough surface data can be obtained using a profilometer. For model evaluation, rough surface generation is very important and popular in diverse fields such as tribology, geophysics, and computer graphics. It can both simulate and simplify the true rough surfaces and the surface-related random phenomena by artificially creating surfaces. By the simplification of the surfaces and related phenomena, the research work on the true surfaces can be much easier.

Many methods used in generating rough surfaces can be found in past literatures. Here, two popular algorithms of generating fractal surfaces, namely, the random midpoint displacement method and the Weierstrass-Mandelbrot (W-M) fractal function, are introduced. However, only the W-M fractal function method is discussed in the current work.

a) Random midpoint displacement

This method, first introduced by Fournier [26], is one of the simplest algorithms for surface generation. It can also be called top-down generation [27]. Based on the method, a rough surface profile can be created by displacing the midpoint of a straight line with some random amount, then continue the operation in the midpoint of new-generated line. After repeating this process for many times until the line segment becomes shorter than can be drawn, a simple rough surface profile can be obtained.

The shortcoming of the random midpoint displacement method lies in that it requires the

generation of a large quantity of random numbers [28]. Moreover, since the length of each line is halved at each step, after several iterations the line segments to be halved will be very short, so that the generated rough surface can be oversimplified and the details of the rough surface are not recognizable.

b) Weierstrass-Mandelbrot (W-M) fractal function

The Weierstrass-Mandelbrot (W-M) fractal function is the most well-known method in characterizing and simulating fractal profiles and has been widely applied in the field of contact mechanics and tribology. It has the properties of continuity, non-differentiability and statistically self-affinity, which satisfies the characteristics of fractal geometry. The W-M function has a fractal dimension which varies between 1 and 2 and the format of it is given below [24, 29, 30]:

$$z(x) = \sum_{n=n_1}^{n_2} \frac{G^{(D-1)} \cos(2\pi\gamma^n x)}{\gamma^{(2-D)n}} \qquad 1<D\leq 2 \tag{12}$$

where $z(x)$ is the surface height, and γ is the fractal scaling parameter, it determines the density of the spectrum and controls the randomization of the phases of frequency modes for the generated surfaces [29]. It is shown that 1.5 is a suitable γ value for high spectral density and phase randomization [29]. In addition, the power of γ can form a geometric series. n is the fractal scale index，n_1 and n_2 are the lowest and highest cut-off frequencies separately which depend on the sampling length L and sampling resolution s. They are given as $\gamma^{n_1} = 1/L$ and $\gamma^{n_2} = 1/s$. Russ described the W-M function as a summation operation that adds

non-fractal sinusoidal shapes together to generate a fractal result [28] and he also mentioned that the W-M function is an algorithm, as it adds a series of sine waves together such that their frequencies are not a linear sequence.

For the fractal surface, its spectral density, $P(\omega)$, and structure function, $S(\tau)$, are:

$$P(\omega) = \frac{G^{2D-2}}{\omega^{5-2D}} \tag{13}$$

$$S(\tau) = E\{[z(x) - z(x+\tau)]^2\} = 2[R(0) - R(\tau)] = K\tau^{(4-2D)} \tag{14}$$

where $R(\tau)$ is the autocorrelation function (ACF), which will be discussed later, and

$$K = \frac{\pi G^{2D-2}}{2\Gamma(5-2D)\sin[(2-D)\pi]} \tag{15}$$

The autocorrelation function and the structure function can be related to the spectral density by using the following equations:

$$R(\tau) = \int_0^\infty P(\omega)\cos(\omega\tau)d\omega \tag{16}$$

$$S(\tau) = 2\int_0^\infty P(\omega)[1-\cos(\omega\tau)]d\omega \tag{17}$$

Some people believed that the W-M function can be extended into two dimensions. Ausloos and Berman [31] tried to extend it using the following function:

$$z(x,y) = L\left(\frac{G}{L}\right)^{(D-2)}\left(\frac{\ln\gamma}{M}\right)^{1/2}\sum_{m=1}^{M}\sum_{n=1}^{n'_{\max}}\gamma^{(D-2)n} \times\left\{\cos\phi_{m,n} - \cos\left[\frac{2\pi\gamma^n(x^2+y^2)^{1/2}}{L}\times\cos\left(\tan^{-1}\left(\frac{x}{y}\right)-\frac{\pi m}{M}\right)+\phi_{m,n}\right]\right\} \tag{18}$$

where $2<D\leq 3$, $n'_{\max} = \mathrm{int}\left(\frac{\log(L/\Delta)}{\log\gamma}\right)$ is the maximum frequency level, M is the number of superposed ridges used to construct the surface and $\phi_{m,n}$ is a random variable representing phase.

Whereas, Wu [32] pointed out that by using this equation, the spectrum density function $P(\omega) = P\left(\sqrt{\omega_x^2 + \omega_y^2}\right)$ of a obtained surface cannot hold for all (ω_x,ω_y), so Ausloos and Berman version of the W-M function cannot be used in two dimension of surfaces with confidence.

1.6 Relationship between statistical parameters and fractal parameters

Majumdar and Tien [24] found that for fractal surfaces, the relationship between the statistical parameters and the fractal parameters are:

$$R_q^2 = \frac{G^{2(D-1)}}{(4-2D)}\left(\frac{1}{\omega_l^{(4-2D)}} - \frac{1}{\omega_h^{(4-2D)}}\right) \tag{19}$$

$$\left(\frac{dy}{dx}\right)^2 = \frac{G^{2(D-1)}}{(2D-2)}\left(\omega_h^{2D-2} - \omega_l^{2D-2}\right) \tag{20}$$

$$\left(\frac{d^2y}{dx^2}\right)^2 = \frac{G^{2(D-1)}}{2D}\left(\omega_h^{2D} - \omega_l^{2D}\right) \tag{21}$$

$$\omega_l = \frac{\pi}{L} \tag{22}$$

$$\omega_h = \frac{\pi}{s} \tag{23}$$

where ω_l is the lower wave number limit, ω_h is the higher wave number limit, L is sampling

length and *s* is the sampling resolution, $(\frac{dy}{dx})^2$ is the mean square slope and $(\frac{d^2y}{dx^2})^2$ is the mean square curvature. Eq. (19) will be used in later chapter 2 to calculate the *G* values in the experiment.

Sayles and Thomas [33] found that the statistical parameters can be expressed by the structure function and fractal dimension:

$$R_q^2 = R(0) \tag{24}$$

$$(\frac{dy}{dx})^2 = \frac{2}{x^2}[R(0) - R(x)] = Kx^{2-2D} \tag{25}$$

$$(\frac{d^2y}{dx^2})^2 = \frac{2}{x^4}[3R(0) - 4R(x) + R(2x)] = (4 - 2^{4-2D})Kx^{-2D} \tag{26}$$

After comparing with Eqs. (20) and (21), Wu [34] found that Eqs. (25) and (26) are more suitable for the calculation of these statistical parameters.

1.7 Goal of the work

The goal of this work is to analyze the structure of roughness over multiple scales with respect to current fractal and multi-scale techniques. As we know, in characterizing fractal geometry, the fractal dimension (*D*) is a very popular parameter but its usefulness in describing real surfaces is questionable. Four different methods are employed to calculate the fractal dimension (*D*) of various surfaces. The results of these methods are then compared and discussed. And the applicability of the one dimension W-M function used for generating and describing real rough surfaces is also evaluated and analyzed.

Chapter 2

2 Experiment and methodology

2.1 Experiment

2.1.1 Preprocessing of surface data

A Veeco Dektak 150 surface profilometer (scan length=5000μm, scan duration=0.16 sec, 5000 points, tip radius=2.5μm, vertical resolution<1nm, lateral resolution = 1μm/sample) (see Figure 7) was used to measure the surfaces with various finishes of a standard reference surface (S-22 Microfinish Comparator Surface Finish Scale as shown in Figure 8).

In this work, six different surfaces were measured which are classified as 63G, 63M, 63P, 2L, 4L and 8L, here G(ground), M(milled), P(profiled) and L(lapped) represent different ways to process the surfaces. After measuring the surfaces with the profilometer, six surface profile data sets were obtained, and then a fitted line needed to be obtained by fitting the data between the point position and the point height. Subtracting the fitted value from the measured data, the leveled surface profile data can be obtained to help calculate the precise parameters which estimate the differences of diverse rough surfaces. Figure 9 shows an example surface profile after leveling the surface profile data (the leveled profiles for the other five rough surfaces are in the Appendices).

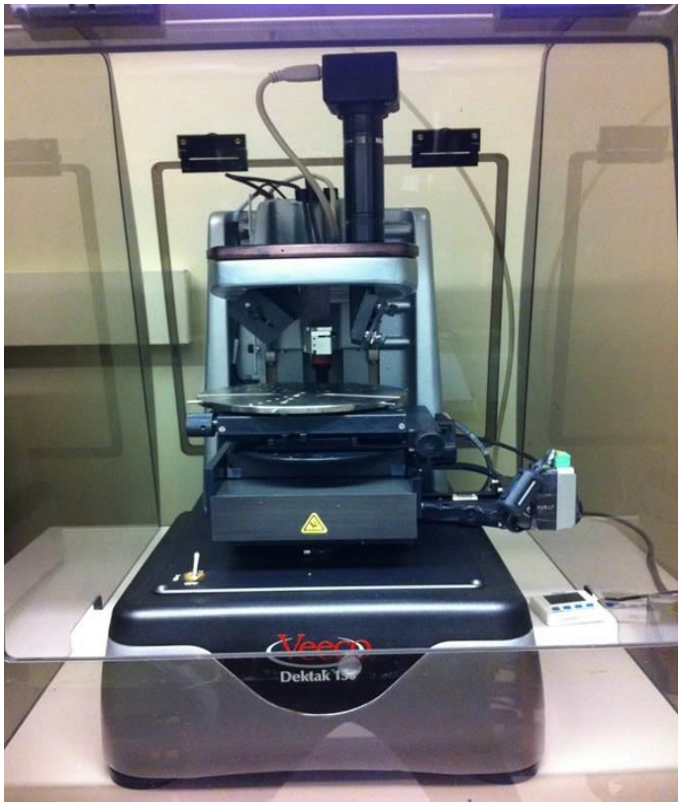

Figure 7: Profilometer used in the experiment

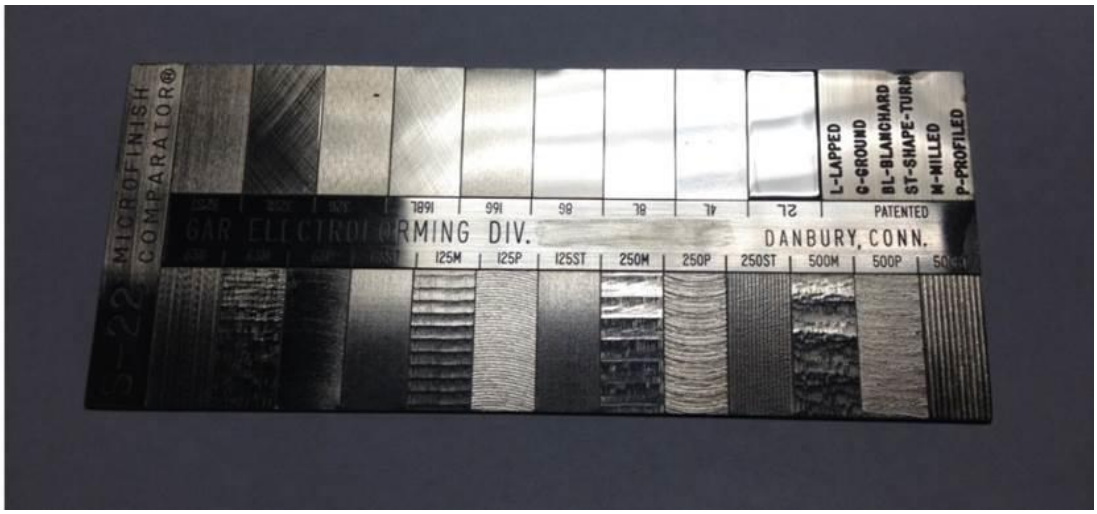

Figure 8: Standard reference surface

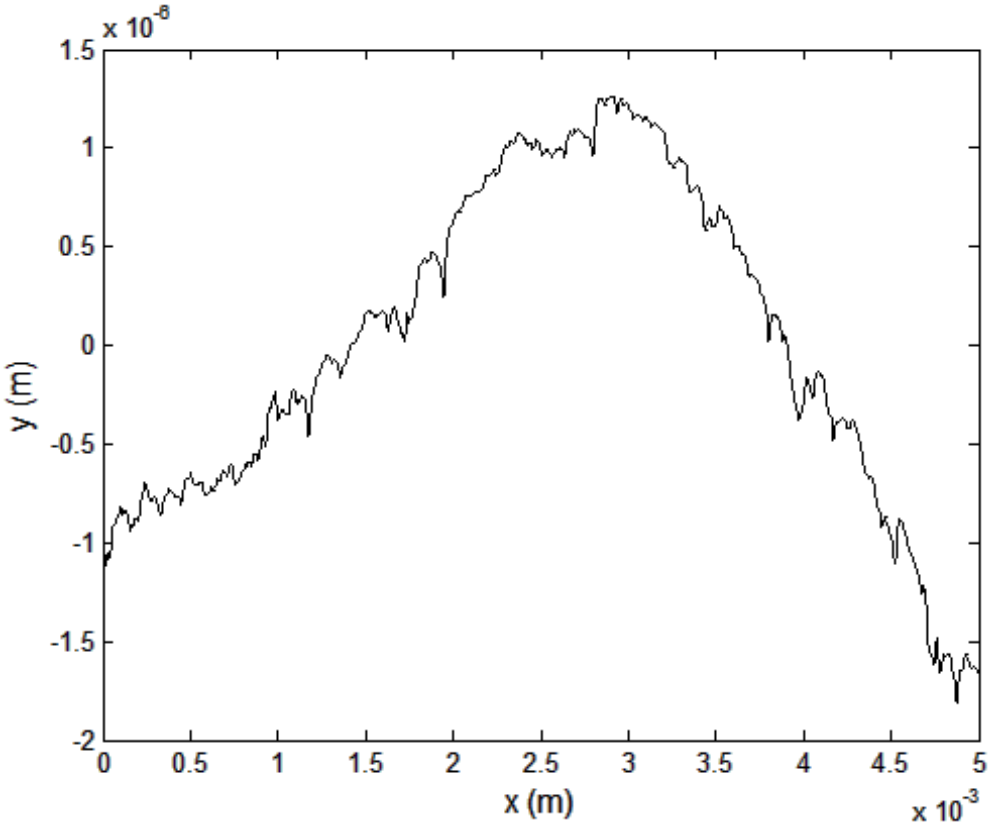

Figure 9: 8L Rough surface profile after leveling

Rough surfaces are multi-scale in nature, which means surfaces usually have scales of roughness that span from the atomic scale to the macro scale (see Figure 10). Archard [35] was the first man who developed the initial multi-scale model that can be described as "protuberances on protuberances". However, because of its unrealistic surface structure (i.e. it used spheres stacked on spheres), this model cannot be practically used on a real rough surface [36].

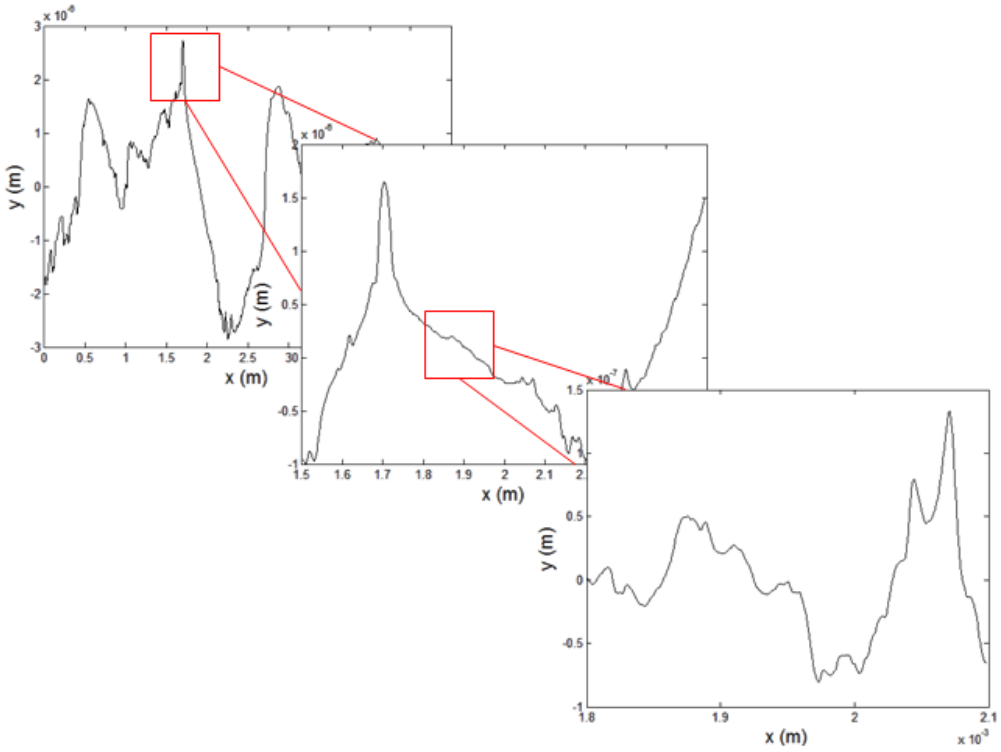

Figure 10: Multi-scale nature of rough surfaces

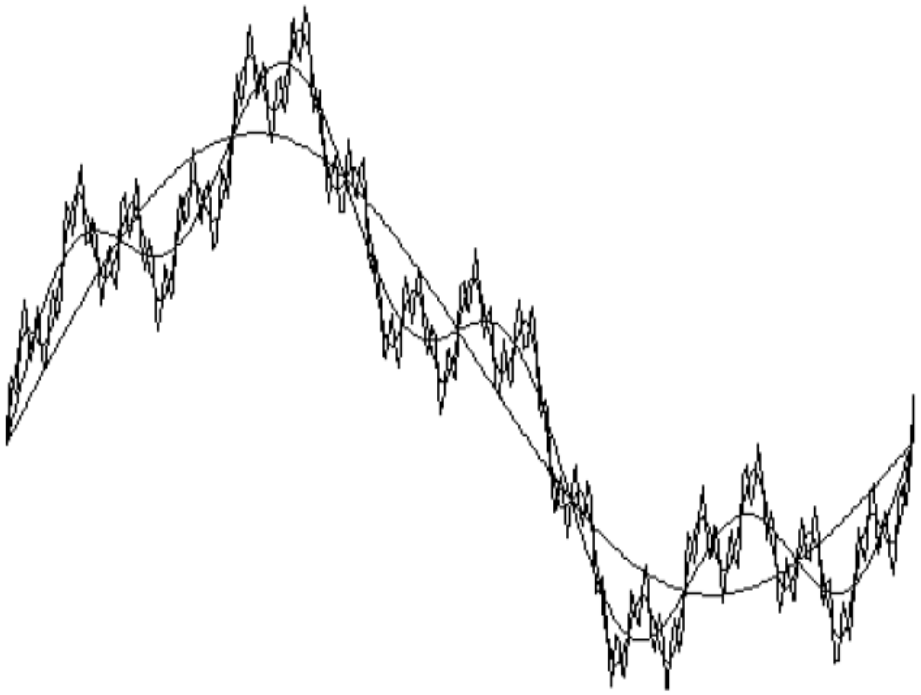

A Simplified Model of Multi-scale Electrical Contact Resistance and Comparison to Existing Closed Form Models

Figure 11: Multi-scale surface profile [37]

For now, another multi-scale model is used which can simplify the complex surface structure by superimposing many sine waves (Figure 11). Each wave represents a different scale of roughness. By using the multi-scale model the assumption of self-affinity imposed by fractal mathematics can be alleviated and how the mechanics are considered is improved [37].

Multi-scale rough surface profiles can be characterized using two different types of mathematical series – arithmetic series and geometric series. Arithmetic series are the series for which every term is computed from the previous one by adding or subtracting a constant. While geometric series are the sum of a sequence in which a constant ratio is held between the continuous terms. Geometric series are the simplest example of an infinite series with a finite sum, and the Grandi's series ($1 - 1 + 1 - 1 + \cdots$) is a specific geometric series. The Fourier series is an example of an arithmetic series and will be used to characterize the rough surfaces in this work in addition to geometric fractal series.

These two series are used to compute the relationship between the amplitude (Δ) and wavelength (λ). Similarly, the connection between the asperity aspect ratio (B), which indicates the ratio of the amplitude (Δ) of the sinusoidal surface at a scale to the wavelength (λ) of that scale, and the wavelength (λ) is also determined using the same method.

For a self-similar rough surface, the relationship between the aspect ratio and the wavelength is a constant as the sinusoidal geometry is replicated exactly at each scale. If B is plotted verse λ, for a self-similar surface, this results in a straight horizontal line. However, for a self-affine rough surface, the sinusoidal features are distorted from one scale to the next in a

predictable monotonic trend. Then if B is plotted verse λ, the line will have a slope. For W-M function generated surfaces, the slope will be negative.

Based on the two different types of mathematical series, the measured rough surfaces were decomposed into Fourier series (using the fast Fourier transform (FFT)) and into geometric series using an equation given as:

$$z(x) = \sum_{n=n_1}^{\infty} A \sin(2\pi x l^n + \phi_n) \tag{27}$$

where A describes the amplitude of each scaled sinusoidal wave and l is the self-similar fractal scaling parameter, it controls the 'distance' between the scales in the geometric series and can vary just like γ in the W-M function. When l=1.5, like γ=1.5 in the W-M function, it can provide adequate surface separation between scales [38]. In the current work, l was varied from a small value of 1.2 to a large value 1.8 (as shown in Figure 12 and Figure 13). After implementing the arithmetic and geometric scaling, the resulting amplitude (Δ) versus wavelength (λ) for rough surfaces are plotted in a log-log curve and shown in Figure 12 (two examples are shown for surfaces 8L and 63P). Then B versus λ for the rough surfaces in this experiment can also be obtained (see Figure 13). The plots for the other measured rough surfaces about these two relationships are in the Appendices.

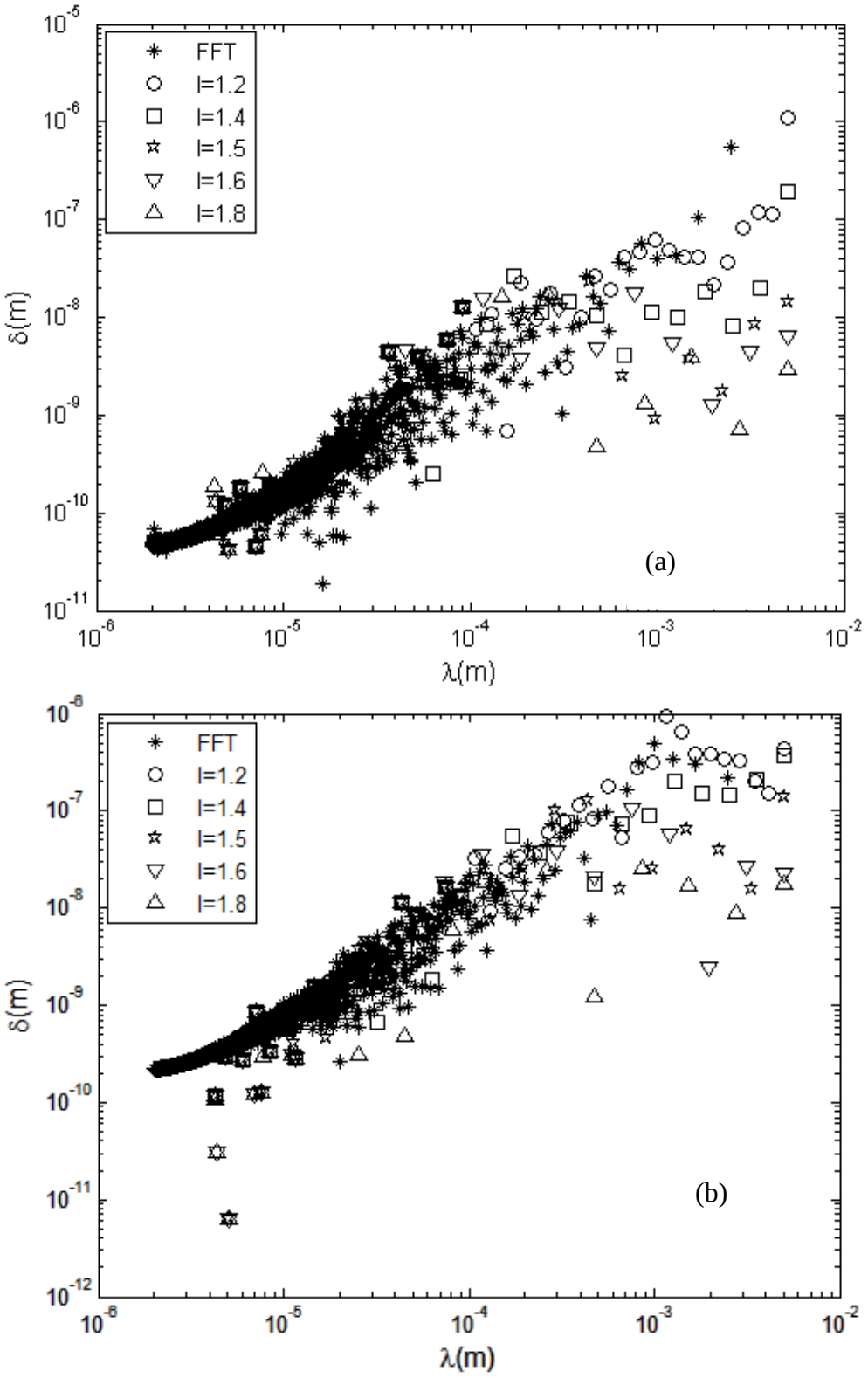

Figure 12: Δ vs. λ for measured rough surfaces
(a) 8L rough surface; (b) 63P rough surface

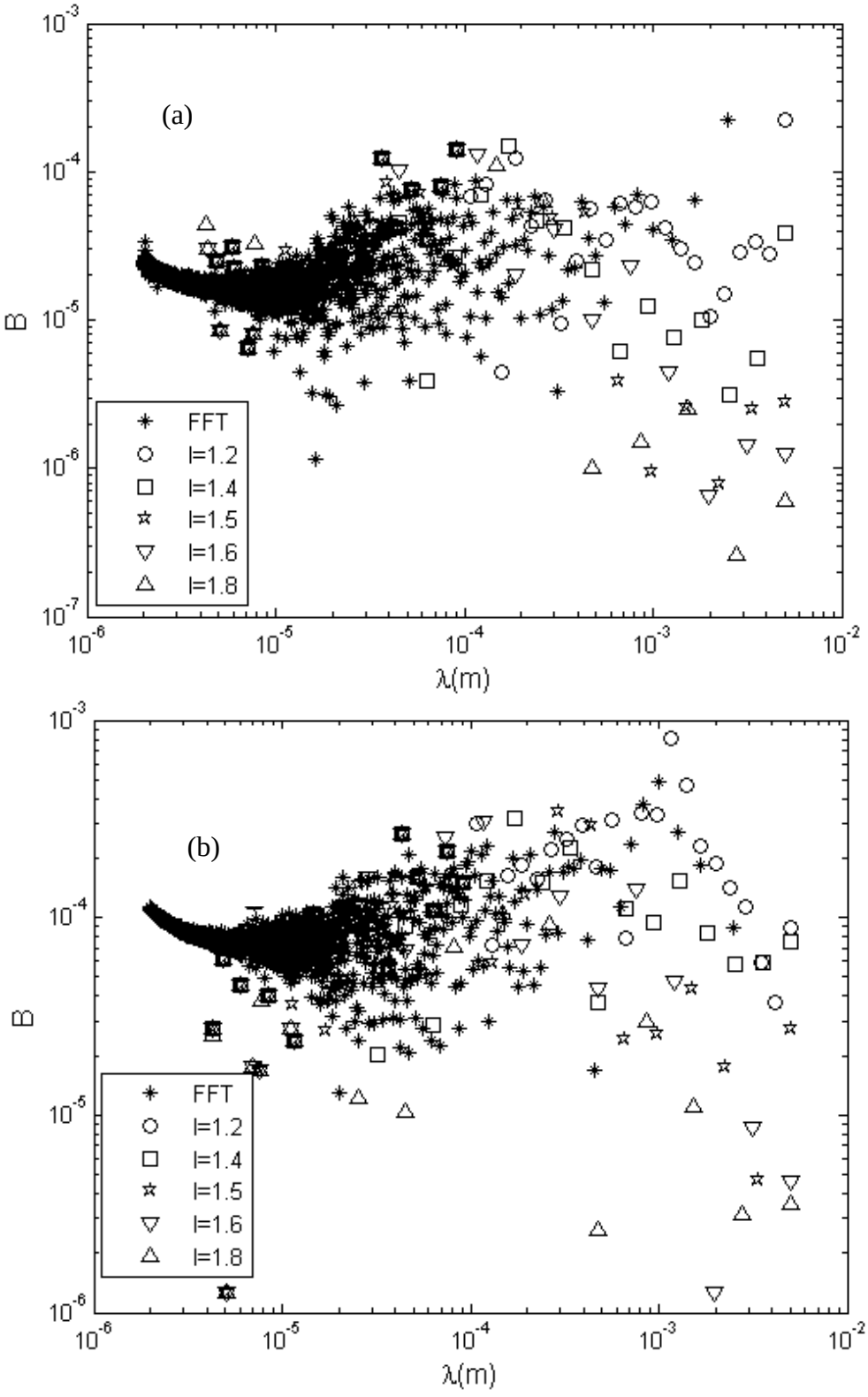

Figure 13: *B* vs. λ for measured rough surfaces
(a) 8L rough surface; (b) 63G rough surface

Interestingly, not only the 8L and 63P rough surfaces, but all these rough surfaces shown in this experiment appeared to have the same line and follow the same trend as shown in Figure 12 and Figure 13. The slope in Figure 12 is nearly one which means as the scale of the surface feature increases, their relative wavelength increases, and the slope between B and λ are all approximately zero with the meaning of that the aspect ratio is nominally constant for all scales and series, like the same conclusion in [38]. In addition, the variation of B appears to be less than four orders of magnitude, the average B values for all the rough surfaces are also calculated and shown in 2.1.4.

Later, the degree of self-similar of all the measured surfaces will also be characterized by finding the average slope, $dB/d\lambda$. Since the spectrum nominally stays the same, this also suggests that the surfaces possess a continuous spectrum. They also show a random distribution around the average B value.

2.1.2 Different methods in calculating the fractal dimension, *D*

(1) Methods description

The fractal dimension (D) is a popular and arguably important parameter in describing fractal rough surfaces, many well-known methods are used in the research of it, e.g. the classic Richardson plot [39], the compass method [40, 41] and the variogram analysis [25, 42]. In the current work, four different methods were adopted to calculate D: the Fourier analysis [28], the roughness-length method [43], the box-counting method [44] and the power spectrum method

[42, 45].

a) Fourier analysis

In analyzing the fractal profile data, Russ [28] used the Fourier analysis, which is based on the Fourier series, to plot the relationship between the logarithm of the magnitude squared and the logarithm of the frequency after conducting FFT for the profile data (as shown in Figure 17(a)). It shows a linear variation between these two parameters, and the slope of the line, β, is related to the fractal dimension, D, as:

$$D = \frac{(4 + \beta)}{2} \tag{28}$$

Russ [28] also emphasized that this method is most often applied to time-varying signals and can be applied to self-affine as well as self-similar data sets as it provides one of the most direct, easily understood and powerful techniques for the analysis of fractal profiles and surfaces.

b) Roughness-length method

In this method, the profile roughness is measured as the root-mean-square value of the residual on a linear trend fitted to the sample points in a window of length, w, [43, 46] (see Figure 14). Then, the root-mean-square roughness including the effect of window length by altering Eq. (3) is calculated:

$$R_q = \frac{1}{n_w} \sum_{i=1}^{n_w} \sqrt{\frac{1}{m_i - 2} \sum_{j \in w_i} (y_j - \bar{y})^2} \tag{29}$$

where n_w is the total number of data points in a window of length w, y_j is the surface height or residual of the trend and $\bar{y}$ is the mean height or residual in the ith window w_i , m_i is the number of points in window w_i.

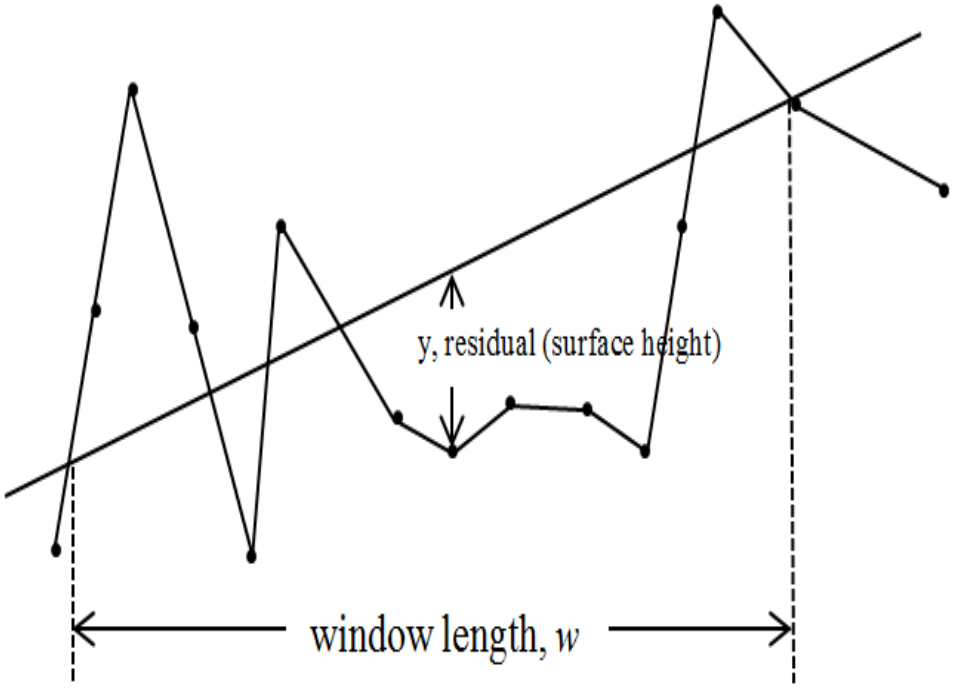

Figure 14: Computational process of roughness-length method

The RMS roughness, R_q, is then plotted as a function of the window length, w, on a log-log scale. The slope of the log-log plot between RMS and window length, w, is H, which is called the Hurst exponent [16]. It is directly related to the fractal dimension (D):

$$D=2-H \tag{30}$$

In this equation, the value of the Hurst exponent lies between 0 and 1, when the Hurst exponent equals to 0.5 (i.e. fractal dimension is 1.5), it indicates the series is a geometric random walk (fractional Brownian motion).

The roughness-length method is a widely used method and it can also be extended to 2D and 3D situations. In 1988, Wilson and Dominic [47] first used this method to evaluate the fractal characteristics of topography and structure in the study area of the Appalachian mountains. Kulatilake and Um [48] applied this method for calculating fractal dimension of 2D profiles. By using 3D laser scan data of rock mass discontinuity surfaces, Fardin [49] originally proposed this method to calculate the fractal dimension of 3D surfaces.

c) Box-counting method

Schroeder [50] is the first man who proposed the formal definition of box-counting method. In this method, the surface profile is first overlapped with a grid or an array of identical boxes. Then the box size is changed by the power of 2 and the box number needed to cover the surface profile is counted for each size of box. Its basic principle to estimate the D value is based on the concept of self-similarity [44]. The D value of a bounded set in Euclidean n-space is defined as

$$D = \lim_{r \to 0} \frac{\log(N_r)}{\log(1/r)} \tag{31}$$

where r is the side length of box. N_r is the least number of the boxes required to cover the set and N_r varies from $1/r$ for a smooth surface profile to $1/r^2$ for a rough surface profile. By using the box-counting method, the values were plotted on a log-log curve and D was exactly the slope of the fitted line.

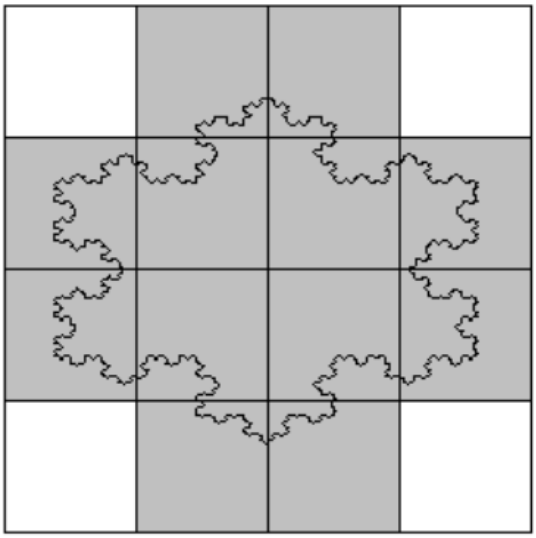

r=4 log(1/4)=-0.602
N_r=12 log(12)=1.079

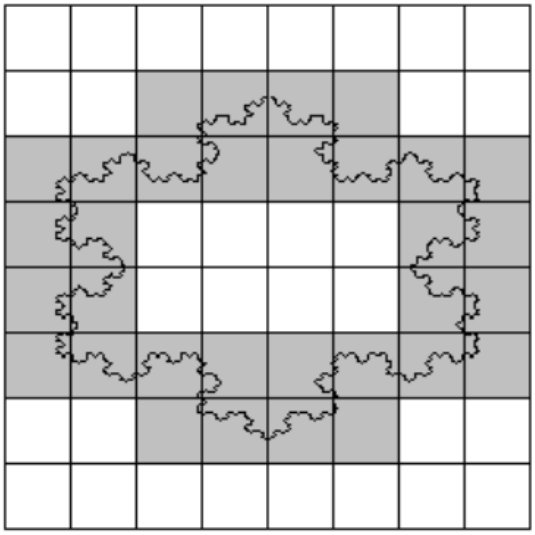

r=2 log(1/2)=-0.301
N_r=32 log(32)=1.505

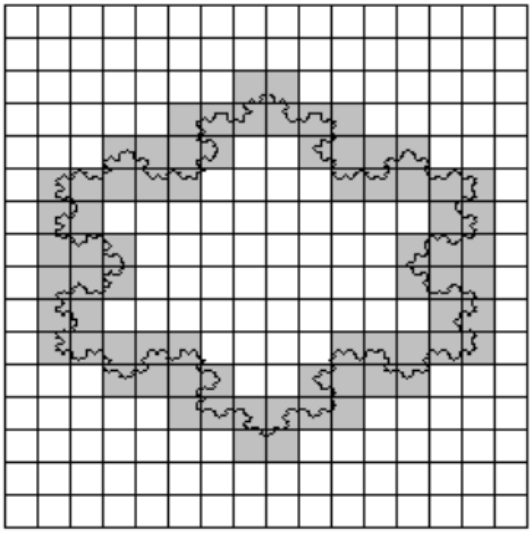

r=1 log(1)=0
N_r=71 log(71)=1.851

Closed Contour Fractal Dimension Estimation by the Fourier Transform [51]

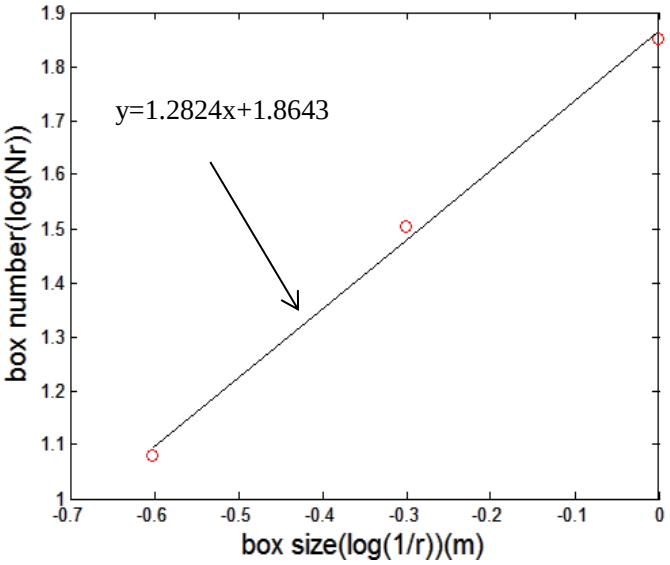

The slope of fitted line is 1.2824, so the fractal dimension of the Koch snowflake is 1.2824.

Figure 15: Process of box-counting method

The whole process of box-counting method is illustrated in Figure 15 [51]. After calculating all the logarithmic values of the box size and box number, a line was fitted and the slope of the fitting equation (i.e. the fractal dimension) was obtained. Since the box size is changed as a power of two, the boxes will rapidly cover the data with few points being shown in the log-log curve [52] and the box size will be evenly spaced in the log-log plot (see Figure 17).

Note again that this method is used unequivocally for self-similar geometries. Only if the size of the box is small with respect to the vertical range of the profile data can this method be used for self-affine fractals [41, 53].

d) Power spectrum method

The power spectrum method is a method that needs much more data processing than the other methods, and was developed by Blackman and Turkey [54] based on the Wiener-Khinchin

theorem. In this method, the autocorrelation function (ACF) of the surface profile (see Eq. 32), which contains useful spatial information and is the most popular way to represent spatial variation [4], was calculated first (see Figure 16).

$$R(\tau) = \frac{1}{(n-\tau)R_q^{\,2}} \sum_{t=1}^{n-\tau} (y(t) - \mu)(y(\tau + t) - \mu) \tag{32}$$

where τ is the changing distance.

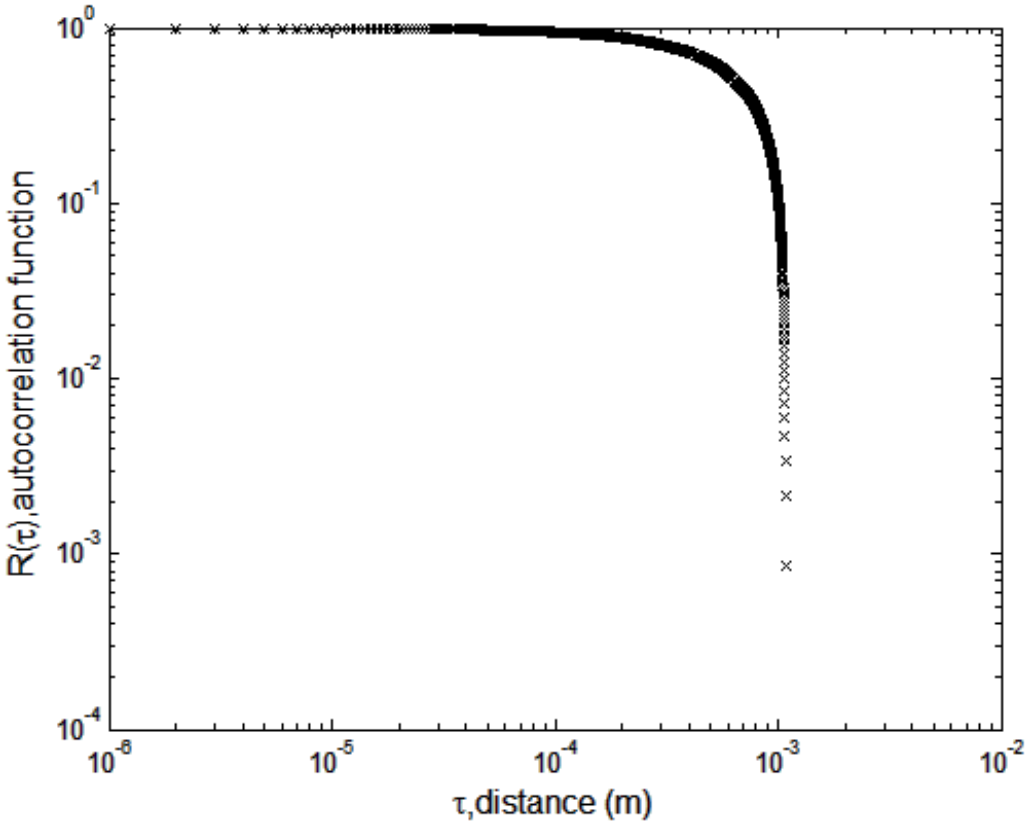

Figure 16: Autocorrelation function for 8L rough surface

The FFT algorithm then was implemented on the autocorrelation function to obtain a power spectrum, which describes how the power of a signal or time series is distributed with frequency [42]:

$$S(f) = cf^{-\beta} \qquad 1 \leq \beta < 3 \tag{33}$$

where *f* represents the spatial frequency and *c* is the scaling parameter.

Taking the logarithm on both sides of Eq. (33), the slope of the fitted line for the power spectrum on a log-log plot can be used to estimate the β value. From β, the D value can be calculated according to Eq. (34):

$$D = \frac{5 - \beta}{2} \tag{34}$$

(2) Results and discussion

Examples of these four methods of calculating *D* for surface 8L are showed in Figure 17 (the plots for the other measured rough surfaces are in the Appendices). Comparing these four different methods, the values calculated from the box-counting method had less variation and followed a linear trend more than when using the other three methods (which results in a better fit). Therefore, the value of *D* from the box-counting method is less affected by the resolution or length of the surface data and is less ambiguous in evaluating the value of *D*.

However, the box-counting method is designed for self-similar surfaces, and as will be shown in this chapter categorizes many surfaces. Here D_0 represents the fractal dimension with the Fourier analysis, D_1 corresponds to the fractal dimension calculated using the roughness-length method，D_2 is the dimension calculated using the box-counting method and D_3 is from the power spectrum method. The resulting values of fractal dimension, *D*, for all measured surfaces are listed in Table 1.

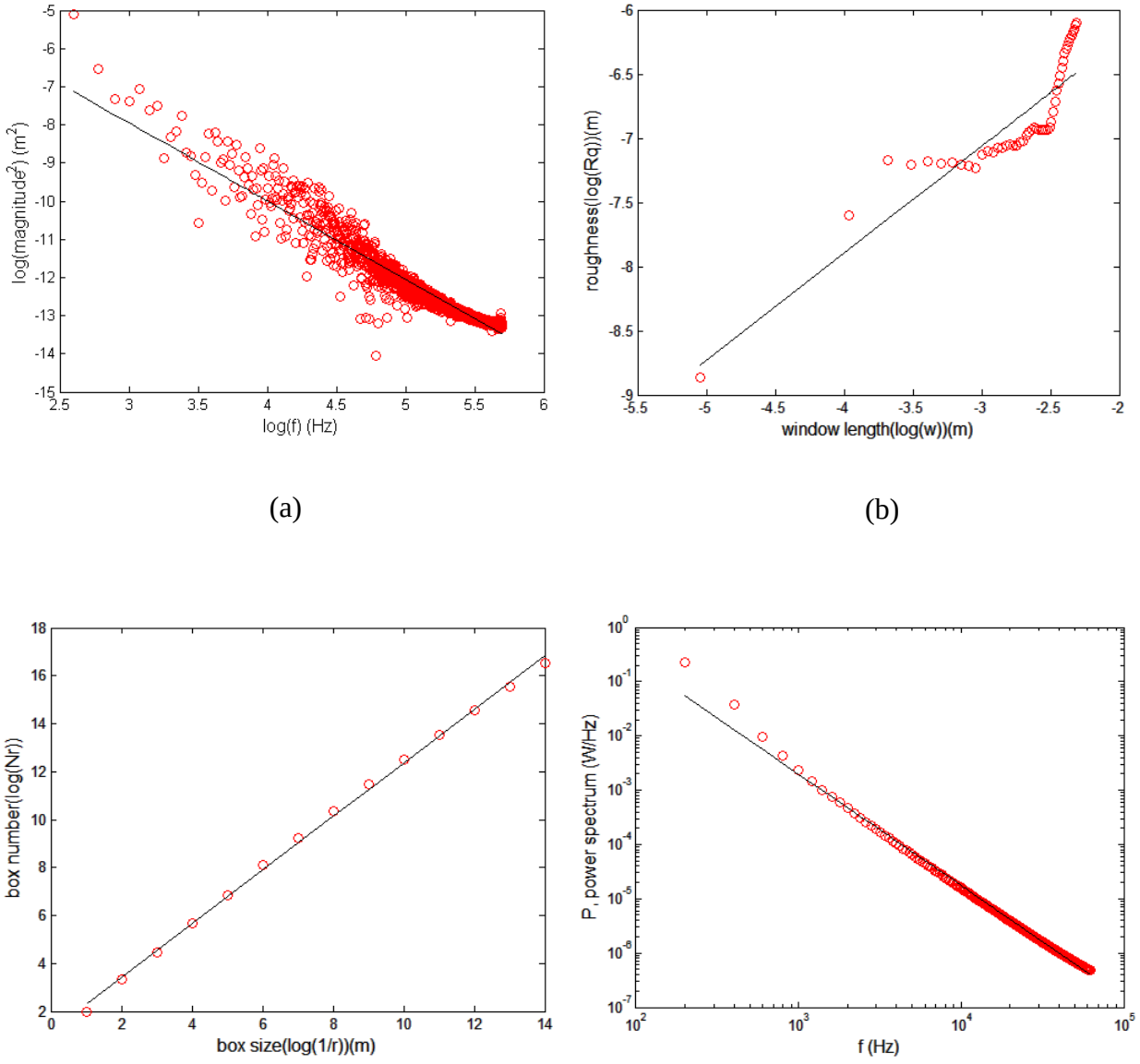

(a) (b)

(c) (d)

Figure 17: The results of four different ways in calculating *D* (choosing 8L surface as an example). (a) Fourier analysis; (b) Roughness-length method; (c) Box-counting method; (d) Power spectrum method
The lines are fitted to the points calculated from the real surfaces

Comparing the fractal dimension values in Table 1, the values of D_0, D_1 and D_2 are much smaller than the D_3 values from the power spectrum method. D_0 have the minimum fluctuation around unity and has some values less than one. The D_2 values are all larger than 1, but the differences with D_0 and D_1 are not so obvious. D_3 has the largest values and all the values are around 1.5 and sometimes D=1.5 indicates the fractional Brownian motion. Since D_2 is relatively close to D_1 and D_0 and unity, it might indicate that the surfaces are nominally self-similar.

It is obvious that some values of D_0 and D_1 are less than one which suggests that the results stay in somewhere between the dimension of a point (D=0) and the dimension of a line (D=1). Since the fractal dimension is a measure of the "space-filling" ability of a system [55], the fractal dimension of a straight line will be less than one when holes or spaces exit in it. A famous example of the fractal dimension less than one is the Cantor dust [56], which also be called Cantor set, it has the fractal dimension of log2/log3 (approximately 0.631).

2.1.3 Discussion of *G* value

In characterizing a multi-scale surface, the fractal roughness parameter (G) is another scale-invariant parameter. It was calculated using Eq. (19) based on the W-M function, which is also listed in Table 1. It was found that G varies widely over many orders of magnitude between the surfaces whose roughness (R_q and R_a which will be shown in Table 2) varies by less than an order of magnitude. To explain this 17 order of magnitude spread in G, the relationship between D and G was also investigated in the work.

Table 1: *D* and *G* values for measured rough surfaces

surface types	D_0	D_1	D_2	D_3	G ($m^{-(D-1)}$)
2L	1.0514	0.838	1.1188	1.4733	2.00e-29
4L	0.8272	0.953	1.1024	1.4740	1.64e-32
8L	0.9766	1.17	1.1192	1.4732	4.19e-30
63G	1.0415	1.25	1.1269	1.4985	2.94e-27
63M	0.9801	1.19	1.1397	1.5018	1.22e-24
63P	0.8380	1.63	1.2407	1.5311	3.36e-15

Note: D_0-Fourier analysis; D_1-Roughness-length method; D_2-Box-counting method; D_3-Power-spectrum method.

The *D* value was changed from 1 to 2 using an increment of 0.01 and the initial R_q value is from 8L surface, by using the Eq. (19) the corresponding *G* value was calculated and the final results are showed in Figure 18, in which the black line is the fitted line for the scattered values.

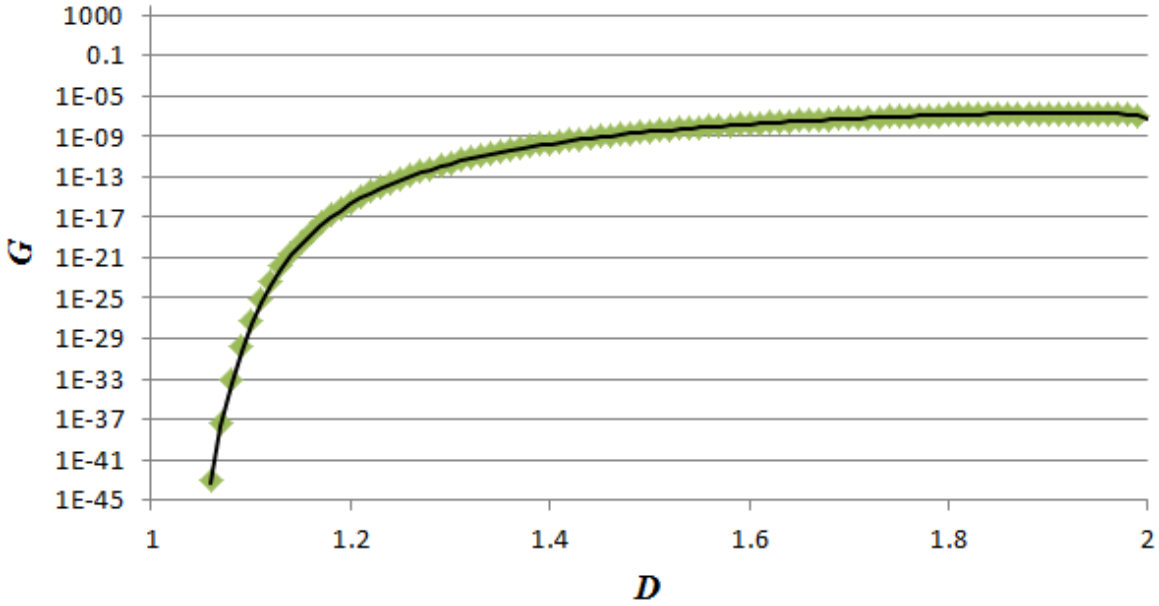

Figure 18: Relationship between *D* and *G*

In Figure 18, it appears that the *G* values are non-linearly proportional to the *D* values or vice-versa. Since the moving average method was used when fitted the data, it can be predicted

from the fitted line that G approaches an asymptotic value when D tends to 2, and when D approaches 1, G becomes infinitesimal. The data in Table 1 conforms to this trend. Therefore, it may be difficult to use G as a characterizing parameter of the rough surfaces.

2.1.4 Parameters calculated in the experiment

Additionally, several statistical and multi-scale roughness parameters are also calculated, such as B_{ave}, $(dB/d\lambda)_{ave}$, R_a, R_q, SK and K. These parameters are computed as references to provide further insight into the comparison of different kinds of rough surfaces. They are all listed in Table 2.

Since the degree of self-similarity might be quantified by calculating the slope of B versus λ, the average slopes (i.e. $(dB/d\lambda)_{ave}$) were calculated and listed in Table 2. In addition, the value of $dB/d\lambda$ for varying l values and the FFT method which are shown in Figures 12 and 13 are listed in Table 3. When $(dB/d\lambda)_{ave}$ equals zero everywhere, the measured rough surfaces could be said to be perfectly self-similar. For actual rough surfaces, the slopes will never be exactly zero. Due to the trend of all the $(dB/d\lambda)_{ave}$ values and the values listed in Table 3 being relatively close to zero, all the measured surfaces tended to be nominally self-similar. It can also be found from Table 3 that not all the values are negative ($dB/d\lambda<0$ and will be discussed in section 3.2), which would suggests that the surfaces do not exactly follow the self-affine structure of the W-M fractal.

Table 2: Parameters calculated in the experiment

surface types	R_q (m)	R_a (m)	m_2	m_4	SK	k	B_{ave}	σ_B (m)	$(dB/d\lambda)_{ave}$ (m^{-1})
2L	1.01e-06	8.76e-07	7.18e-05	-0.824	-0.538	1.98	2.14e-05	1.08e-05	0.0079
4L	1.28e-06	1.10e-06	6.10e-05	-0.356	-0.631	2.14	3.94e-05	1.68e-05	0.0100
8L	8.16e-07	7.02e-07	-9.87e-05	-0.592	-0.161	1.99	3.12e-05	1.01e-05	0.0045
63G	1.17e-06	9.56e-07	4.40e-04	-3.10	-0.507	2.59	9.90e-05	4.60e-05	0.0053
63M	1.36e-06	1.14e-06	-3.53e-04	2.75	-0.174	2.21	1.11e-04	4.62e-05	0.0120
63P	2.03e-06	1.68e-06	1.52e-04	7.48	-0.349	2.36	2.91e-04	1.29e-04	-0.0060

Table 3: Values of *db/dλ* for varying *l* and FFT method

surface types	l=1.2	l=1.4	l=1.5	l=1.6	l=1.8	FFT
2L	0.0169	-0.0028	-0.0067	-0.0074	-0.0077	0.0549
4L	0.0185	-0.0079	-0.0133	-0.0124	-0.0128	0.0907
8L	0.0083	-0.0062	-0.0098	-0.0095	-0.0082	0.0549
63G	-0.0019	-0.0066	-0.0200	-0.0181	-0.0218	0.0975
63M	-7.91e-04	-0.0125	-0.0211	-0.0199	-0.0246	0.1498
63P	-0.1095	-0.0622	-0.0630	-0.0689	-0.0579	0.3244

2.2 Bearing area curve

In the field of engineering and manufacturing, sometimes it is needed to estimate the area in contact between two rough surfaces, and then the rate of wear can be accessed. The bearing area curve (BAC), which was proposed by Abbott and Firestone [57], can give an indication of the rate of wear and how the asperity peaks are distributed. It can also help to understand the property of sealing area.

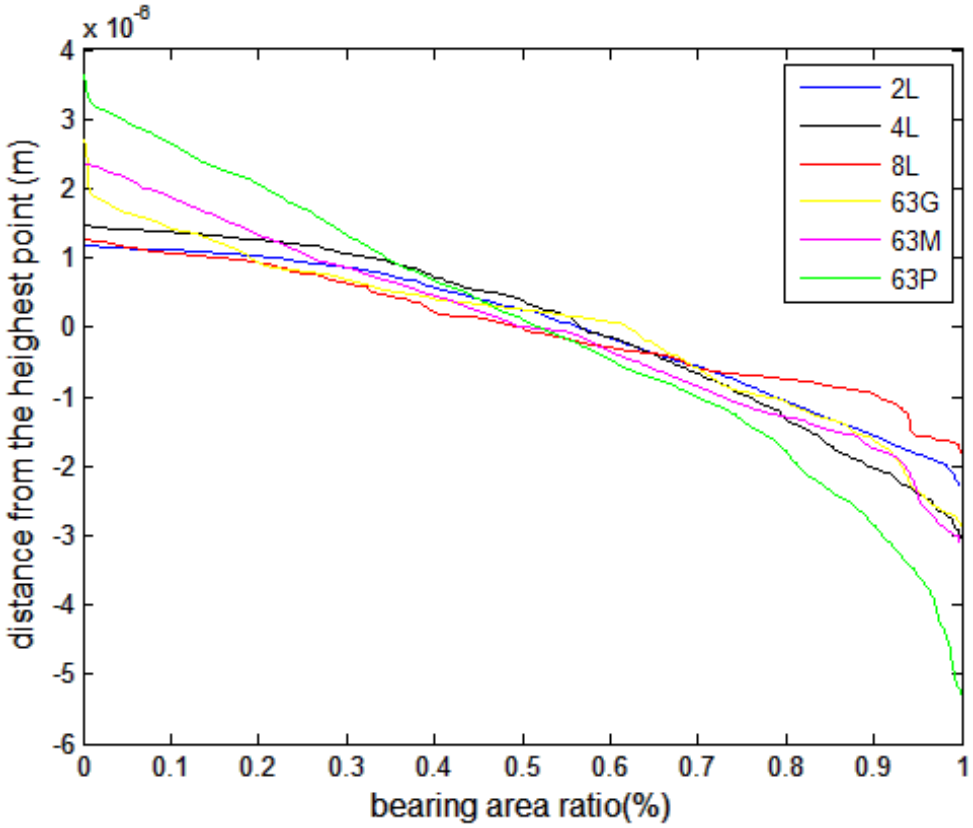

Figure 19: Bearing area curve for 8L surface

The curve could be established from a profile trace by drawing lines parallel to the datum and measuring the fraction of the line which lies within the profile [58], and the bearing area curve for a measured rough surface is shown in Figure 19. Mathematically, the bearing area curve is the cumulative form of the height distribution, and it can be calculated by integrating the profile trace [59].

Combining Table 2 and Figure 19, it can be found that at the initial height, much rougher surfaces have many peaks, so their bearing area ratio are much larger. The peaks of less rough surfaces can be worn out quickly because of fewer peaks they have. The less rough surfaces can become smooth surfaces much more easily than the rougher surfaces.

Specifically, if a height distribution of a surface profile is approximately a Gaussian distribution, the bearing area curve becomes the famous cumulative error function of classical statistics. Then at any height, the bearing area fraction relative to the mean line can be obtained by simple inspection of the tables [4].

Chapter 3

3 Generated W-M fractal rough surfaces

3.1 Surfaces generation based on the W-M function

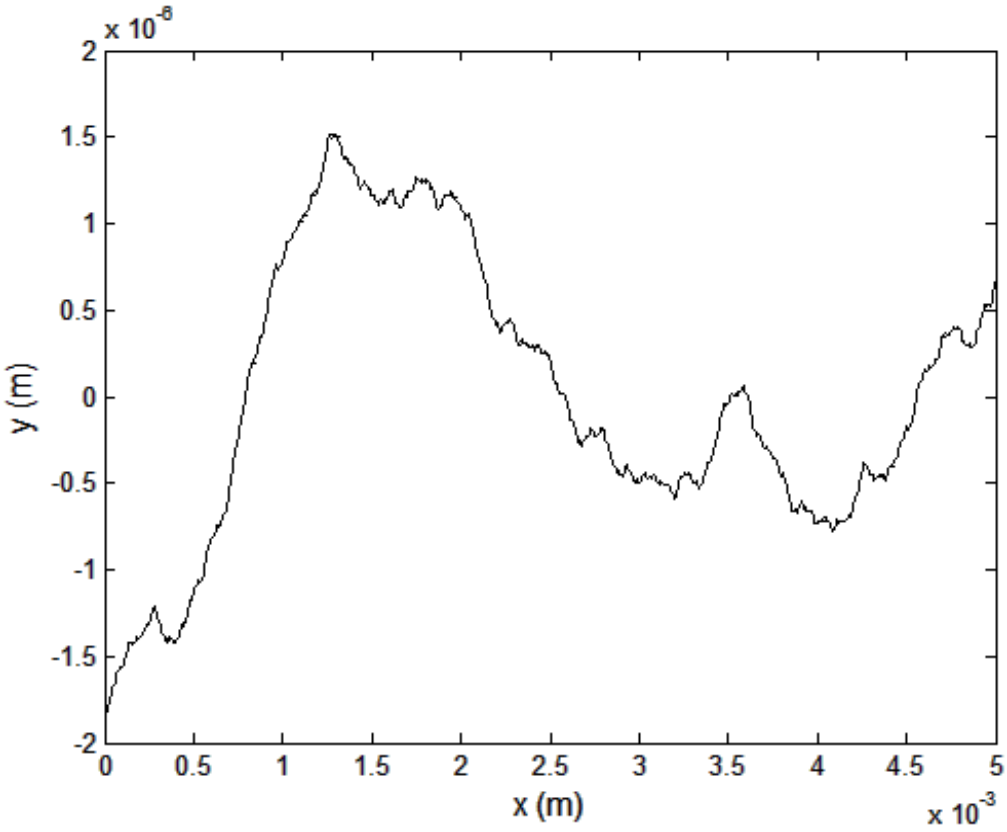

Figure 20: Generated 8L surface by using the W-M function

When the constants 'G', 'D', 'γ', 'n_1' and 'n_2' are known, then the surface profile can be determined from the W-M function (Eq. (12)) at any length scale. To test the applicability of the W-M function used for describing real rough surfaces, rough surfaces have been generated

according to the W-M function for each rough surface in Table 1. Since the results from the box-counting method appear to be more reliable, so D_2 is implemented in generating rough surfaces using the W-M function. And the corresponding G values for all rough surfaces were used to achieve a matching R_q between the original surfaces and generated surfaces (see Table 2). An example generated rough surface for 8L is shown in Figure 20 (the rough surface profiles for the other generated rough surfaces are in the Appendices).

3.2 Discussion of parameters in generated rough surfaces

According to the W-M function, the expression for the aspect ratio (B) is shown below:

$$B = \left(\frac{\Delta}{\lambda}\right) = \frac{G^{(D-1)}}{\gamma^{(1-D)n}} = G^{(D-1)}\gamma^{(D-1)n} \tag{35}$$

From the discussion in the last chapter, when the surface is a self-similar surface, B is supposed to be a constant. Based on Eq. (35), B varies with n, only when D=1 can B remain constant. So for a generated W-M surface profile, the D value must equal to one if rough surfaces are self-similar surfaces. As noted in the chapter 1, this relationship between D and self-similarity is not true for all fractals (i.e. a fractal surface in general could have a $D \neq 1$ but still be self-similar). That is an unnecessary restraint that is imposed by the W-M function.

Then four different methods introduced in section 2.1.2 were implemented in evaluating the values of the fractal dimension for all generated rough surfaces (the plots for all the generated rough surfaces are in the Appendices), and they are listed in Table 4. Other statistical roughness surface parameters (as in Table 2) were also computed. They are listed in Table 5.

Table 4: Fractal dimension values for generated rough surfaces

surface types	D_0	D_1	D_2	D_3
2L	1.0758	1.0330	1.1137	1.4737
4L	1.0870	1.1000	1.1009	1.4739
8L	1.0842	0.9672	1.1036	1.4870
63G	1.0724	1.2359	1.1136	1.4761
63M	1.0679	1.2533	1.1036	1.4879
63P	1.0754	1.1085	1.1530	1.4794

Note: D_0-Fourier analysis; D_1-Roughness-length method; D_2-Box-counting method; D_3-Power-spectrum method.

Table 5: Parameters calculated based on W-M function

surface types	R_q (m)	R_a (m)	m_2	m_4	SK	k	B_{ave}	σ_B (m)	$(dB/d\lambda)_{ave}$ (m^{-1})
2L	1.02e-06	8.46e-07	-3.55e-04	0.366	-0.6121	2.42	4.53e-05	3.16e-05	0.0851
4L	1.24e-06	1.02e-06	-4.47e-04	-1.18	-0.0988	2.25	5.72e-05	3.95e-05	0.0864
8L	8.11e-07	6.76e-07	-6.91e-05	-0.191	0.0366	2.21	4.03e-05	2.06e-05	0.0169
63G	1.16e-06	9.90e-07	3.68e-04	-0.102	-0.079	1.92	3.58e-05	2.47e-05	0.0071
63M	1.38e-06	1.14e-06	-6.18e-04	0.564	0.3254	2.60	6.11e-05	3.19e-05	0.0612
63P	2.06e-06	1.82e-06	-4.97e-04	-4.93	0.5527	1.84	5.13e-05	4.10e-05	0.0777

Again, in generating rough surfaces using the W-M function, D_2 in Table 1 was set as the inputted values. Comparing all fractal dimension values in Table 4 with the initial set values, D_3 are much greater than the inputted data, so the power spectrum method does not appear to be a reliable method for calculating the D value when the rough surfaces seem to be self-similar.

Simultaneously, the relationships Δ vs. λ and B vs. λ for these generated rough surfaces were also obtained and are shown in Figure 21 and Figure 22 separately (the plots for the other four generated rough surfaces are in the Appendices). Although all the trends appear to be in

accordance with the relationship found in the measured surfaces, there are many evenly spaced peaks in the trend. These peaks correspond to the discrete frequencies represented in the surface by the W-M function (Eq. (12)). Real surfaces do not display this trend because their spectrum is continuous. This is one reason the W-M function may not be very suitable for characterizing real surfaces or generating artificial surfaces. Table 6 shows the value of $dB/d\lambda$ with varying l values and the FFT method for the generated rough surfaces corresponding to Figure 22.

In addition, an analytical solution between λ and $dB/d\lambda$ for different D values is also derived according to Eq. (35):

$$\lambda = \frac{1}{\gamma^{n}} \tag{36}$$

After taking the logarithm in both side of Eq. (36), the obtained expression of n can be used in Eq. (35). Then Eq. (35) is rearranged as:

$$B = G^{(D-1)}\gamma^{(D-1)\cdot(-\frac{\ln\lambda}{\ln\gamma})} \tag{37}$$

The derivative of Eq. (37) with respect to λ is taken which is shown in Eq. (35). And the trend between λ and $dB/d\lambda$ based on this analytical solution is shown in Figure 23.

$$\frac{db}{d\lambda} = (1 - D)G^{(D-1)}\lambda^{-D} \tag{38}$$

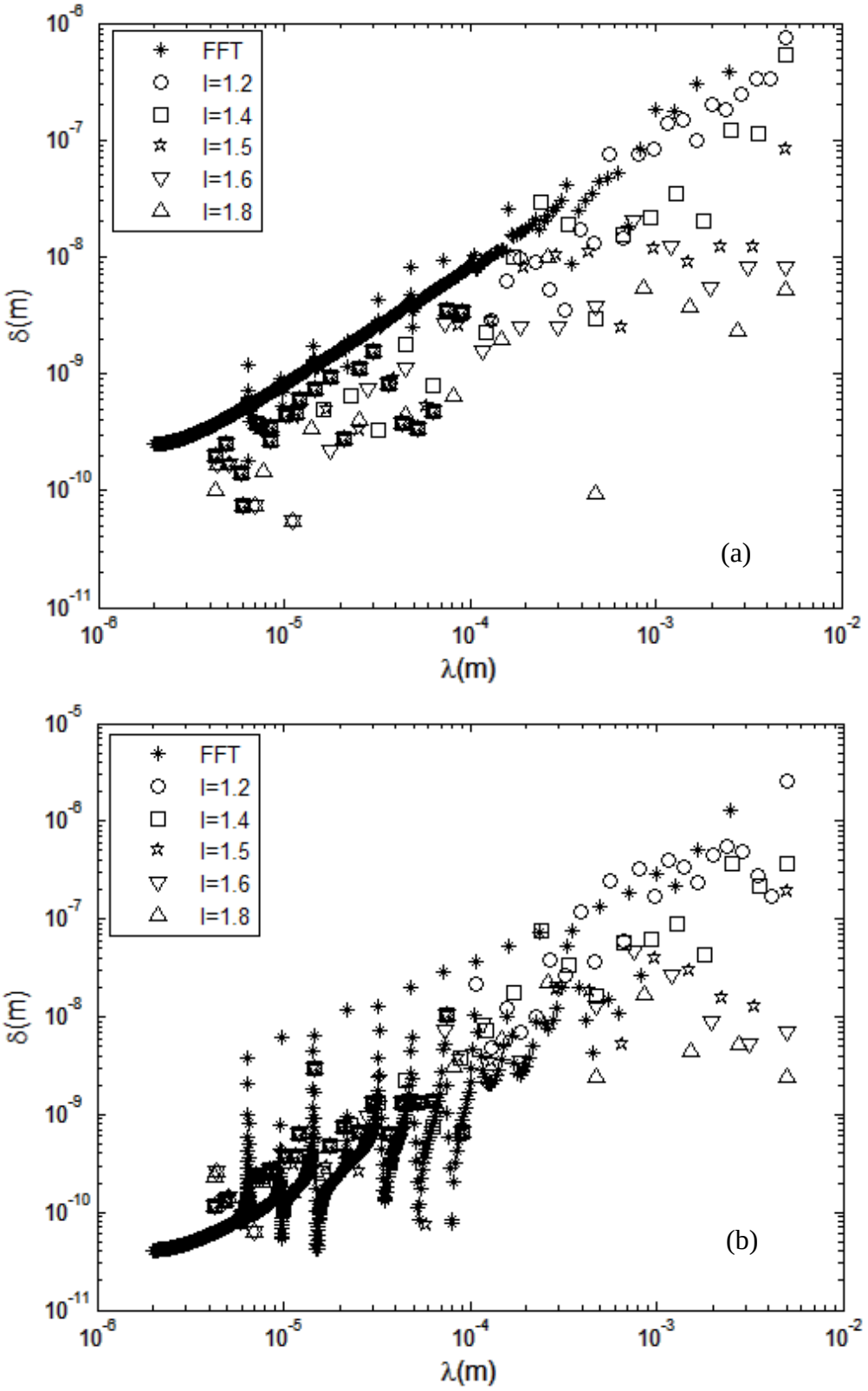

Figure 21: Δ vs. λ for the generated rough surfaces
(a) generated 8L surface; (b) generated 63P surface

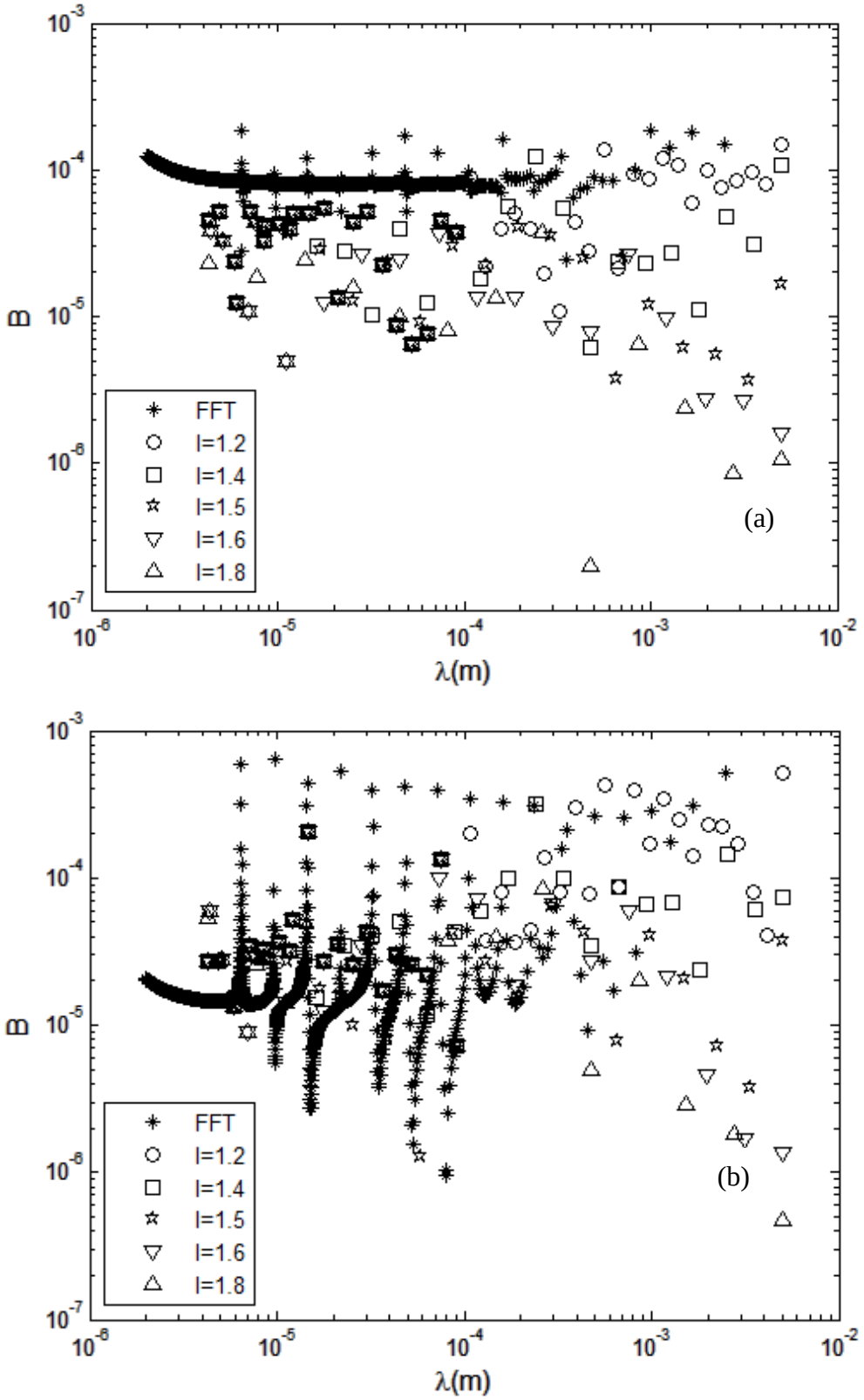

Figure 22: *B* vs. *λ* for the generated rough surfaces
(a) generated 8L surface; (b) generated 63P surface

Table 6: Values of *db/dλ* for different *l* and FFT method of generated surfaces

surface types	*l*=1.2	*l*=1.4	*l*=1.5	*l*=1.6	*l*=1.8	FFT
2L	0.0236	0.0070	-0.0073	-0.0074	-0.0082	0.0043
4L	0.0287	0.0099	-0.0089	-0.0101	-0.0110	0.0066
8L	0.0189	0.0070	-0.0068	-0.0080	-0.0081	0.0021
63G	0.0228	0.0055	-0.0066	-0.0074	-0.0077	0.0116
63M	0.0262	0.0041	-0.0132	-0.0132	-0.0145	0.0085
63P	0.0488	0.0088	-0.0096	-0.0101	-0.0039	0.0362

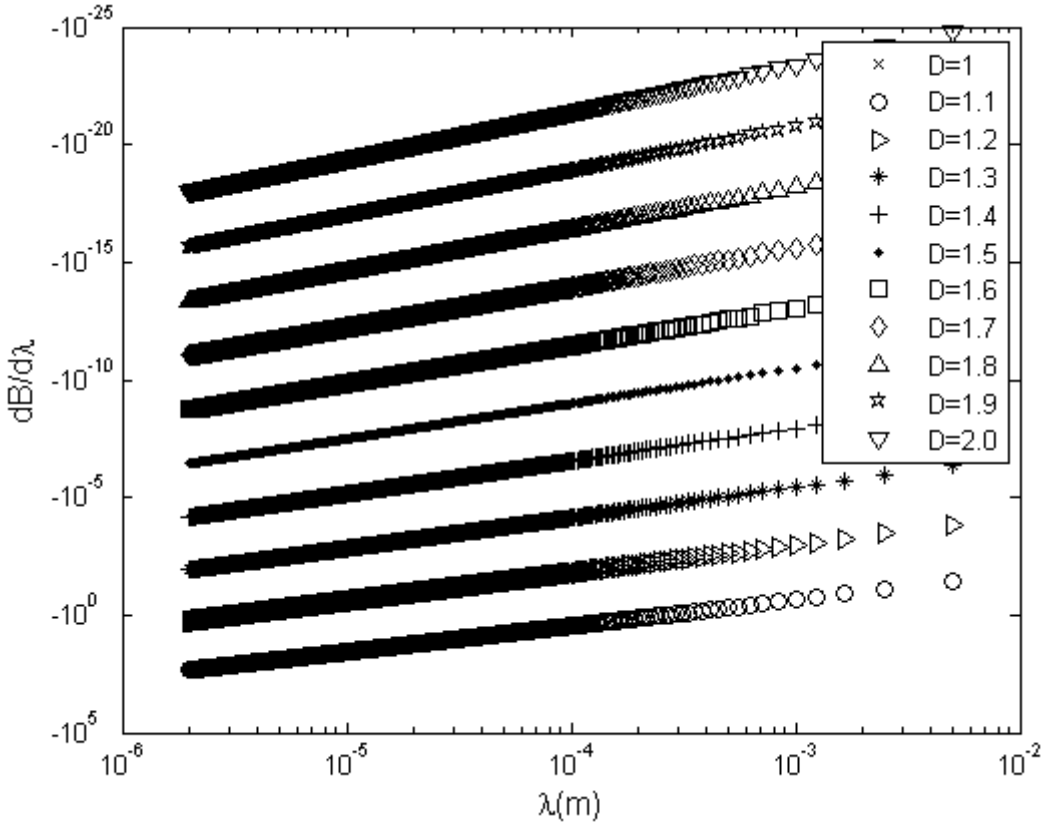

Figure 23: *dB/dλ* vs. *λ*

Interestingly, the *dB/dλ* values in Figure 23 are all negative except as *D*=1 it is zero. *D*=1.1 has the smallest value and *D*=2 has the biggest value. In contrast, in both Table 3 and Table 6, the *dB/dλ* values are not all negative, especially using the FFT method for all the rough surfaces

which shows the opposite trend of the self-affine W-M function. Therefore, the W-M function is not an effective way for charactering the rough surfaces.

3.3 Parameters comparison between measured rough surfaces and generated rough surfaces

Some parameters in Table 2 and Table 5 are also compared graphically. Bar graphs for the statistical parameters are shown in Figure 24 and for the multi-scale parameters are shown in Figure 25. R_q does not need to be shown here because G is fit such that the Rq values for the real and generated surfaces are identical (Eq. (19)). However, for a better comparison, we still show R_q and R_a.

In Figure 24, the compared parameters between these two kinds of rough surfaces are not so consistent. The differences between m_2 and m_4 in Figure 24 are very obvious, and the absolute values of m_2 and m_4 for the generated rough surfaces are much larger than for the measured rough surfaces. All the skewness values for the measured rough surfaces is negative, which means the rough surface profile data for the rough surfaces lies most on the right side of all the average values. However, for the generated rough surfaces it has some positive values. As we know, for a standard normal distribution, its kurtosis equals 3. Here, kurtosis for all the rough surfaces are smaller than 3, so the distribution of rough surface profile data either for original rough surfaces or the generated rough surfaces is flatter than the standard normal distribution.

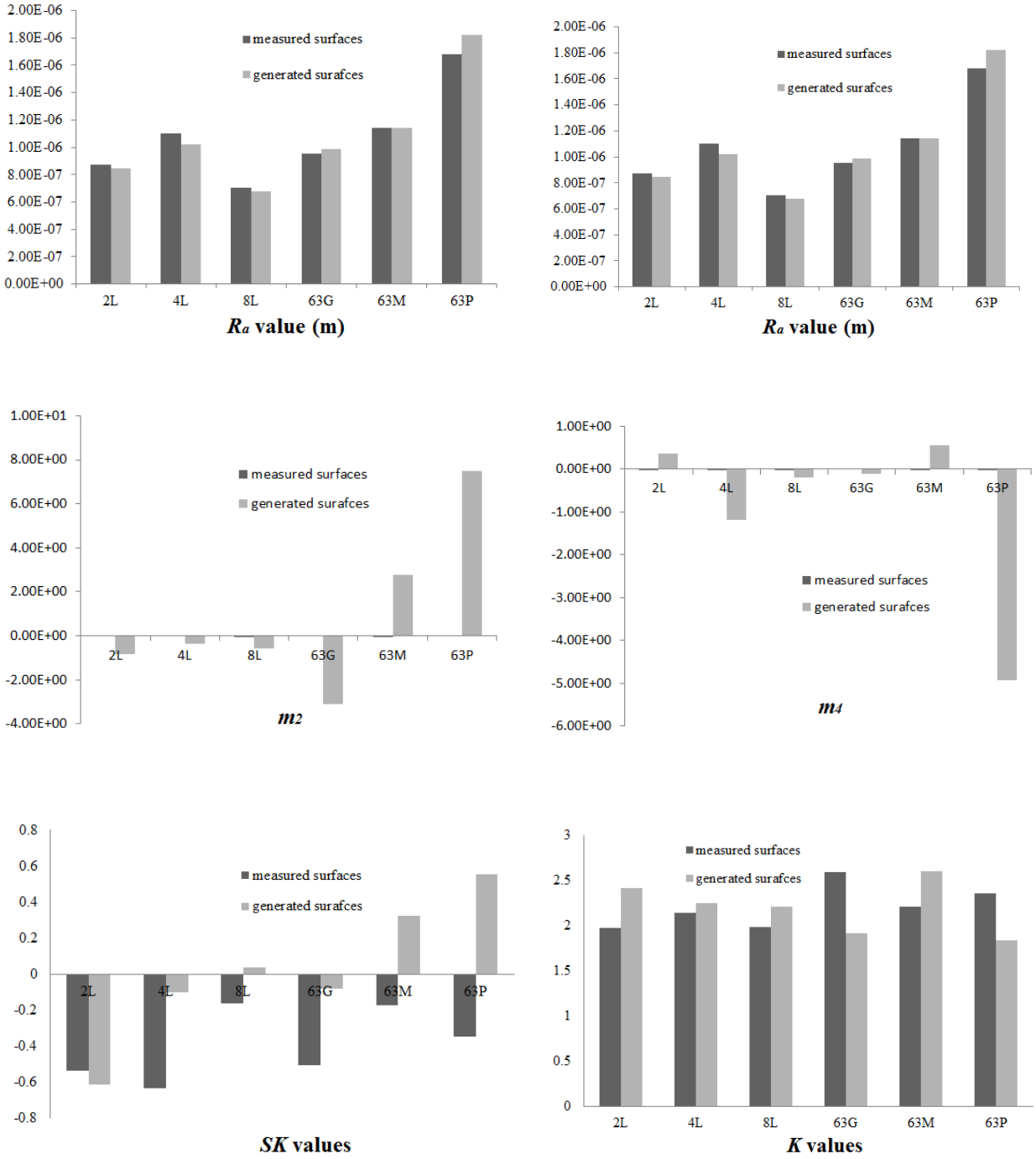

Figure 24: Comparison of statistical parameters between original rough surfaces and generated rough surfaces

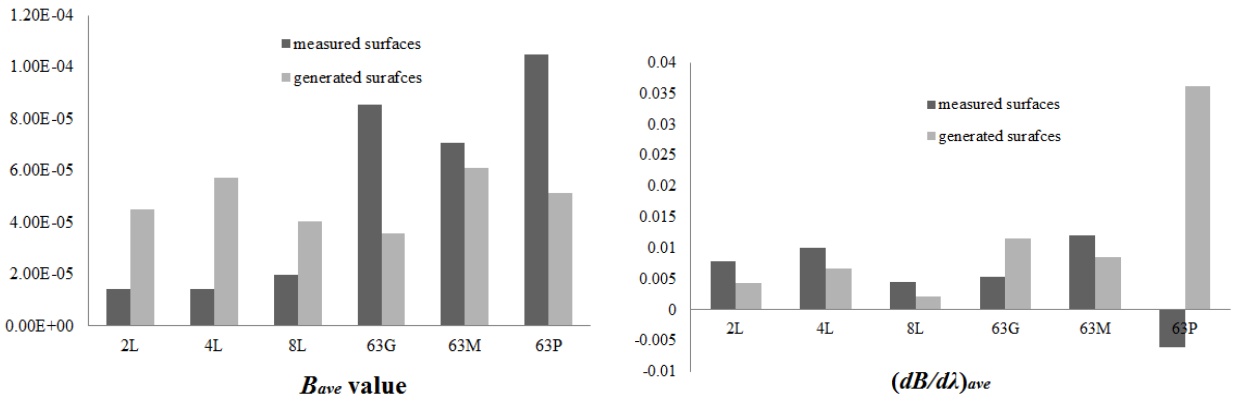

Figure 25: Comparison of multi-scale parameters between original rough surfaces and generated rough surfaces

The B_{ave} values and the $dB/d\lambda$ values do not follow the same trend (see previous section for the analysis) according to Figure 25. This is because the W-M function does not create a rough surface with a continuous spectrum. The measured roughest 63P surface has the highest B_{ave} so that its asperities are on average much more acute than the other surfaces. Whereas, for the generated rough surfaces, 63M has the highest B_{ave} with lower R_q value compared with R_q value in 63P generated rough surfaces.

Values from Table 3 and Table 6 are also compared and shown as Figure 26. It is obvious that all the values of $dB/d\lambda$ are approximately one, which indicates that both the measured rough surfaces and the generated rough surfaces are nominally self-similar surfaces. For the measured rough surfaces, the largest absolute values of $dB/d\lambda$ are from the roughest surfaces (i.e. the 63P surface), but this trend did not occur in the generated W-M rough surfaces.

Values of $db/d\lambda$ from l=1.5, l=1.6 and l=1.8 for all the surfaces are negative, which follows the trend obtained in section 3.2 that $dB/d\lambda$ should be negative according to the self-affine W-M

function. When l=1.2, the $dB/d\lambda$ values for the measured rough surfaces of 2L, 4L and 8L is positive and for the other three measured rough surfaces it is negative. However, the $dB/d\lambda$ values for the generated rough surfaces at l=1.2 are positive. When l=1.4, the $dB/d\lambda$ value is negative for the measured rough surfaces and positive for the generated rough surfaces. For the FFT method, all the values of $dB/d\lambda$ are positive, which is the exact opposite of the result in section 3.2. At l=1.5, and values closer to that, the wavelengths being considered by the spectrum should better align with the W-M function and therefore better capture the self-affine fractal structure.

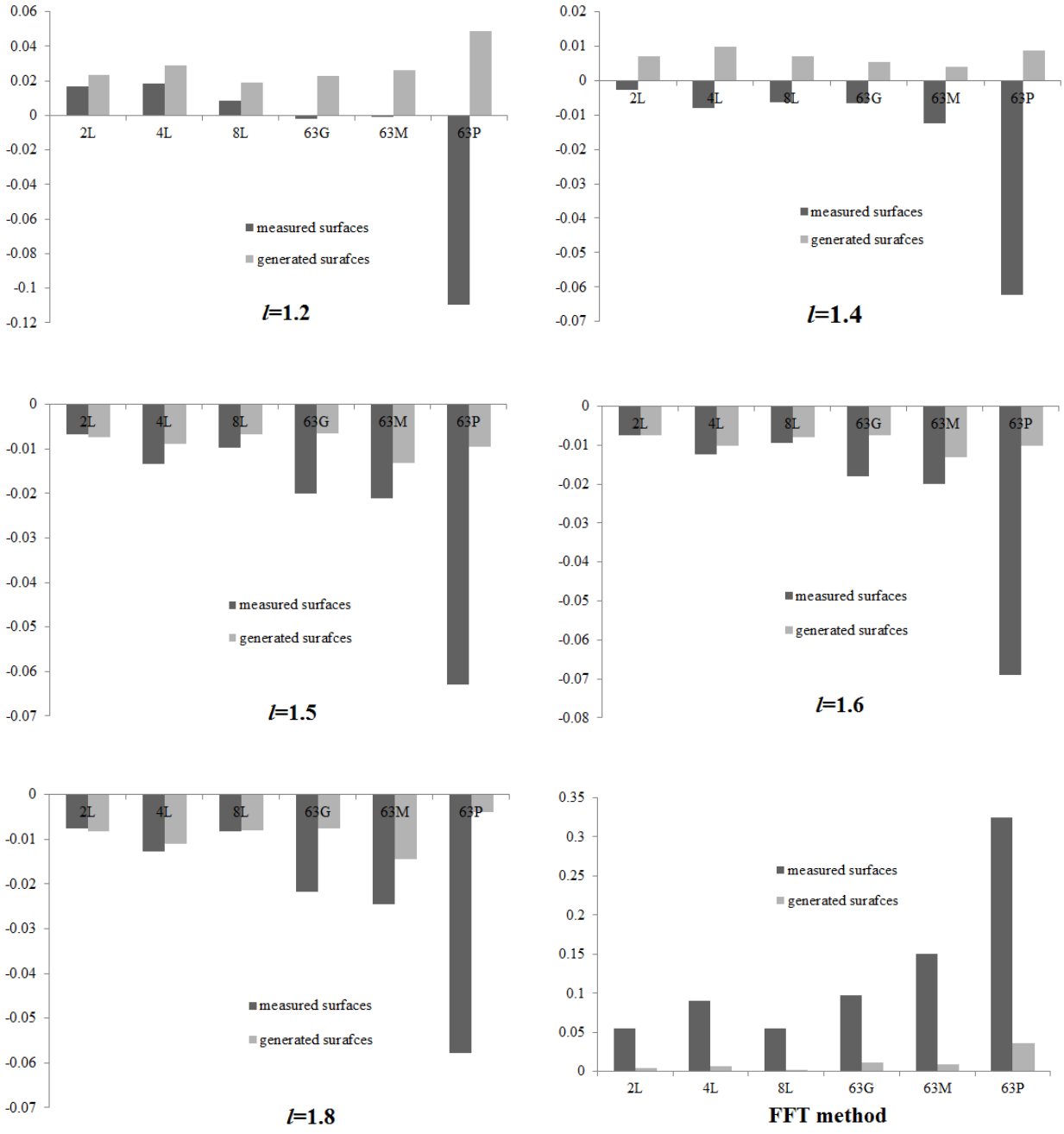

Figure 26: Comparison of *dB/dλ* calculated with varying *l* values and FFT method for measured rough surfaces and generated rough surfaces

Chapter 4

4 Analysis

4.1 The analysis of the W-M function

The W-M function $z(x)$ is mathematically self-affine [24, 29, 60, 61], so the generated surfaces based on the W-M function in our work are also self-affine but only at discrete wavelengths. In terms of Figures 24 and 25, the differences of parameters between the original real surfaces and the generated self-affine surfaces are not small, especially the statistical parameters, m_2, m_4 and SK, and the multi-scale parameters, B_{ave} and $(dB/d\lambda)_{ave}$, show the most disagreement. Moreover, after comparing the $dB/d\lambda$ values from different l values and FFT method (see Figure 26), one may find that not only a inconformity between the measured rough surfaces and the generated rough surfaces but not all the $dB/d\lambda$ values are negative which expected to be based on the result obtained in section 3.2. So the W-M function is not recommended for characterizing the true rough surfaces which appear to be nominally self-similar.

Another result was also obtained that the D value should equal one if the surface is self-similar according to Eq. (35). However, a self-similar fractal surface not described by the W-M function is generally not required to follow this rule. For instance, a self-similar surface

could have a D between 1 and 2 (such as Korch Curve [13], Sierpinski Triangle [14] and the coast lines illustrated in [40]).

From the above analysis, we know that the popular W-M function cannot be used with confidence to characterize real surfaces, and using it to generate surfaces is not practical. Wu [32] also derived a similar conclusion in his paper.

4.2 The analysis of different methods in calculating the fractal dimension, *D*

Table 7: Comparison between different methods in evaluating *D*

initial values	methods	calculated values	precision /%
D=1.1	Fourier analysis	1.0762	97.84
	Roughness-length method	1.0744	97.67
	Box-counting method	1.1030	99.73
	Power-spectrum method	1.4792	65.53
D=1.3	Fourier analysis	0.9873	75.95
	Roughness-length method	1.3148	98.86
	Box-counting method	1.2114	93.18
	Power-spectrum method	1.4817	86.02
D=1.5	Fourier analysis	1.0488	69.92
	Roughness-length method	1.5296	98.03
	Box-counting method	1.2969	86.46
	Power-spectrum method	1.4999	99.99
D=1.7	Fourier analysis	0.9764	57.44
	Roughness-length method	1.6941	99.65
	Box-counting method	1.3990	82.29
	Power-spectrum method	1.6031	94.30

Attention should also be paid to the fractal dimensions in Table 1 and Table 3. As we mentioned in 2.1.4, the values of D_0, D_1 and D_2 are all nominally equal to one whereas most of the D_3 values are much larger than one. And all the D_3 values are around 1.5. So it appears that

all the measured surfaces and generated surfaces are nominally self-similar only according to the W-M function.

Table 7 shows a comparison of the precision between different methods in evaluating *D* values. One may find that the degree of precision for the roughness-length method always results in a relatively precise prediction. The Fourier analysis is only effective on the W-M function when *D* has low values, which means that the rough surfaces are nearly self-similar surfaces according to W-M function. Since the box-counting method is used unequivocally for self-similar geometries as mentioned before, so with the *D* value increasing, its accuracy is decreasing, as the W-M function produces surfaces that are more self-affine. The variation of *D* values calculated by power spectrum method is very small, and when the *D* value becomes larger, the precision of this method grows higher.

Therefore, conclusions can be drawn that: (1) The roughness-length method is a good choice when evaluating the fractal dimension; (2) The box-counting method needs to be avoided to use when the fractal dimension is a little large; (3) The Fourier analysis is not effective for the W-M function because the W-M function does not create a continuous spectrum, or a spectrum whose wavelengths correlate with the Fourier series; (4) When the surfaces are self-similar, the power spectrum method is not reliable in calculating fractal dimension, as it can cause a spectrum to appear self-affine.

In many previous studies and discussions [25, 43, 62], the ACF-based power spectrum method is a popular method in evaluating the fractal dimension, and when the initial fractal

dimension value is large enough, this method can have a high accuracy in predicting it. However, in the current work, it appears that a value near D=1.5 is consistently predicted. This situation is perhaps caused by the use of the discrete form of the autocorrelation function used to calculate the power spectrum and the rough surfaces created by the W-M function also have a discontinuous spectrum. Then a large difference existed between the calculated fractal dimension values and the initial fractal dimension values. Klinkenberg [25] stated briefly that every method using in calculating the fractal dimension has one common drawback that discretization of the phenomenon being investigated (i.e. the rough surfaces) will result in a measured fractal dimension that is different from its theoretical fractal dimension. Therefore, the coarser the discretization is, the greater the expected difference will be.

The Fourier analysis can have higher precision in determining fractal dimension only when the surface has a continuous spectrum or one that aligns with the Fourier series. This conclusion is not the same as in [28], perhaps this is because the way the surfaces generated are not the same (Russ used the midpoint displacement technique) and the input parameters may have some impact on the process of generating rough surfaces. Real surfaces may also be more effective.

T. Candela [63] also used a method known as the Fourier power spectrum (FPS) method, which is similar to the Fourier analysis, to analyze the fractal property of self-affine surfaces. They concluded that this method is the most accurate and reliable method in evaluating the Hurst exponent. This is probably because when they used this method, the spectrum of the

entire surface is calculated by stacking all 1-D Fourier transforms for the reduction of the noise associated with individual profiles.

In addition, the 1-D surface profiles they used to analyze were extracted from the 2-D Digital Elevation Model (DEM) of 2-D surfaces. A set of 1-D parallel profiles in the specific direction were extracted, detruded and analyzed for each surface. These 1-D profiles are all self-affine and the input exponent in extracting rough surface profiles can also cause the rough surface profiles to be absolutely self-affine.

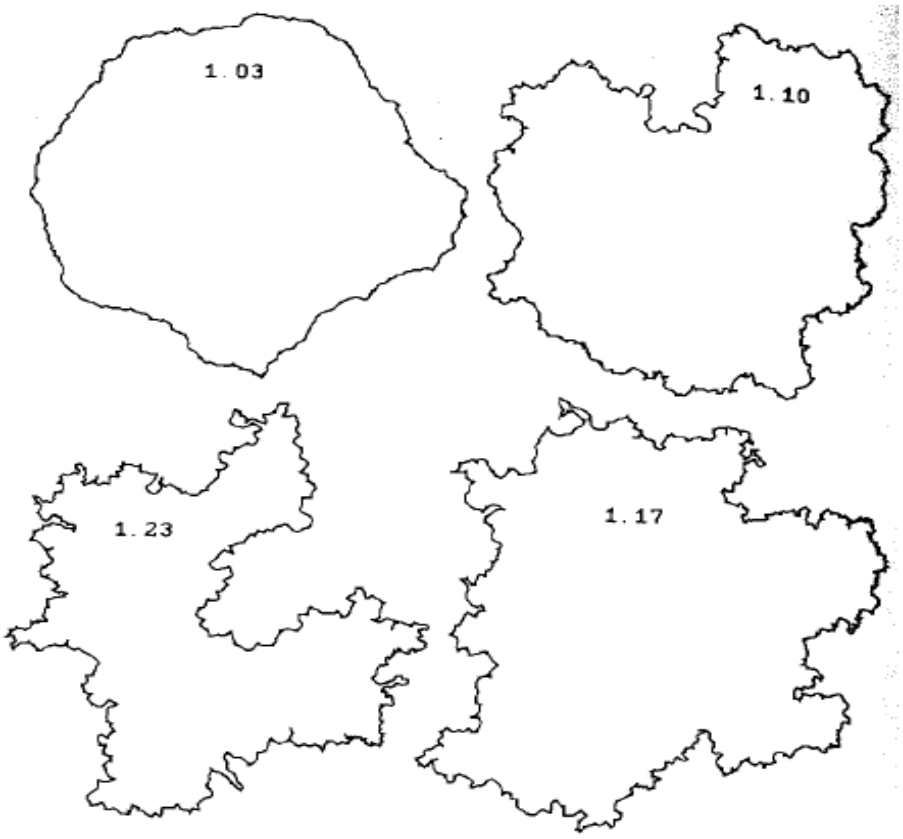

Surface Characterization: Fractal Dimensions, Hurst Coefficients, and Frequency Transforms

Figure 27: Random fractal outlines generated with varying fractal dimensions [64]

Russ [64] described that the fractal dimension can provide an efficient descriptor of the

roughness. This is because the increase in the perceived irregularity of the boundary line can be well mapped by increasing the measured fractal dimension of the line. He also showed a figure to help illustrate this trend which is shown here as Figure 27.

From the figure 27, one may find that the larger the fractal dimension is, the rougher the outline is. However, from the Table 1 and Table 4, the larger *D* values do not always correspond to larger roughness. So the point of view of Russ is not exactly correct and the role of the fractal dimension, *D*, in describing the real rough surfaces need to be questioned.

4.3 The analysis of autocorrelation function (ACF) in power spectrum method

The version of the power spectrum used in this work is based on the FFT of the ACF. First used in 1946 on surface roughness [65], the ACF is applied to create a spectrum of the surface that is smooth by finding the peaks that are correlated laterally. This is required for analyzing surfaces generated by the W-M function because their power spectrum is not continuous like a real surface.

However, when the ACF is calculated, the small scales naturally correlate better and therefore they are amplified, and larger scales do not match as well at larger wavelengths. This is a natural behavior of real rough surfaces [66]. By enlarging the amplitudes at small scales, the power spectrum artificially causes the self-affinity of the surface to be amplified.

Chapter 5

5 Conclusions and future work

In this work, surfaces with various finishes were analyzed. It is found that all the measured rough surfaces are nominally self-similar, and not self-affine as many of the popular fractal models assumed. They do show random variation about this self-similar structure. Different rough surfaces were generated by using the W-M function. According to the W-M function, the fractal dimension, *D*, must equal to one if rough surfaces are self-similar which has been proved to be an unnecessary restraint imposed by the W-M function.

Since the fractal dimension, *D*, is a popular parameter for fractal surfaces, four different methods were implemented to calculate the value. It is found that the values of fractal dimension from the Fourier analysis, box-counting method and roughness-length method are mostly consistent with each other, which might indicate that the measured rough surfaces are nominally self-similar. However, the values of fractal dimension from the power spectrum method are all approximately 1.5, for all the measured surfaces and the W-M function generated surfaces. It is much higher than the other three methods, so the power spectrum method can cause a spectrum to appear self-affine when it is not.

The degree of self-similarity of all the measured surfaces is characterized by the average

slope, $dB/d\lambda$. When it equals zero everywhere, the measured surfaces could be said to be perfectly self-similar. In the current work, the values of average slope for all the rough surfaces are relatively close to zero (see Table 2 and Table 3), which means that the measured surfaces tend to be nominally self-similar.

The relationship between the fractal dimension, D, and the fractal roughness parameter, G, was also analyzed. It appears that when D approaches 2, G becomes an asymptotic value, the differences between the G values are not so obvious when D becomes larger than 2. In addition, G becomes infinitesimal when D tends to 2. Hence, it demonstrates that G may not be a good choice in characterizing the rough surfaces.

Moreover, the real rough surfaces were compared with the W-M function generated rough surfaces. The statistical parameters, m_2, m_4 and SK, and the multi-scale parameters, B_{ave} and $dB/d\lambda$, show much disagreement. The relationship between $dB/d\lambda$ and λ was also investigated which shows that the trend of these two parameters in the real rough surfaces is not always consistent with the trend derived by the W-M function.

In analyzing the B_{ave} and $(dB/d\lambda)_{\text{ave}}$ for the generated rough surfaces, one may find that there are many spaced peaks in the trend which correspond to the discrete frequencies existing in the W-M function generated rough surfaces. This phenomenon can also be found in evaluating the fractal dimension by using the Fourier analysis in Chapter 4. In determining the fractal dimension, the Fourier analysis can only have higher precision when the rough surfaces have a continuous spectrum. Whereas, this method is not effective for the W-M generated rough

surfaces (see Table 5) because of the discontinuous spectrum created by the W-M function. Therefore, the W-M function does not represent a continuous spectrum that is represented in most surfaces.

When calculating the fractal dimension based on the power spectrum method, the discrete type of the autocorrelation function was used. The resulting calculations suggest that the autocorrelation function can amplify the amplitude at small scales. Therefore, when using the power spectrum method, it can enlarge the self-affinity of the rough surfaces.

From the above analysis, it can be found that when calculating the fractal dimension for self-similar rough surfaces, one should avoid using the power spectrum method because it can cause the spectrum to appear self-affine. Moreover, a discrepancy exists between the generated rough surfaces and real rough surfaces. Since no real surface follows the W-M function, and the measured surfaces in this experiment were self-similar, not self-affine, the W-M function is not recommended for charactering rough surfaces. This area of multi-scale surface characterization deserves much more work and focus in the future.

References

[1] Y. Jeng, "Characterization of Surface Height Distributions", Journal of the Chinese Society of Mechanical Engineers, 19(4), pp. 417-423, 1998.

[2] B. Bhushan, "Surface Roughness Analysis and Measurement Techniques", in Modern Tribology Handbook, CRC Press, 2000.

[3] M. Zecchino, "Characterizing Surface Quality:Why average Roughness is not Enough".

[4] T. R. Thomas, "Rough Surfaces", Longman, 1982.

[5] J. I. McCool, " Comparison of Models for the Contact of Rough Surfaces", Wear, 107(1), pp. 37-60, 1986.

[6] D. J. Whitehouse, "Handbook of Surface and Nanometrology", CRC Press, 2010.

[7] R. L. Jackson, L. Kogut, "A Comparison of Contact Modeling Utilizing Statistical and Fractal Approaches", Journal of Tribology, 128(1), pp. 213-217, 2006.

[8] A. Majumdar, B. Bhushan, "Fractal Model of Elastic-plastic Contact Between Rough Surfaces", Journal of Tribology, 113(1), pp. 1-11, 1991.

[9] A. Eftekhari, "Fractal Geometry of Texts: An Initial Application to the Works of Shakespeare", Journal of Quantitative Linguistics, 13(2-3), pp. 177-193, 2006.

[10] B. B. Mandelbrot, A. Blumen, "Fractal Geometry: what is it, and what does it do?", Proc.

R. Soc. Lond. A, 423(1864), pp. 3-16, 1989.

[11] D. Shiffman, "The Nature of Code: Simulating Natural Systems with Processing", The nature of code, 2012.

[12] P. M. Iannaccone, M. Khokha, "Fractal Geometry in Biological Systems: An Analytical Approach", CRC Press; 1 edition, 1996.

[13] F. Kenneth, "Fractal Geometry: Mathematical Foundation and Applications", John Wiley & Sons, 1990.

[14] A. Karplus, "Self-similar Sierpinski Fractals", Science Fair, 2008.

[15] M. S. El Naschie, "A Fractal Menger Sponge Space-Time Proposal to Reconcile Measurements and Theoretical Predictions of Cosmic Dark Energy", International Journal of Modern Nonlinear Theory and Application, 2(2), pp. 107-121, 2013.

[16] B. B. Mandelbrot, "The Fractal Geometry of Nature", New York: W.H. Freeman, 1983.

[17] B. B. Mandelbrot, "Self-Affine Fractal Sets", Fractals in Physics, pp. 3-28, 1986.

[18] P. A. Burrough, "Fractal Dimensions of Landscapes and Other Environmental Data", Nature, 294, pp. 240-242, 1981.

[19] A. Majumdar, "Fractal Surfaces and Their Applications to Surface Phenomena", University of California, Berkeley, 1989.

[20] D. Greening, "Scrum Self-Similarity: Creating Organizational Fractals", 2009, retrieved from http://senexrex.com/scrum-fractals/.

[21] M. Frame, B. Mandelbrot, and N. Neger, "Fractal Geometry", Yale University, 2009.

[22] J. C. Russ, "Measurement of the Fractal Dimension of Surfaces", Journal of Computer-Assisted Microscopy, 3(3), pp. 127-144, 1991a.

[23] P. K. Srivastava, "Proceedings of All India Seminar on Advances in Product Development", APD 2006, New Age International Pvt Ltd Publishers, 2006.

[24] A. Majumdar, and Tien, C. L., "Fractal Characterization and Simulation of Rough Surfaces", Wear, 136(2), pp. 313-327, 1990.

[25] B. Klinkenberg, "A Review of Methods Used to Determine the Fractal Dimension of Linear Features", Mathematical Geology, 26(1), pp. 23-46, 1994.

[26] A. Fournier, D. Fussell, and L. Carpenter, "Computer Rendering of Stochastic Models", Communications of the ACM, 25(6), pp. 371-384, 1982.

[27] I. Norros, P. Mannersalo, and J. L. Wang, "Simulation of fractional Brownian motion with conditionalized random midpoint displacement", Advances in Performance Analysis, pp. 77-101, 1999.

[28] J. C. Russ, "Fractal Surfaces", New York and London: Plenum Press, 1994.

[29] A. Majumdar, B. Bhushan, "Role of Fractal Geometry in roughness Characterization and Contact Mechanics of Surfaces", Journal of Tribology, 112(2), pp. 205-216, 1990.

[30] M. V. Berry, Z. V. Lewis, "On the Weierstrass-Mandelbrot Fractal Function", Proc. Royal. Soc. A, 370(1743), pp. 459-484, 1980.

[31] M. Ausloos, B. H. Berman, "A Multivariate Weierstrass-Mandelbrot Function", Proc. Royal. Soc. A, 400(1819), pp. 331-350, 1985.

[32] J.-J. Wu, "Characterization of fractal surface", Wear, 239(1), pp. 36-47, 2000.

[33] R. S. Sayles, T. R. Thomas, "Measurement of the Statistical Microgeometry and Engineering Surfaces", Journal of Lubricant Technology, 101(4), pp. 409-428, 1979.

[34] J.-J. Wu, "Spectral Analysis for the Effect of Stylus Tip Curvature on Measuring Rough Profiles", Wear, 230(2), pp. 194-200, 1990.

[35] J. F. Archard, "Elastic Deformation and the Laws of Friction", Proc. R. Soc. Lond. A, 243(1233), pp. 190-205, 1957.

[36] Y. Xu, "An Analysis of Elastic Rough Contact Models", Mechanical Engineering, Auburn University, Auburn, 2012.

[37] R. L. Jackson, R. D. Malucci, and S. Angadi, *et al.* "A Simplified Model of Multiscale Electrical Contact Resistance and Comparison to Existing Closed Form Models", in Electrical Contacts, 2009 Proceedings of the 55th IEEE Holm Conference on, pp. 28-35, 2009.

[38] R. L. Jackson, "An Analytical Solution to an Archard-Type Fractal Rough Surface Contact Model", Tribology Transactions, 53(4), pp. 543-553, 2010.

[39] L. F. Richardson, "The Problem of Contiguity: An appendix to Statisics of Deadly Quarrels", in Yearbook of the Society for General Systems Research, Ann Arbor, 1961, pp. 140-187.

[40] B. Mandelbrot, "How Long Is the Coast of Britain? Statistical Self-Similarity and Fractional Dimension", Science, 156(3775), pp. 636-638, 1967.

[41] B. B. Mandelbrot, "Self-affine Fractals and Fractal Dimension", Physica Scripta, 32(4), pp. 257-260, 1985.

[42] R. Wen, R. Sinding-Larsen, "Uncertainty in Fractal Dimension Estimated from Power Spectra and Variograms", Mathematical Geology, 29(6), pp. 727-753, 1997.

[43] A. Malinverno, "A Simple Method to Estimate the Fractal Dimension of A Self-affine Series", Geophysical Research Letters, 17(11), pp. 1953-1956, 1990.

[44] A. S. Balghonaim, J. M. Keller, "A maximum likelihood estimate for two-variable fractal surface", IEEE Transactions on Image Processing, 7(12), pp. 1746-1753, 1998.

[45] B. B. Mandelbrot, J. W. van Ness, "Fractional Brownian Motions, Fractional Noises and Applications", SIAM Review, 10(4), pp. 422-437, 1968.

[46] T. Babadagli, K. Develi, "Fractal Fracture Surfaces and Fluid Displacement Process Fractured Rocks", 10th Int. Conf. of Fracture, 2001.

[47] T. H. Wilson, J. Dominic, "Fractal Interrelationships Between Topography and Structure", Earth Surface Processes and Landforms, 23(6), pp. 509-525, 1998.

[48] P.H.S.W.Kulatilake, J. Um, "Requirements for Accurate Quantification of Self-affine Roughness Using the Roughness-length Method", International Journal of Rock Mechanics and Mining Sciences, 36(1), pp. 5-18, 1999.

[49] N. Fardin, Q. Feng and O. Stephansson, "Application of A New in Situ 3D Laser Scanner to Study the Scale Effect on the Rock Joint Surface Roughness", International Journal of Rock Mechanics and Mining Sciences, 41(2), pp. 329-335, 2004.

[50] M. Schroeder, "Fractals, Chaos, Power Laws: Minutes from an Infinite Paradise", New York: W. H. Freeman and Company, 1991.

[51] B. Florindo, O. M. Bruno, "Closed Contour Fractal Dimension Estimation by the Fourier Transform", Chaos, Solitons and Fractals, 44(10), pp. 851-861, 2012.

[52] B. Dubuc, S. W. Zucker, and C. Tricot, et al., "Evaluating the Fractal Dimension of Surfaces", Proc. R. Soc. Lond. A, 425(1868), 1989a.

[53] J. Fender, "Fractals", New York: Springer US, 1988.

[54] R. B. Blackman, J. W. Tukey, "The Measurement of Power Spectra", New York: Dover Publications, 1958.

[55] A. Sadana, "Binding and Dissociation Kinetics for Different Biosensor Applications Using Fractals", Elsevier, 2003.

[56] M. Ciesla, J. Barbasz, "Random Sequential Adsorption on Fractals", Journal of Chemical Physics, 137(4), 2012.

[57] E. J. Abbott, F. A. Firestone, "Specifying Surface Quality - A method based on Accurate Measurement and Comparison", Mechanical Engineering, 55(1933), pp. 569-572, 1933.

[58] K. L. Johnson, "Contact Mechanics", Cambridge University Press, 1985.

[59] G. W. Stachowiak, A. W. Batchelor, "Engineering Tribology", Butterworth-Heinemann, 2005.

[60] P. Sahoo, "Engineering Tribology", New Delhi: Phi Learning Pvt, Ltd., 2005.

[61] D. Gard, A. Tudor, and G. Chisiu, "Fractal Approach for Erodated Wear of Surfaces by Solid Particles," University Politehnica of Bucharest Scientific Bulletin, 76(2), pp. 111-120, 2014.

[62] C. Q. Yuan, J. Li, and X. P . Yan, *et al.* "The Use of the Fractal description to Characterize Engineering Surfaces and Wear Particles", Wear, 255(1-6), pp. 315-326, 2003.

[63] T. Candela, F. Renard. and M. Bouchon, *et al.*"Characterization of Fault Roughness at Various Scales: Implications of Three-Dimensional High Resolution Topography Measurement", Pure and Applied Geophysics, 166(10-11), pp. 1817-1851, 2009.

[64] J. C. Russ, "Surface Characterization: Fractal Dimensions, Hurst Coefficients, and Frequency Transform", Journal of Computer-Assisted Microscopy, 2(3), pp. 161-183, 1990.

[65] H. A. Francis, "Application of Spherical Indentation Mechanics to Reversible and Irreversible Contact between Rough Surfaces", Wear, 45(2), pp. 221-269, 1977.

[66] J. Williams, "Engineering Tribology", Oxford University Press, 1994.

Appendices

A: The other five measured rough surface profiles after leveling

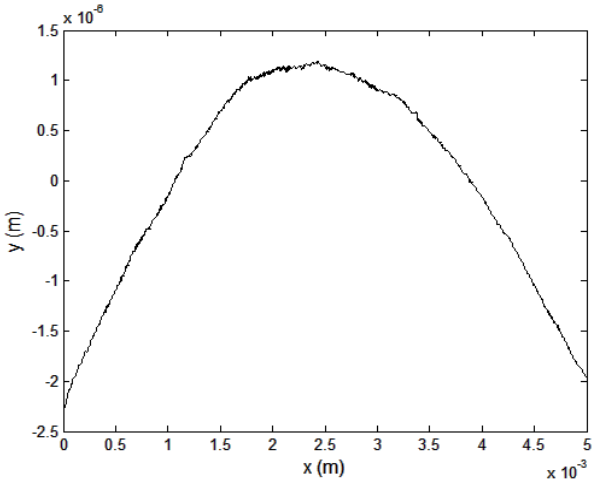

2L rough surface

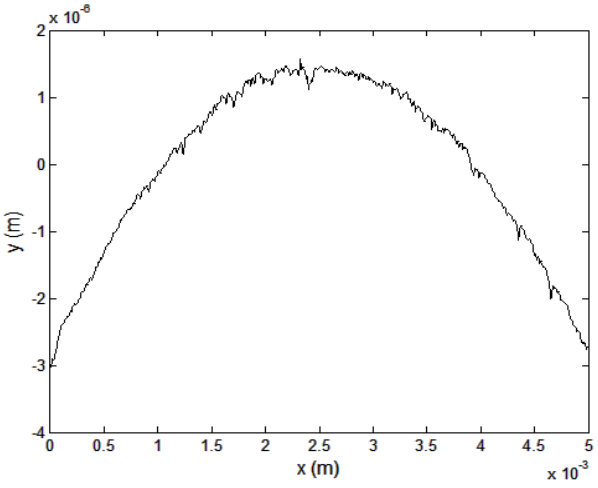

4L rough surface

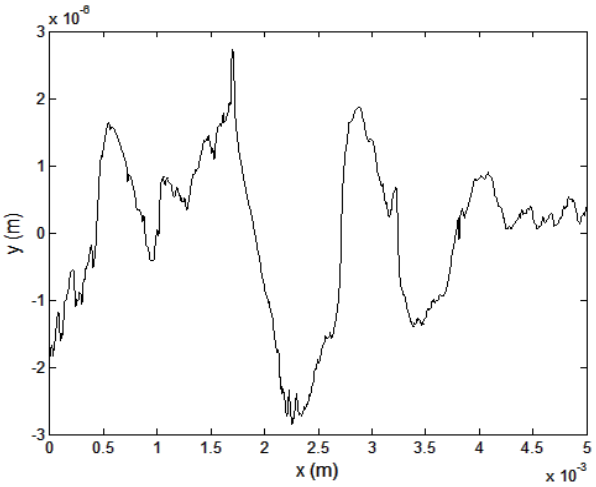

63G rough surface

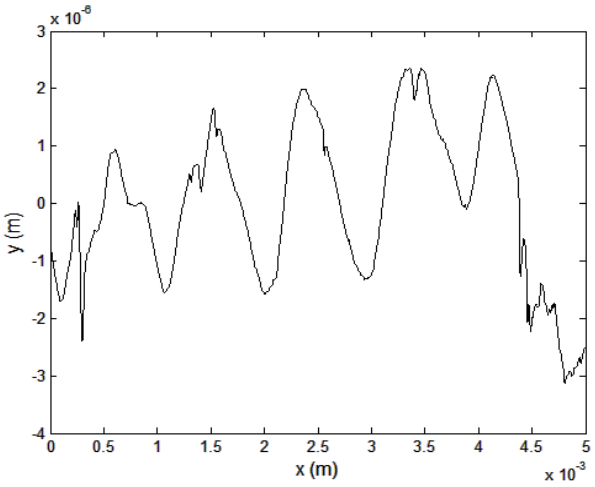

63M rough surface

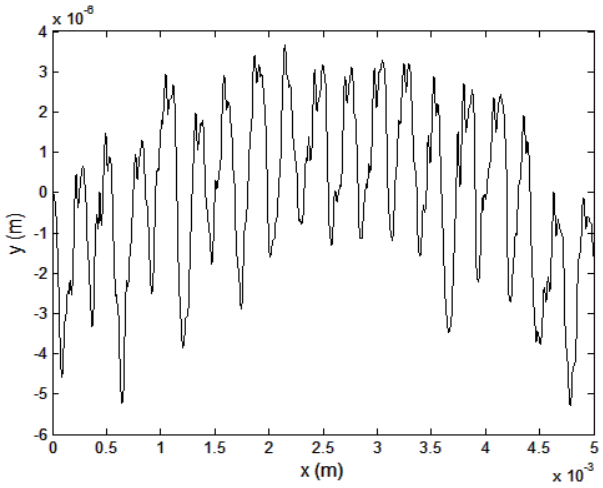

63P rough surface

Figure 28: The other five rough surface profiles after leveling

B: Plots of relationship between amplitude (Δ) versus wavelength (λ) for the other four measured rough surfaces

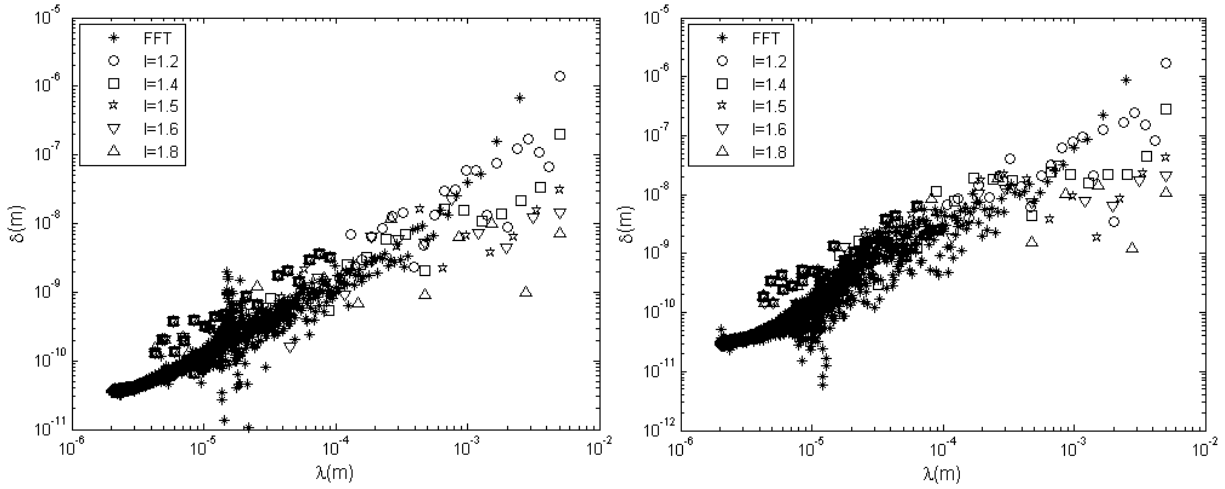

2L rough surface

4L rough surface

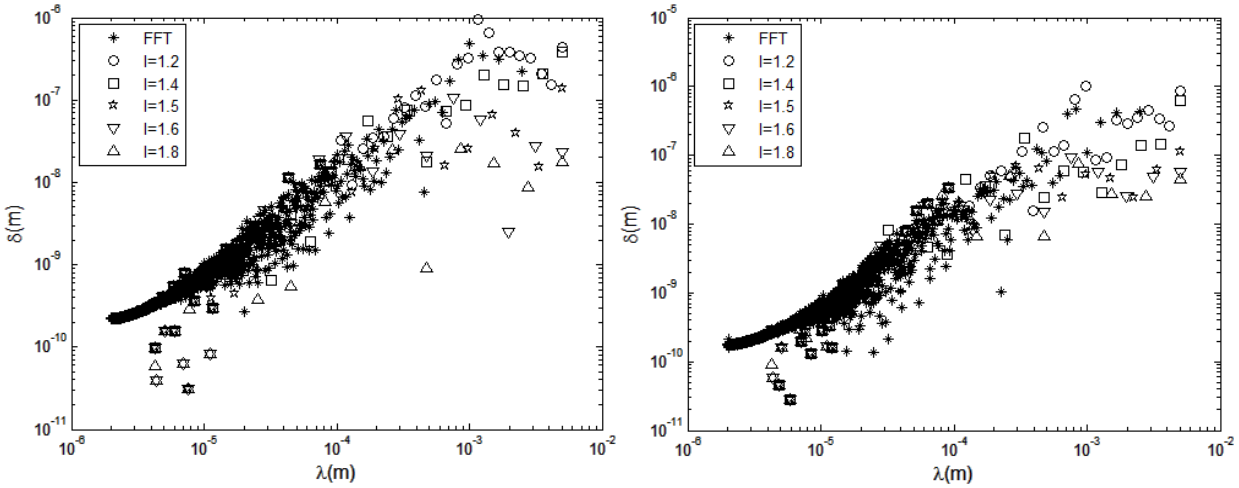

63G rough surface 63M rough surface

Figure 29: Δ vs. λ for the other measured rough surfaces

C: Plots of relationship between *B* and λ for the other four measured rough surfaces

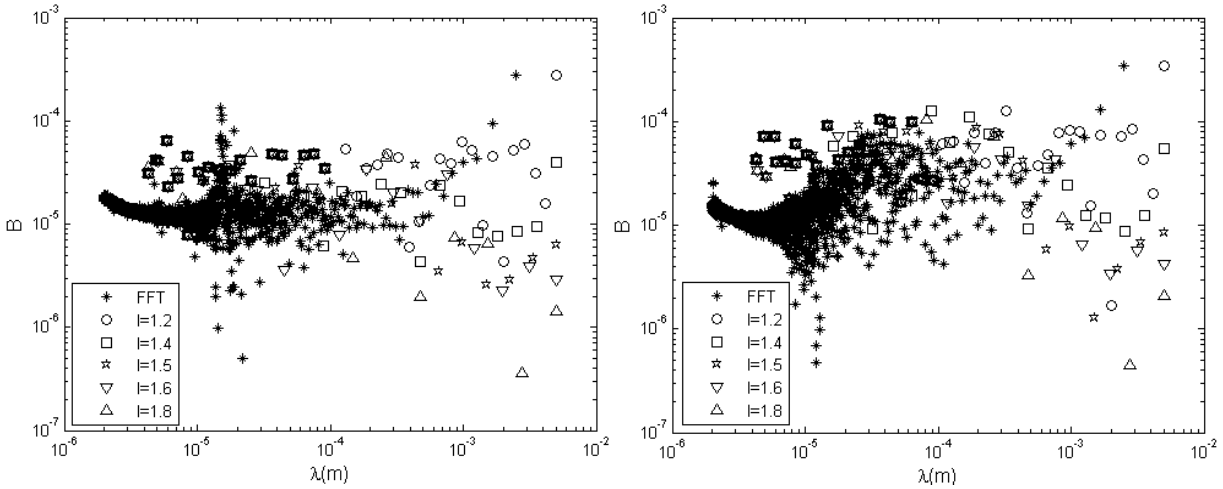

2L rough surface 4L rough surface

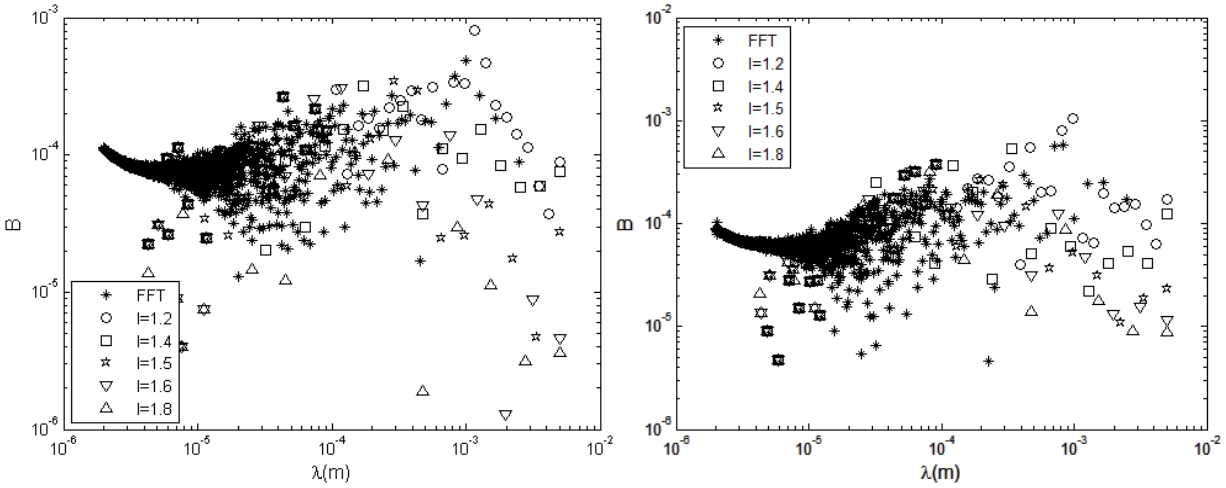

63G rough surface 63M rough surface

Figure 30: *B* vs. λ for the other four measured rough surfaces

D: Schematical illustration of fractal dimension of the other five measured rough surfaces calculated by using different four methods

For 2L rough surface:

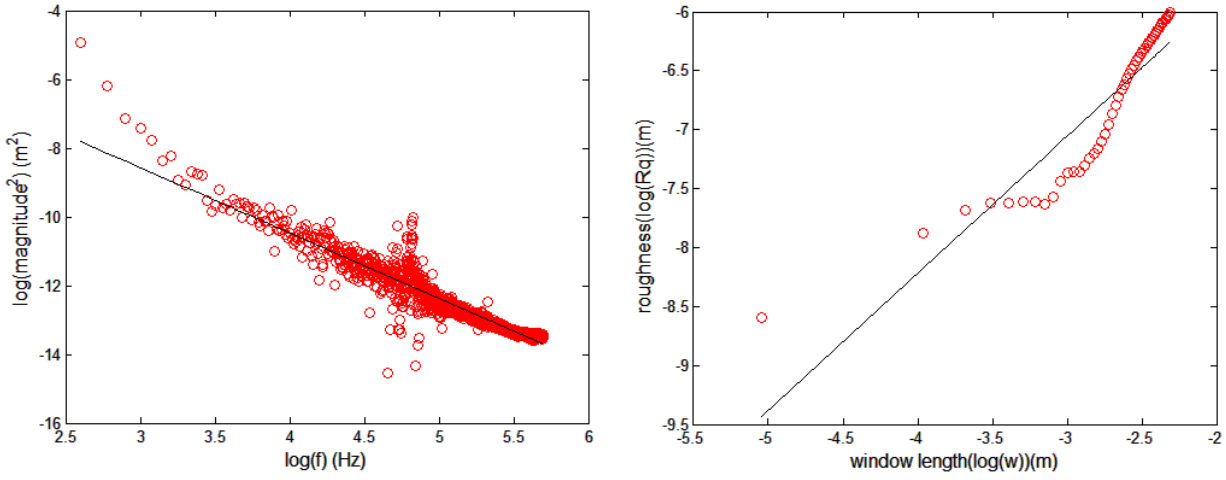

(a) (b)

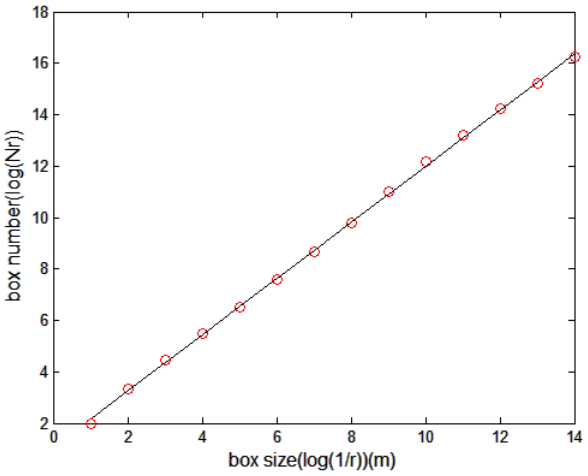

(c)

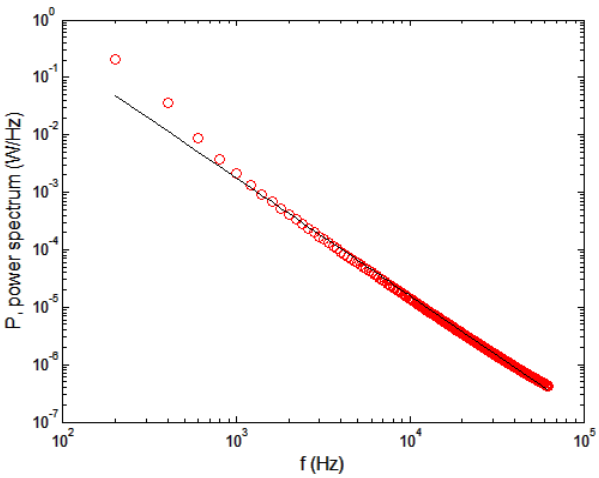

(d)

For 4L rough surfaces:

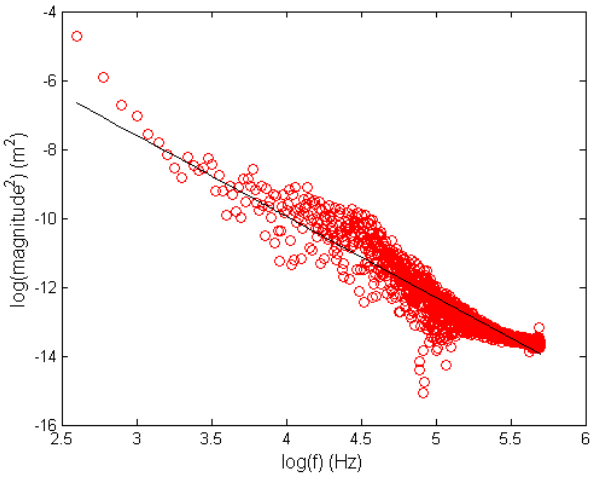

(a)

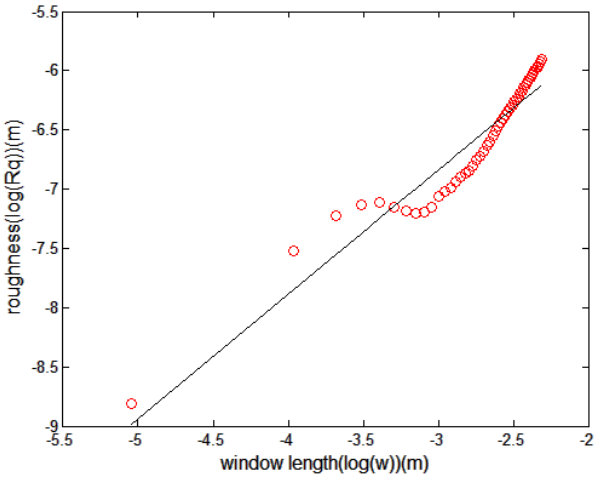

(b)

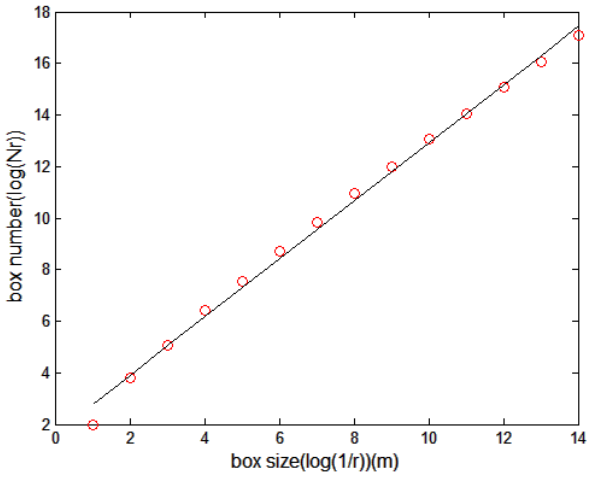

(c)

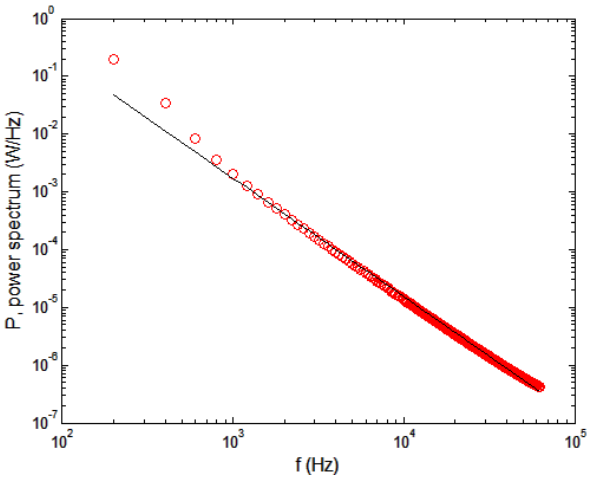

(d)

For 63G rough surface:

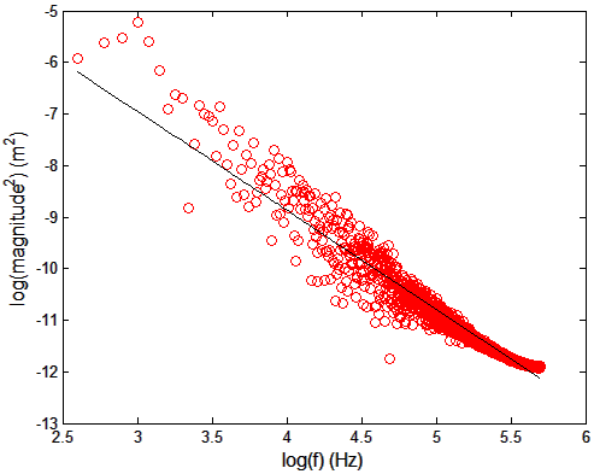

(a)

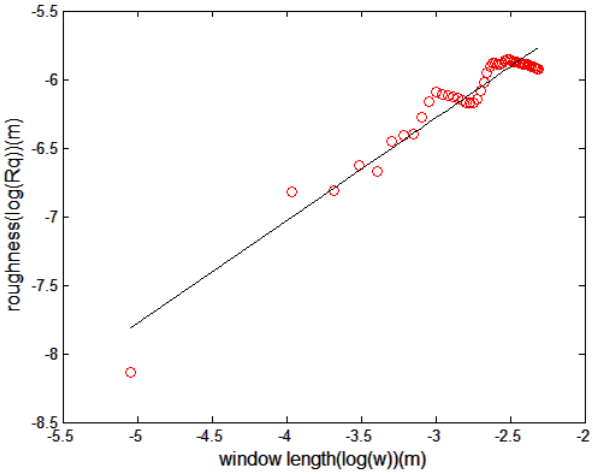

(b)

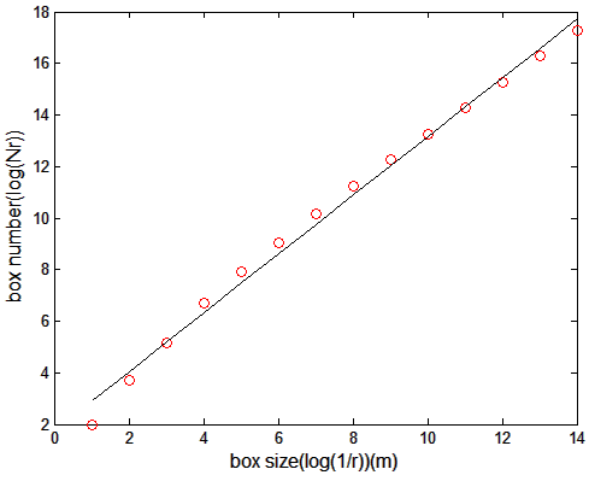

(c)

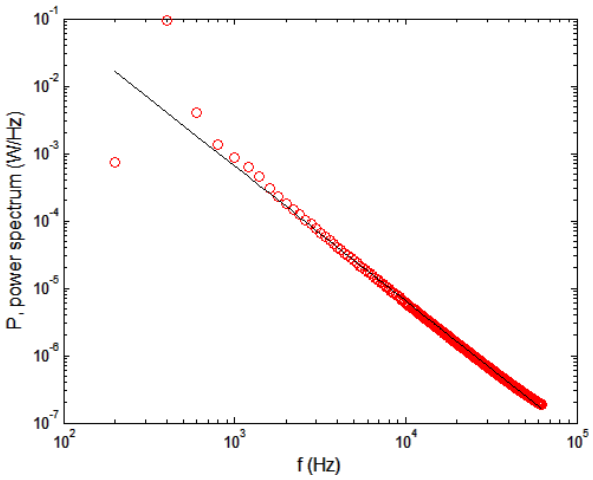

(d)

For 63M rough surface:

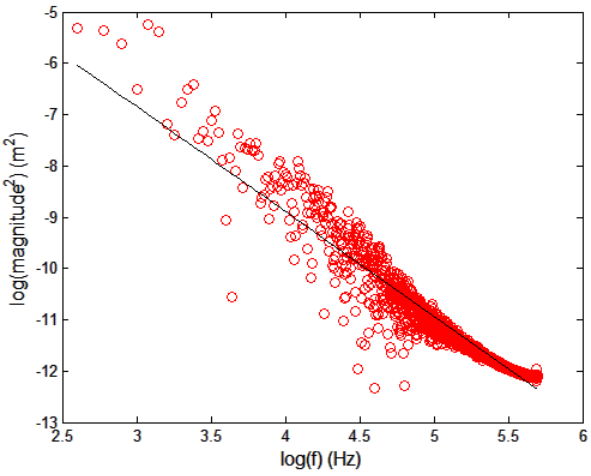

(a)

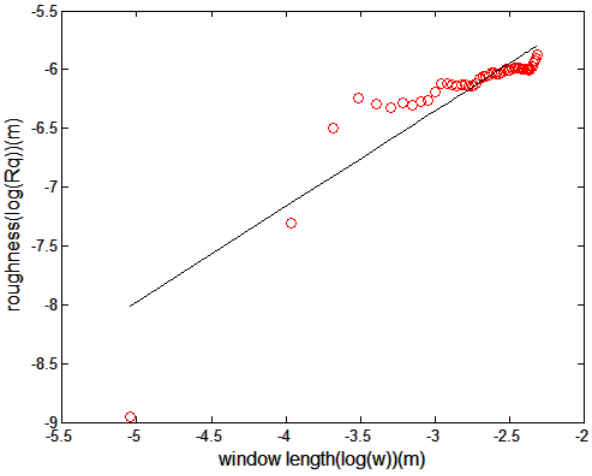

(b)

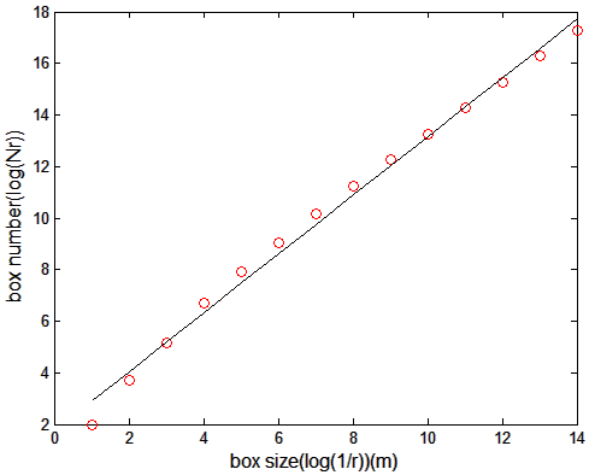

(c)

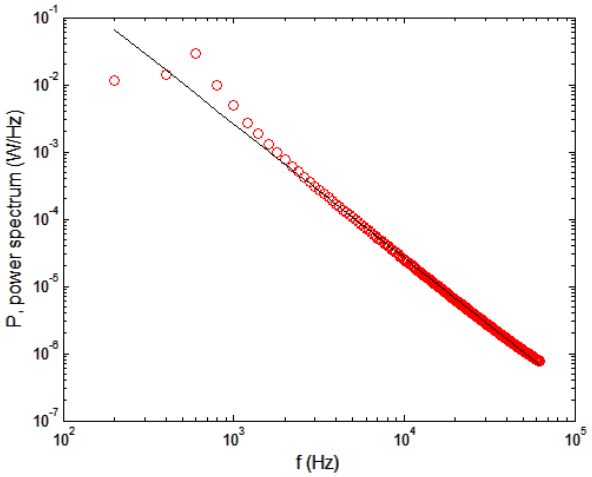

(d)

For 63P rough surface:

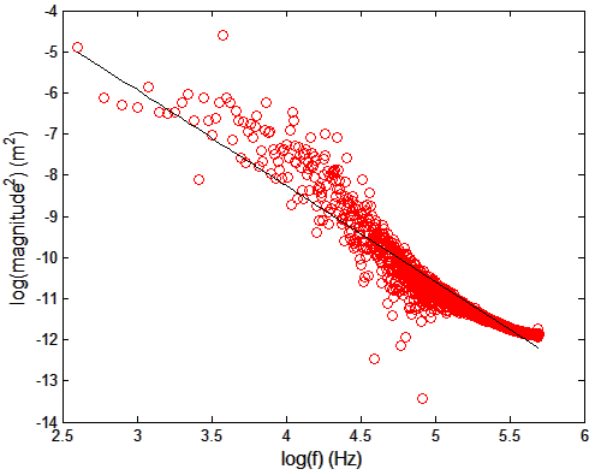

(a)

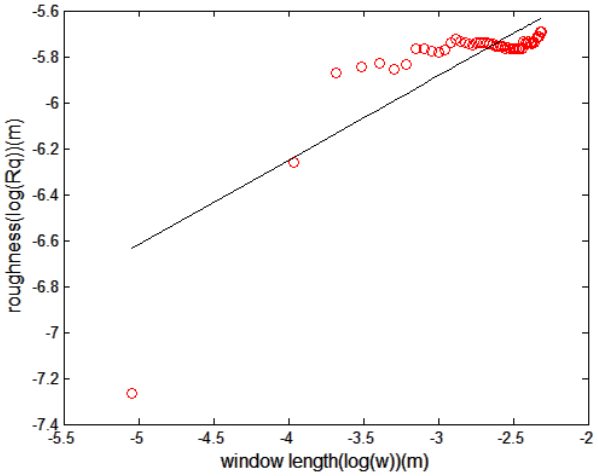

(b)

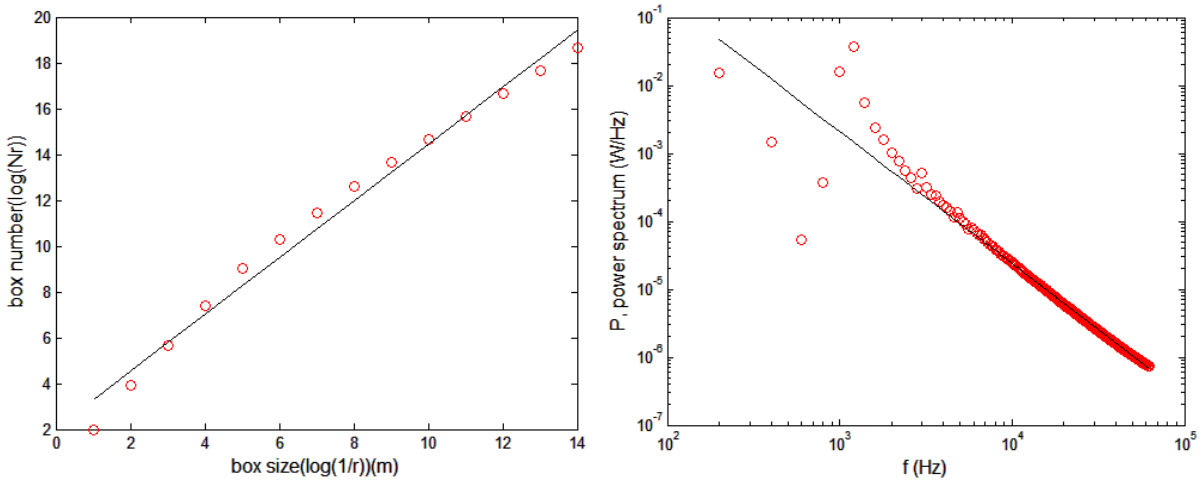

(c) (d)

Figure 31: *D* values calculated by four different methods for the other five measured rough surfaces
(a) Fourier analysis; (b) Roughness-length method; (c) Box-counting method; (d) Power spectrum method
The lines are fitted to the points calculated from the real surfaces

E: The other five generated rough surface profiles after leveling

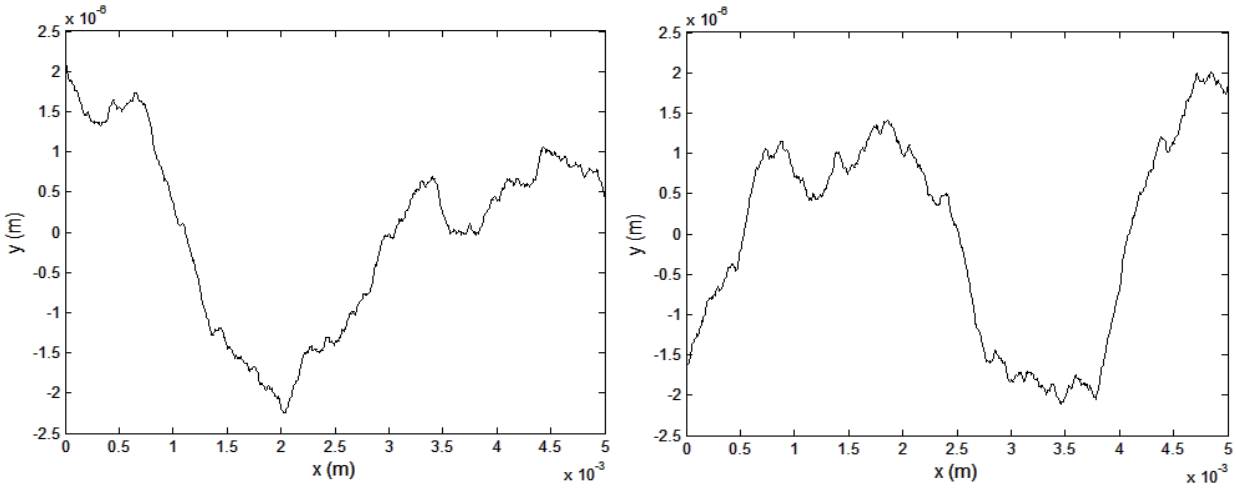

2L rough surface 4L rough surface

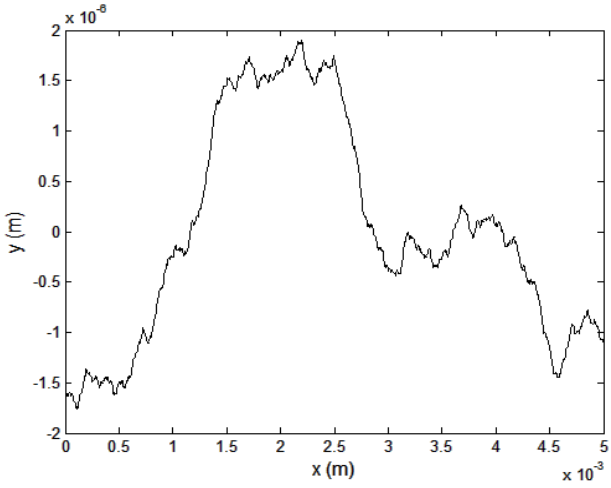

63G rough surface

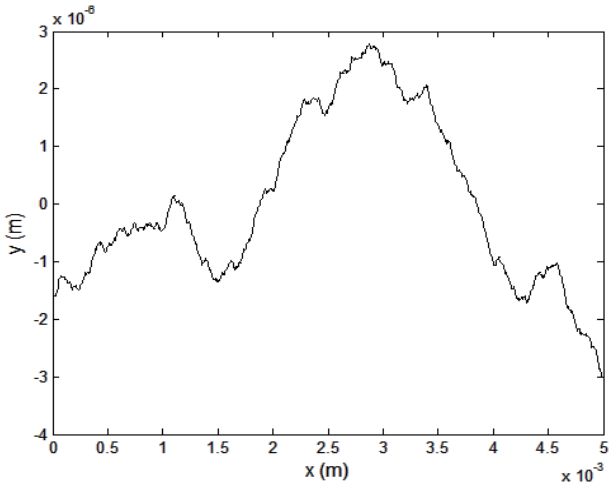

63M rough surface

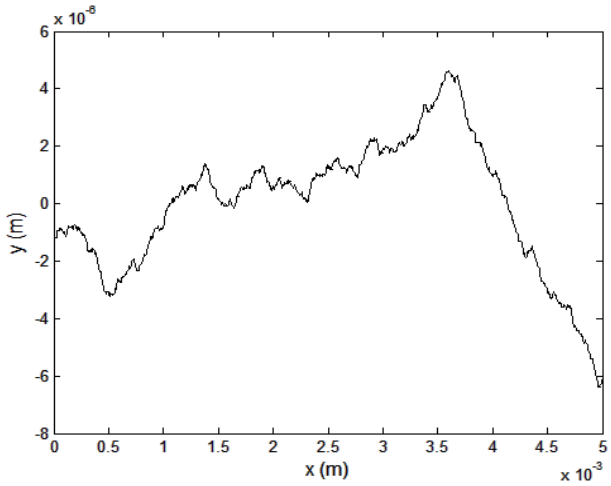

63P rough surface

Figure 32: Surface profiles after leveling for the other five generated rough surfaces

F: Plots of relationship between amplitude (Δ) versus wavelength (λ) for the other four generated rough surfaces

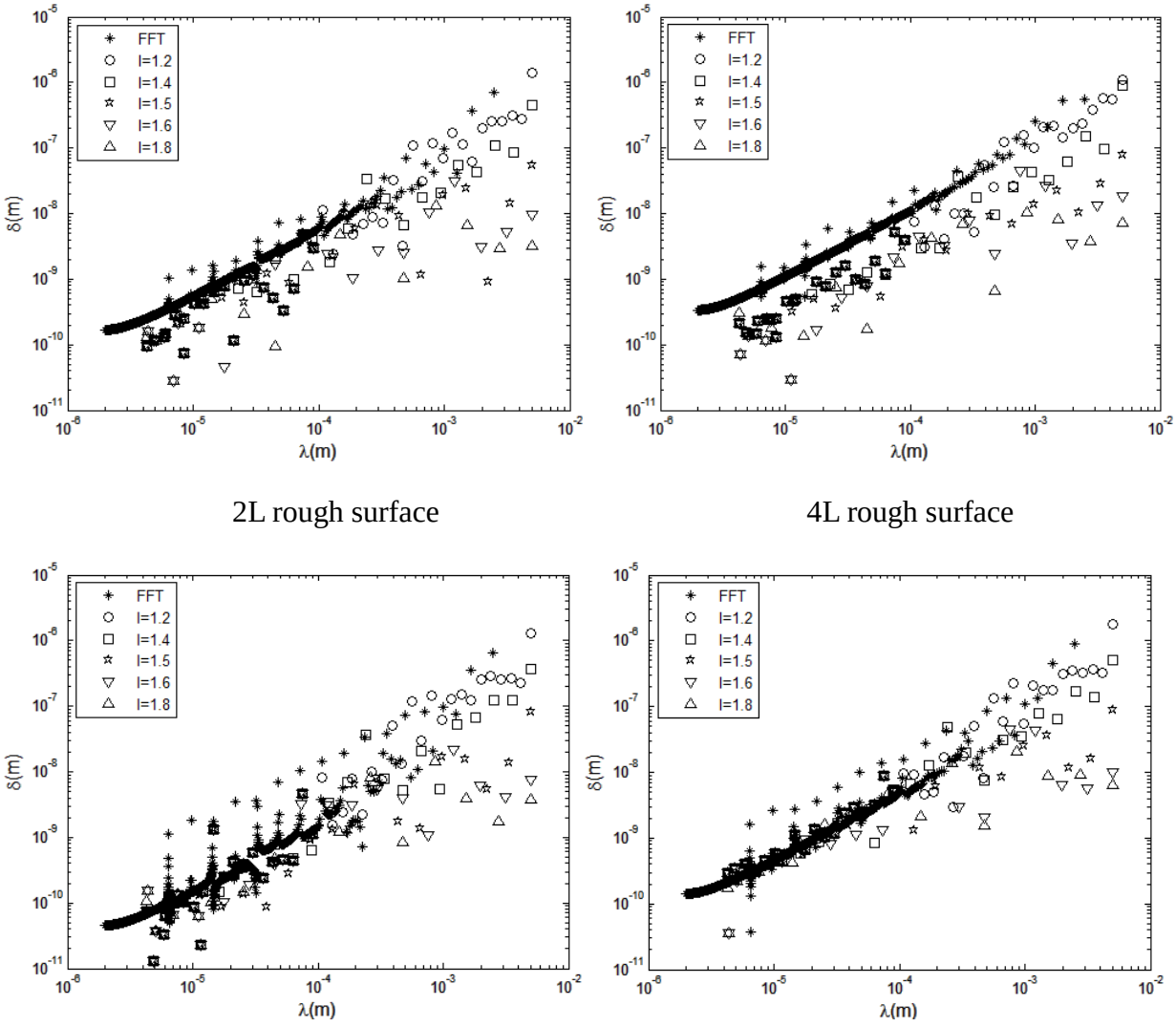

2L rough surface

4L rough surface

63G rough surface

63M rough surface

Figure 33: Δ vs. λ for the other four generated rough surfaces

G: Plots of relationship between *B* and λ for the other four measured rough surfaces

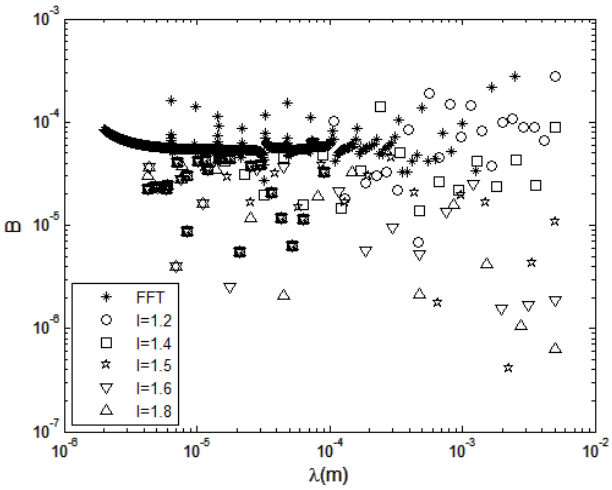

2L rough surface

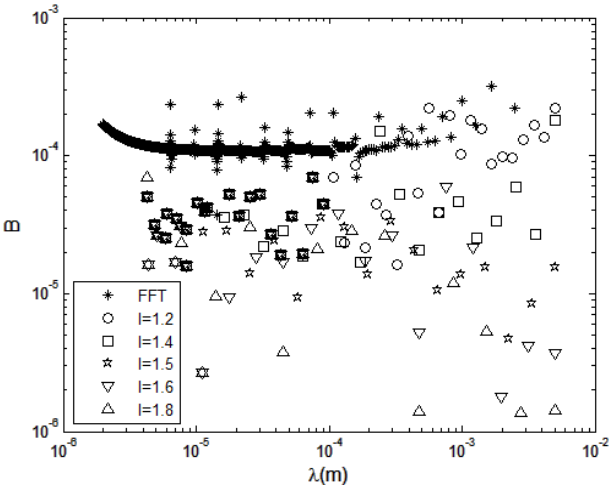

4L rough surface

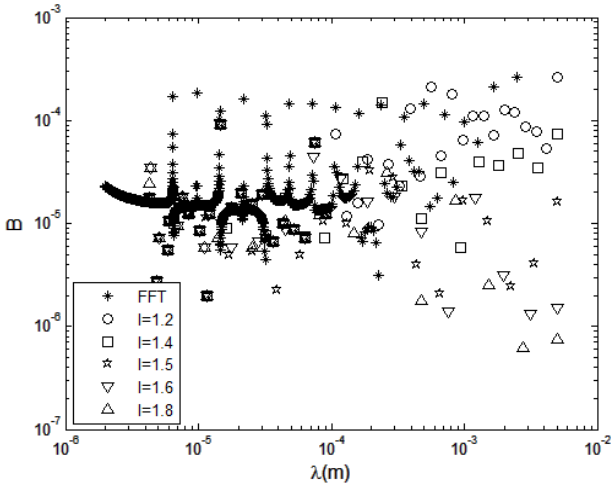

63G rough surface

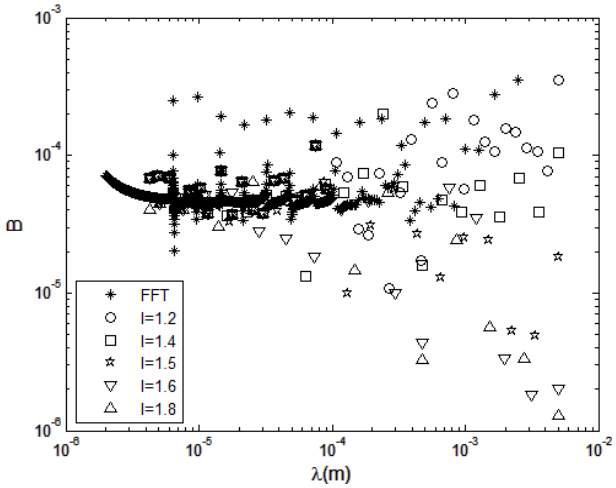

63M rough surface

Figure 34: *B* vs. λ for the other four generated rough surfaces

H: Schematical illustration of fractal dimension of generated rough surfaces calculated by using different four methods

For 2L rough surface:

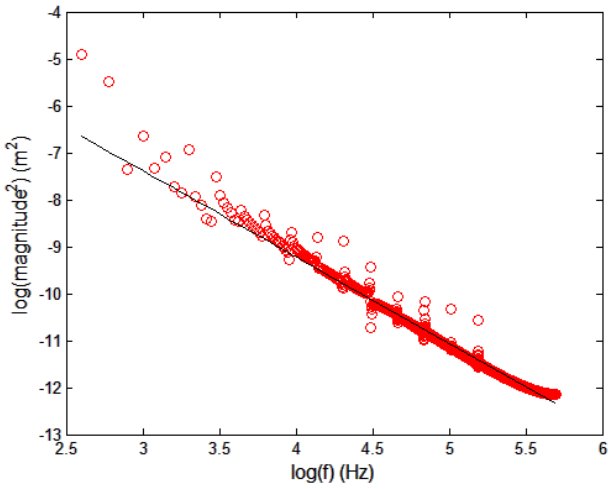

(a)

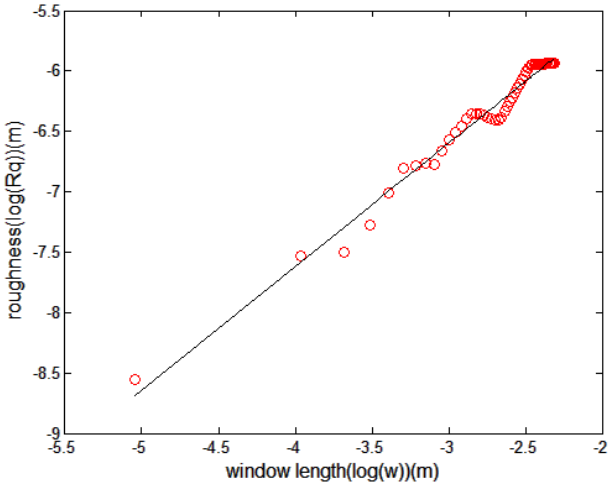

(b)

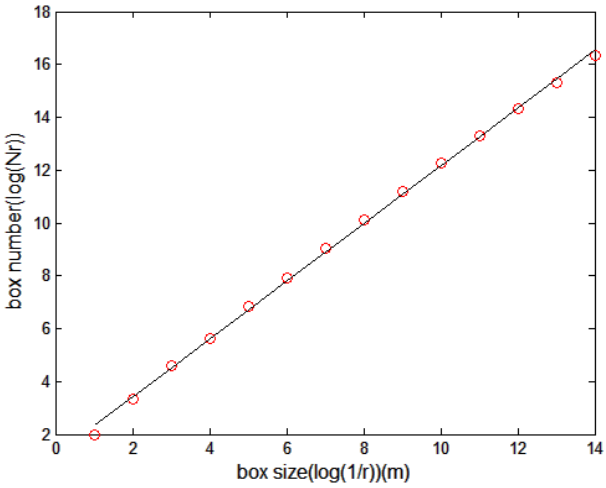

(c)

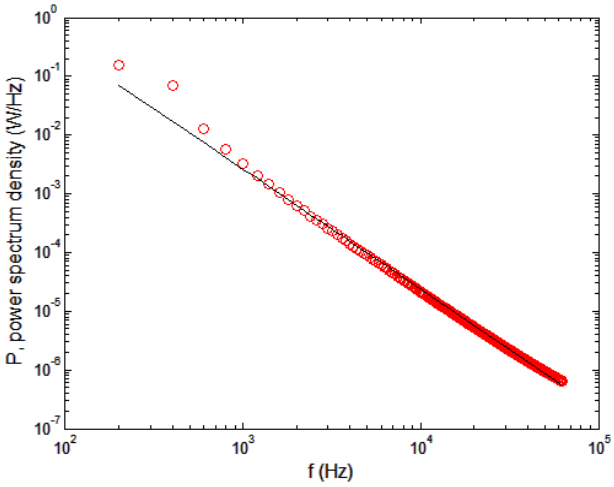

(d)

For 4L rough surface:

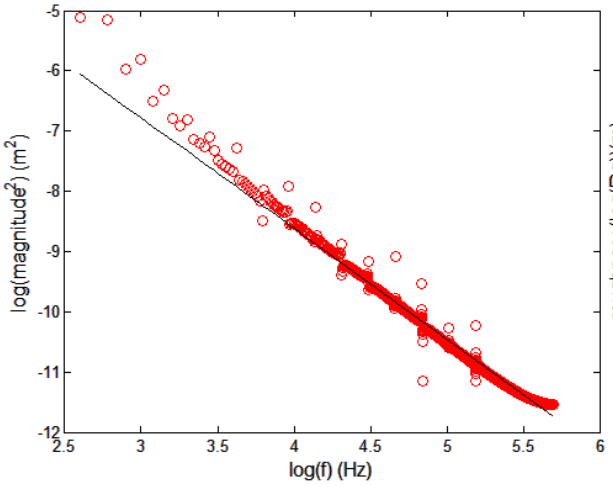

(a)

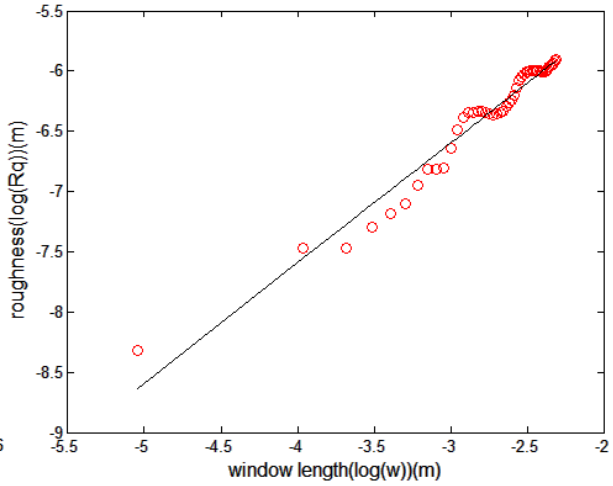

(b)

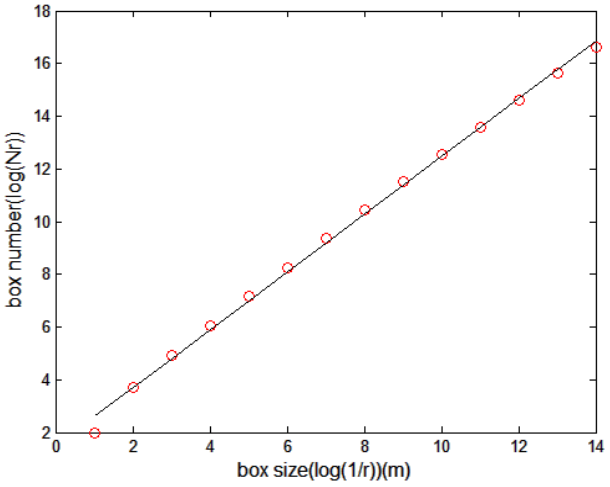

(c)

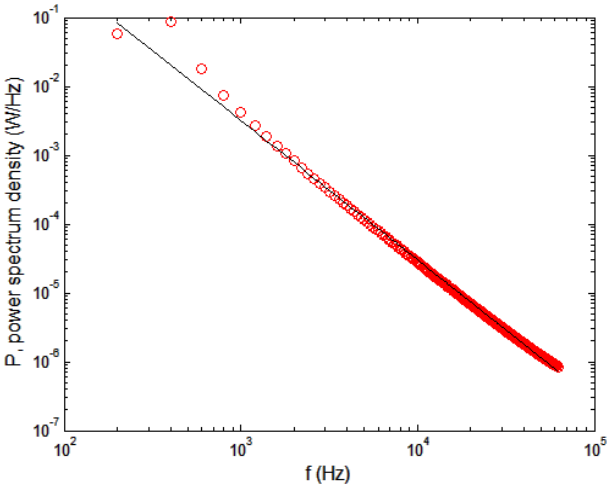

(d)

For 8L rough surface:

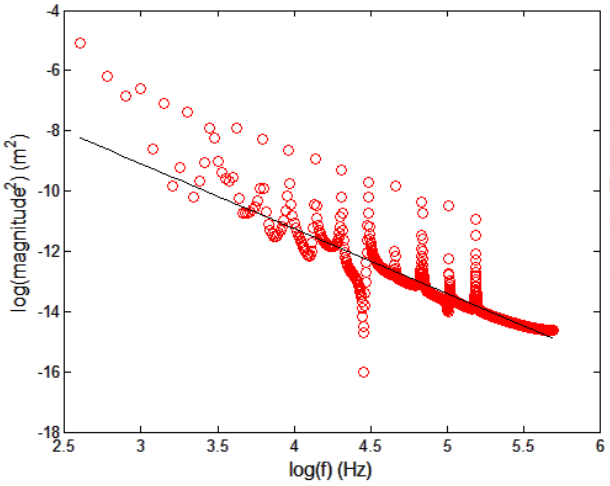

(a)

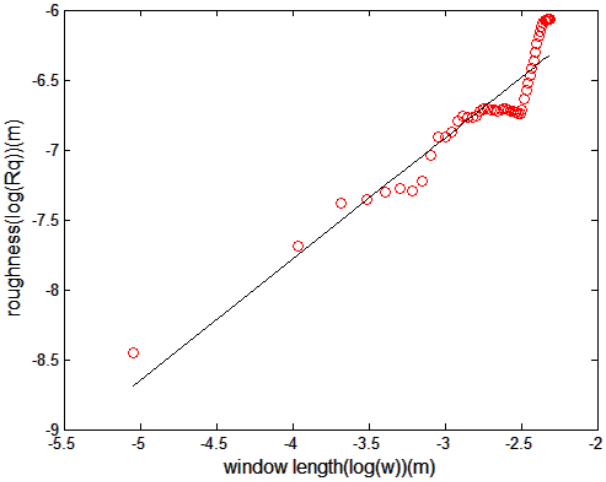

(b)

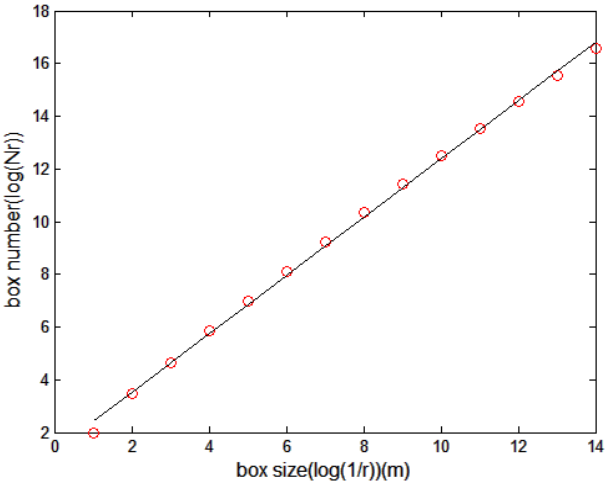

(c)

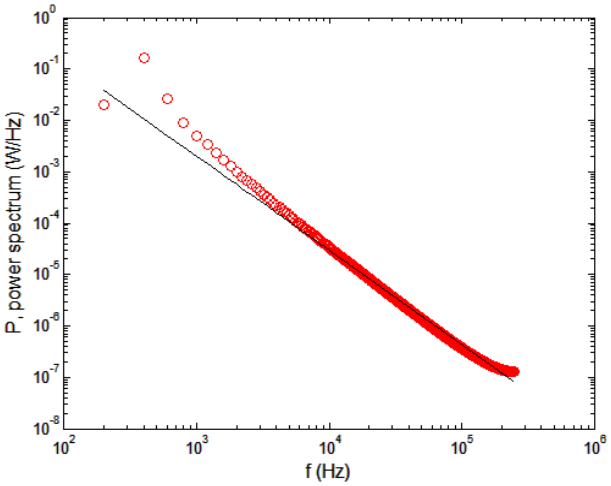

(d)

For 63G rough surface:

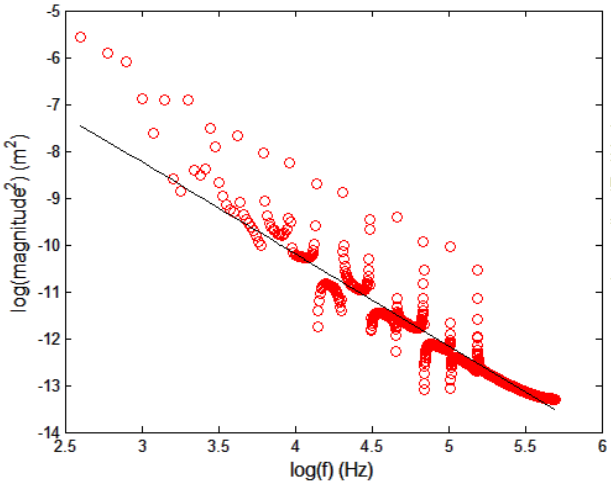

(a)

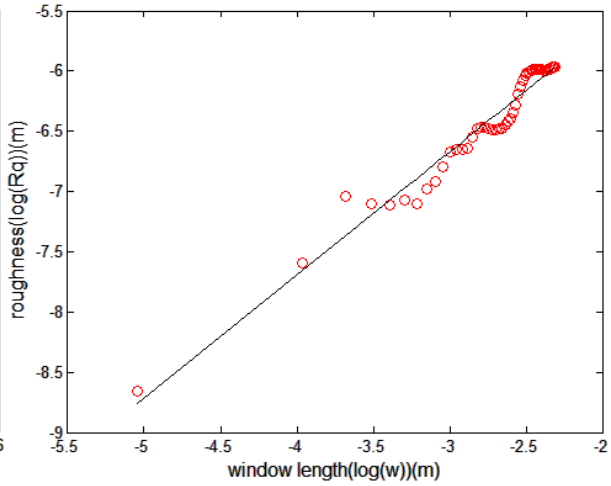

(b)

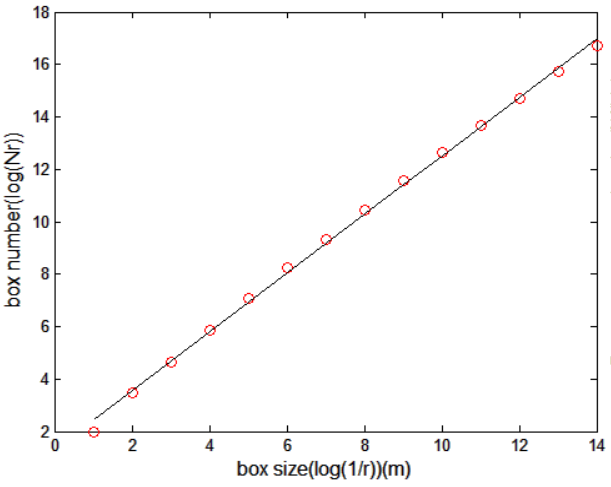

(c)

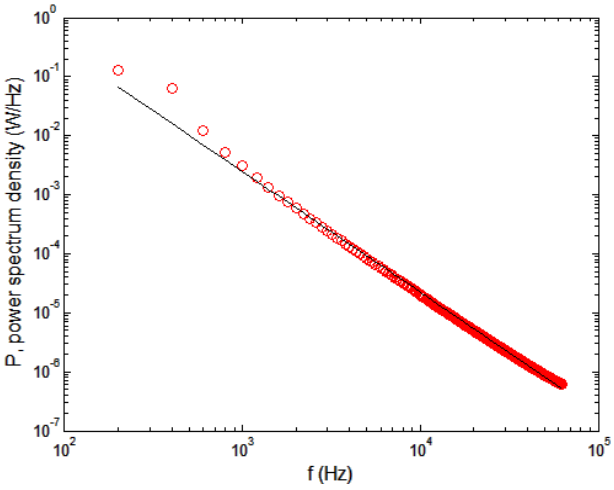

(d)

For 63M roughs surface:

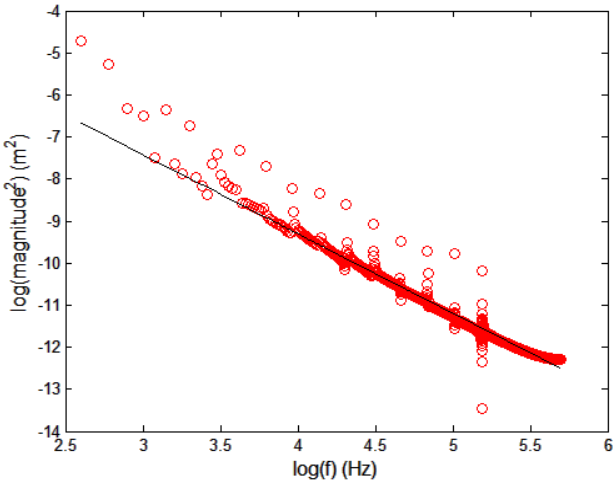

(a)

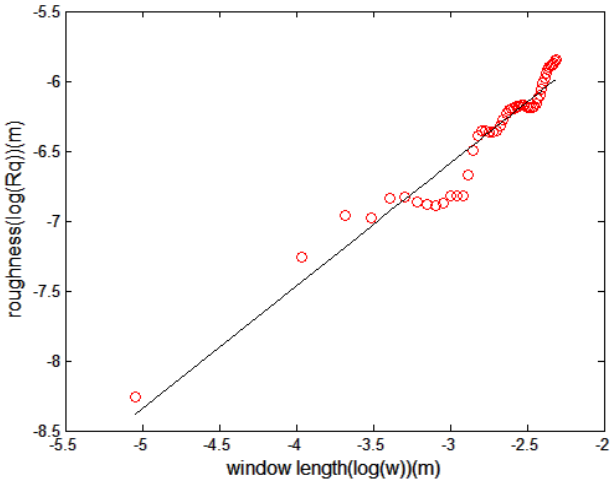

(b)

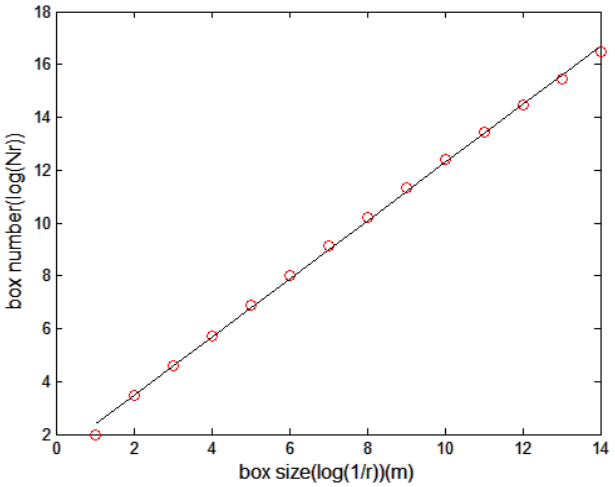

(c)

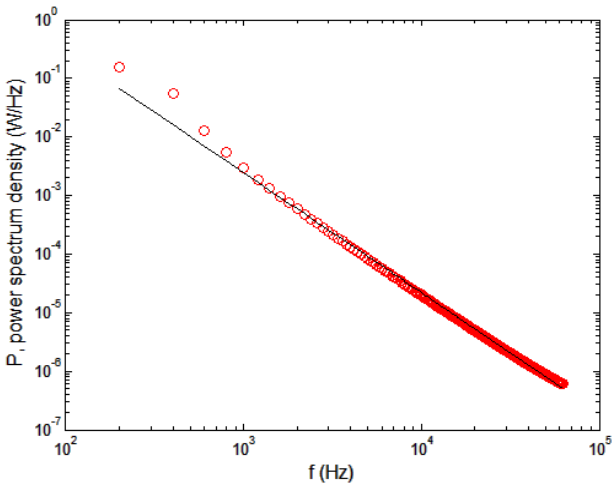

(d)

For 63P rough surface:

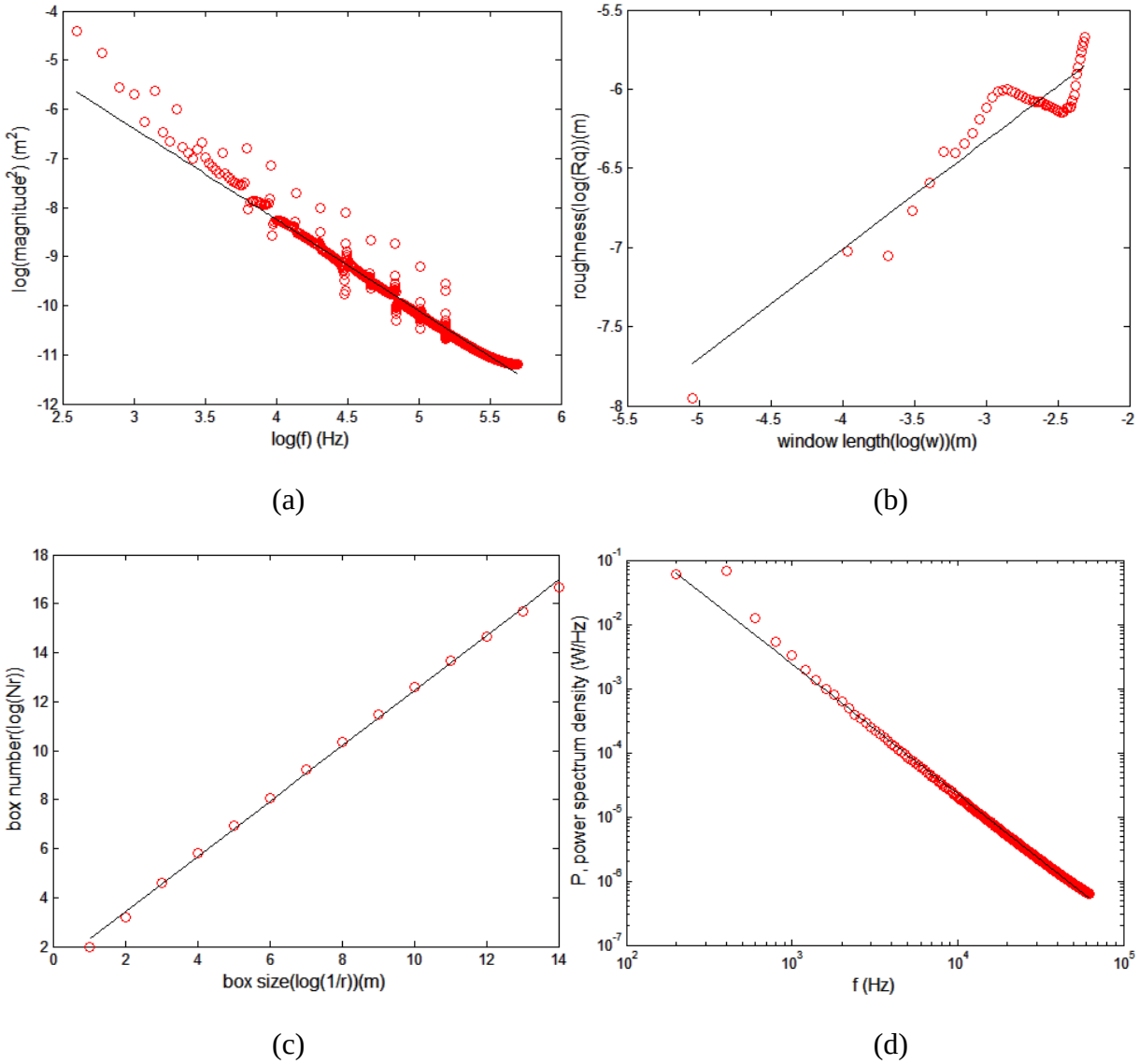

Figure 35: *D* values calculated by four different methods for the other five measured rough surfaces
(a) Fourier analysis; (b) Roughness-length method; (c) Box-counting method; (d) Power spectrum method
The lines are fitted to the points calculated from the generated surfaces